

Summer 8-1-2022

**COASTAL GEOMORPHIC RESPONSE TO SEA-LEVEL RISE,
STORMS, AND ANTECEDENT GEOLOGY: EXAMPLES FROM THE
NORTHERN GULF OF MEXICO**

Clayton Dike

Follow this and additional works at: <https://aquila.usm.edu/dissertations>



Part of the [Geology Commons](#), [Geomorphology Commons](#), [Geophysics and Seismology Commons](#), [Sedimentology Commons](#), and the [Stratigraphy Commons](#)

Recommended Citation

Dike, Clayton, "COASTAL GEOMORPHIC RESPONSE TO SEA-LEVEL RISE, STORMS, AND ANTECEDENT GEOLOGY: EXAMPLES FROM THE NORTHERN GULF OF MEXICO" (2022). *Dissertations*. 2005.
<https://aquila.usm.edu/dissertations/2005>

This Dissertation is brought to you for free and open access by The Aquila Digital Community. It has been accepted for inclusion in Dissertations by an authorized administrator of The Aquila Digital Community. For more information, please contact aquilastaff@usm.edu.

COASTAL GEOMORPHIC RESPONSE TO SEA-LEVEL RISE, STORMS, AND
ANTECEDENT GEOLOGY: EXAMPLES FROM THE NORTHERN GULF OF
MEXICO

by

Clayton Dike

A Dissertation
Submitted to the Graduate School,
the College of Arts and Sciences
and the School of Ocean Science and Engineering
at The University of Southern Mississippi
in Partial Fulfillment of the Requirements
for the Degree of Doctor of Philosophy

Approved by:

Dr. Davin Wallace, Committee Chair

Dr. Stephan Howden

Dr. Leonardo Macelloni

Dr. Michael Miner

Dr. Jessica Pilarczyk

August 2022

COPYRIGHT BY

Clayton Dike

2022

Published by the Graduate School



ABSTRACT

Sea-level rise and tropical cyclone activity are threatening coastlines around the world. Past geologic coastal responses can be used to inform future scenarios. This three-part study examines the response of coastal systems to sea-level rise, storms, sediment supply, and antecedent geology over the past ~ 140 ka.

The first study is of the Bay St. Louis, Mississippi, coastal system along the northern Gulf of Mexico incorporating sediment supply, subsidence, and antecedent topography paired with an examination of geologic response to sea-level fall and rise. I used core and geophysical data that resolve incised valleys and other subsurface deposits from ~ 140 ka to the modern to understand the sequence stratigraphy and extent of geomorphologic change. The response of this previously understudied system can be considered relevant for other Gulf of Mexico systems. I conclude that an eroding bay line is on a trajectory to migrate to a landward Pliocene scarp in ~ 400 years. Infrastructure designed without consideration of this migration may be threatened.

The second study is of sedimentological effects of Hurricane Nate, a Category 1 hurricane, on Ship Island, Mississippi. While major hurricanes receive considerable attention, researchers have not extensively studied and understood the effects of minor hurricanes on barrier islands, and field data are needed to determine the precise role they play. An analysis of trench sediments in overwash fans deposited from Hurricane Nate on Ship Island led to the conclusion that minor hurricanes (categories 1 and 2) can be constructive to barrier islands. The results of this study indicate that minor hurricanes can enhance barrier protection of mainland coastlines on a decadal time scale.

The third study was a database compilation of legacy sediment cores and geophysics created along the Mississippi-Alabama Shelf. These data may be used by researchers to evaluate sediment resource availability for future nourishment projects.

ACKNOWLEDGMENTS

I would like to recognize my advisor Dr. Davin Wallace for his guidance and assistance throughout this process. I would like to recognize my committee members (Dr. Stephan Howden, Dr. Leonardo Macelloni, Dr. Michael Miner, and Dr. Jessica Pilarczyk) for their support and feedback on this dissertation. I would like to acknowledge Dr. Hermann Fritz for providing imagery and survey information. I would also like to acknowledge my lab mates, both past and current, for their help and support over the years: Josh Bregy, Eve Eisemann, Nina Gal, Rob Hollis, Shara Gremillion, Erin Miller, Carrie Miller, and Sarah Monica.

TABLE OF CONTENTS

ABSTRACT ii

ACKNOWLEDGMENTS iv

LIST OF TABLES ix

LIST OF ILLUSTRATIONS x

CHAPTER I - INTRODUCTION 1

 1.1 References 4

CHAPTER II - GEOLOGIC HISTORY OF BAY ST. LOUIS, MISSISSIPPI SINCE OIS
6: IMPLICATIONS FOR FUTURE RESPONSE 7

 2.1 Introduction 7

 2.1.1 Sequence Stratigraphy 7

 2.1.2 Sea-level Rise 8

 2.1.3 Modern Gulf Coast of Mississippi 16

 2.1.3.1 Gulf Coast of Mississippi Geology 16

 2.1.3.1.1 Upper Pliocene 17

 2.1.3.1.2 Sangamon 19

 2.1.3.2 Mississippi Sound 21

 2.1.3.3 Bay St. Louis 23

 2.2 Hypotheses 26

 2.3 Methods 26

2.3.1 Data	26
2.3.1.1 Core Data	26
2.3.1.2 Geophysical Data	27
2.3.1.3 Stratigraphic Bounding Surface Interpretation	32
2.4 Results.....	32
2.4.1 OIS 6.....	32
2.4.2 Undifferentiated Pleistocene	35
2.4.3 OIS 2	35
2.4.4 Holocene Bayhead Delta.....	37
2.4.5 Ravinement Surfaces	39
2.4.6 Holocene Bay Sedimentation.....	41
2.5 Discussion.....	43
2.5.1 OIS 6 and OIS 5.....	43
2.5.2 OIS 2	43
2.5.3 OIS 1	44
2.5.4 Bayhead Delta	47
2.6 Conclusion	50
2.6.1 Morphology.....	50
2.6.2 Bayhead Delta Backstepping and Ravinement	50
2.7 References.....	53

CHAPTER III - SEDIMENTOLOGICAL EFFECTS OF HURRICANE NATE

(CATEGORY 1) ON SHIP ISLAND	61
3.1 Introduction.....	61
3.2 Study Area	64
3.2.1 Regional Setting.....	64
3.2.1.1 Ship Island	66
3.2.1.2 Hurricane Nate	70
3.3 Hypotheses	73
3.4 Methods.....	74
3.4.1 Survey	74
3.4.1.1 Trenches	74
3.4.1.2 Grain Size.....	75
3.4.2 Sediment Flux	78
3.4.3 Image Analysis.....	79
3.5 Results.....	79
3.5.1 Hurricane Nate Deposit Characteristics.....	79
3.5.2 Flux	83
3.5.3 Overwash Volume	83
3.6 Discussion.....	83
3.6.1 Storm Sediment Transport	83

3.6.2 Grain Size Comparison	85
3.6.2.1 West Ship Island and East Ship Island	85
3.6.2.2 Landward Fining.....	87
3.6.3 Flux Comparison: Major Hurricane and Hurricane Nate	91
3.7 Conclusions.....	93
3.8 References.....	95
APPENDIX A – Mississippi Offshore Sediment Resources Inventory.....	104
A.1 References	110

LIST OF TABLES

Table 2.1 Samples Processed at the National Ocean Sciences AMS Laboratory at the Woods Hole Oceanographic Institution and Calibrated Using IntCal20 (Reimer et al., 2020) 37

Table 3.1 Hurricane Nate layer thicknesses and flux (from Equation 1)..... 83

Table 3.2 Comparison of Stratigraphic and Sedimentological Features of Hurricane Nate Deposits to other NGOM Tropical Cyclone Deposits, with Local Setting, Meteorology, and Hydrodynamic Conditions (adapted from [Soria et al., 2017]) 88

Table 3.3 Comparison of Stratigraphic and Sedimentological Features of Tropical Cyclone Deposits Outside of NGOM, with Local Setting, Meteorology, and Hydrodynamic Conditions (adapted from [Soria et al., 2017]) 90

Table A.1 Legacy Core and Geophysical Data Collected in the USM Database 108

LIST OF ILLUSTRATIONS

Figure 2.1 Oxygen Isotope Stages	12
Figure 2.2 NGOM Holocene Sea-level Curve	13
Figure 2.3 NGOM RSL Trends	14
Figure 2.4 Mississippi Coastal Plain.....	15
Figure 2.5 Coastal Mississippi Stratigraphic Column	18
Figure 2.6 Bay St. Louis	24
Figure 2.7 Geology of Bay St. Louis Environments.....	25
Figure 2.8 MDOT Geotechnical Report	29
Figure 2.9 Geotechnical and Geophysical Integration.....	30
Figure 2.10 Data Location	31
Figure 2.11 USM Seismic Line Striking the Top of the Lower Bay	34
Figure 2.12 USM Seismic Line Striking the Lower Bay with MDOT Cores.....	36
Figure 2.13 USM Seismic Line Striking the Lower Bay with USM Core	38
Figure 2.14 USGS Seismic Striking the Lower Bay with Core.....	40
Figure 2.15 USGS Seismic Line Dipping at the Bay Mouth.....	42
Figure 2.16 OIS 6 and OIS 5 Fluvial Extensions.....	45
Figure 2.17 Sequence Boundary	46
Figure 2.18 OIS 1 Bayhead Delta Remnants and Sequence Boundary	48
Figure 2.19 OIS 1 Bayhead Delta Remnants and Bay St. Louis	49
Figure 2.20 Bay St. Louis Paleo Geology	52
Figure 3.1 Mississippi-Alabama Barrier Chain	69
Figure 3.2 Hurricane Nate.....	71

Figure 3.3 East Ship Island after Hurricane Katrina and Hurricane Nate	72
Figure 3.4 Ship Island Survey.....	76
Figure 3.5 Trench Locations.....	77
Figure 3.6 Sedimentological Characteristics	81
Figure 3.7 Trench Distances from Shoreline and Elevations	82
Figure 3.8 Elevation Versus D90.....	86
Figure A.1 NGOM Legacy Core Data Compiled in the USM Database.....	106
Figure A.2 NGOM Legacy Seismic Data Compiled in the USM Database.	107

CHAPTER I - INTRODUCTION

Sea-level rise and tropical cyclone activity are threatening coastlines around the world. Lives and infrastructure are at risk resulting in an increase in the study of geomorphological coastal processes (Munoz et al., 2022) to better understand the evolution of coastal systems. Interacting factors such as flooding, storms, sea-level rise, sediment supply, subsidence, and antecedent topography have led to widespread erosion along the north Gulf of Mexico (NGOM), and these systems are among the most vulnerable in the United States. Coastal inhabitants need to understand these problems and risks so that they may develop strategies for sustainably living in these areas.

Chapter 2 is a study of the Bay St. Louis, Mississippi, coastal system along the NGOM which investigates sediment supply, subsidence, and antecedent topography paired with an examination of geologic response to sea-level fall and rise. This study's design is a reconstruction of past responses to sea level to augment predictions of the response to impending sea-level rise. I used core and geophysical data that resolves incised valleys and other subsurface deposits from ~ 140 ka to the modern to understand the sequence stratigraphy and extent of geomorphologic change controlled by eustatic sea level, sedimentation rates, sediment compaction, and antecedent geology. The eustatic response of this previously understudied system can be considered relevant for other Gulf of Mexico bays. I conclude that an eroding bay line is on a trajectory to migrate to a landward Pliocene scarp in ~ 400 years. Infrastructure designed without consideration of this migration may be threatened.

Chapter 3 is a study of sedimentological effects of Hurricane Nate, a Category 1 hurricane (Achenbach & Sullivan, 2017), on a NGOM barrier island, Ship Island.

Tropical cyclones have profound impacts on barrier islands in the NGOM (Morton et al., 2005; Anderson et al., 2014). Storms cause erosion on short time scales (Morton et al., 2005; Anderson et al., 2014) and increased bedform migration rates (Goff et al., 2015; Campmans, 2018). Sediment removed by major hurricanes, if in the nearshore environment, may be returned by cross shoreface transport or littoral transport energized by minor hurricanes. Major hurricanes are less frequent than minor ones; however, the frequency of major hurricanes may increase with radiative forcing from greenhouse gases (Emanuel, 2013) in addition to storm intensification (Wu et al., 2011; Mousavi et al., 2011; Knutson, 2021; Narita et al., 2009). One of several natural factors affecting barriers, storms cause almost instantaneous geomorphic changes to islands and their shorefaces (Mellet & Plater, 2018; Stutz & Pilkey, 2005). Anthropogenic changes to barriers include beach nourishment, seawall construction (Linhoss, 2018; Stutz & Pilkey, 2005), and coastal development. During tropical cyclones, barrier islands mediate effects on the mainland coastline by breaking or slowing storm waves (Fleming et al., 2018), protecting communities and estuaries (Linhoss, 2018; National Park Service, 2019). Researchers have not extensively studied and understood the effects of minor hurricanes on barrier islands, and field experiments are needed to determine sources and mechanisms of sedimentation associated with minor storms (Stone et al., 2004) to understand their precise role (Stone et al., 1999). The results of this chapter indicate that minor hurricanes enhance barrier protection of mainland coastlines and estuarine fisheries on a decadal time scale. An analysis of trench sediments in overwash fans deposited from a minor hurricane impacting Ship Island led to the conclusion that minor hurricanes (categories 1 and 2) can increase the volume of the dune field and overwash terrace. The

results of this study can be considered for other Gulf barriers frequently impacted by minor hurricanes.

Appendix A describes an ArcGIS collection of legacy core and geophysical data from the NGOM for an offshore sediment resources inventory. These data can be used to locate hard mineral resources of which sand is the most abundant and has the highest near-term leasing potential as it used for beach nourishment (Parker et al., 1993). For example, the Mississippi Coastal Improvements Program was started in 2009 by the U.S. Army Corps of Engineers in collaboration with other federal and state agencies to restore Mississippi barrier islands, including the placement of dredged sand to restore Ship Island (National Park Service, 2019), enhancing mainland protection from storm waves. To better understand coastal hazards, these datasets may be used to reconstruct past responses of coastlines to the sea-level rise rate of the modern and they have supported insightful publications to date.

The overall goal of this dissertation is to inform Mississippi coastal hazard mitigation, complicated by increases in sea-level rise rates and tropical cyclone activity. I expect St. Louis Bay to continue to expand into low lying coastline fringing the bayhead deltas, while the fate of the Ship Island restoration project is unknown. With aid of the legacy data compilation, managers can locate sediment resources needed to augment protection of communities and infrastructure.

1.1 References

Achenbach, J. & Sullivan, P., 2017. *Nate slams Mississippi as the 4th hurricane in an extraordinary year to make landfall in the U.S.* [Online]

Available at: <https://www.washingtonpost.com/news/post-nation/wp/2017/10/08/hurricane-nate-fourth-to-strike-u-s-in-extraordinary-year-slams-mississippi-coast/>

Anderson, J. B. et al., 2014. Variable response of the coastal environments of the northwestern Gulf of Mexico to sea level rise and climate change: Implications for future change. *Marine Geology*, Volume 352, pp. 348-366.

Campmans, G. H. P., 2018. *Modeling storm effects on sand wave dynamics.* [Online]

Available at: <https://research.utwente.nl/en/publications/modeling-storm-effects-on-sand-wave-dynamics>

[Accessed 16 4 2022].

Emanuel, K. A., 2013. Downscaling CMIP5 climate models shows increased tropical cyclone activity over the 21st century. *PNAS*, 110(30), pp. 12219-12224.

Fleming, E. et al., 2018. Coastal Effects. In: D. R. Reidmiller, et al. eds. *Impacts, Risks, and Adaptation in the United States: Fourth National Climate Assessment.*

Washington, DC: U.S. Global Change Research Program, pp. 322-352.

Goff, J. A. et al., 2015. The impact of Hurricane Sandy on the shoreface and inner shelf of Fire Island, New York: large bedform migration but limited erosion.

Continental Shelf Research, Volume 98, pp. 13-25.

Knutson, T., 2021. *Global Warming and Hurricanes.* [Online]

Available at: <https://www.gfdl.noaa.gov/global-warming-and-hurricanes/>

Linhoss, A., 2018. *The Conversation*. [Online]

Available at: <https://theconversation.com/barrier-islands-are-natural-coast-guards-that-absorb-impacts-from-hurricanes-and-storms-103120>

[Accessed 2 April 2022].

Mellet, C. L. & Plater, A. J., 2018. Drowned Barriers as Archives of Coastal Response to Sea-Level Rise. In: Moore, L., Murray, A. (eds) *Barrier Dynamics and Response to Changing Climate*. Springer, Cham, pp. 57-89.

Morton, R. A., Miller, T. & Moore, L., 2005. Historical Shoreline Changes Along the US Gulf of Mexico: A Summary of Recent Shoreline Comparisons and Analyses. *Journal of Coastal Research*, pp. 704-709.

Mousavi, M. E. et al., 2011. Global warming and hurricanes: the potential impact of hurricane intensification and sea level rise on coastal flooding. *Climatic Change*, 104(3), pp. 575-597.

Munoz, S. C. et al., 2022. The timing of postglacial marine transgression in the Ria de Ferrol (NW Iberia): A new multiproxy approach from its sedimentary infill. *CATENA*, Volume 209.

Narita, D., Tol, R. S. J. & Anthoff, D., 2009. Damage costs of climate change through intensification of tropical cyclone activities: An application of FUND. *Climate Research*, 39(2), pp. 87-97.

National Park Service, 2019. *Mississippi Coastal Improvements Program*. [Online]

Available at: <https://www.nps.gov/guis/learn/nature/mscip.htm>

Parker, S. J., Davies, D. J. & Smith, W. E., 1993. *Geological, Economic, and Environmental Characterization of Selected Near-Term Leasable Offshore Sand*

Deposits and Competing Onshore Sources for Beach Nourishment. Tuscaloosa:
Geological Survey of Alabama.

Stone, G. W., Liu, B., Pepper, D. A. & Wang, P., 2004. The Importance of Extratropical and Tropical Cyclones on the Short-Term Evolution of Barrier Islands Along the Northern Gulf of Mexico, USA. *Marine Geology*, 210(1), pp. 63-78.

Stone, G. W. et al., 1999. Studying the importance of hurricanes to the northern Gulf of Mexico coast. *Eos, Transactions American Geophysical Union*, 80(27), pp. 301-305.

Stutz, M. L. & Pilkey, O. H., 2005. The relative influence of humans on barrier islands: Humans versus geomorphology. In: J. Ehlen, W. C. Haneberg & R. A. Larson, eds. *Humans as Geologic Agents*. Boulder(Colorado): Geological Society of America, pp. 137-147.

Wu, Y. et al., 2011. Changes in storm tracks and energy transports in a warmer climate simulated by the GFDL CM2.1 model. *Climate Dynamics*, 37(1), pp. 53-72.

CHAPTER II - GEOLOGIC HISTORY OF BAY ST. LOUIS, MISSISSIPPI SINCE OIS

6: IMPLICATIONS FOR FUTURE RESPONSE

2.1 Introduction

2.1.1 Sequence Stratigraphy

For most coastal systems, the style of deposition tends to repeat itself over glacioeustatic cycles (Anderson et al., 2014; Anderson et al., 2022). The Exxon Production Research Group (Vail & Mitchum, 1977) developed the concept of sequence stratigraphy for reconstructed sea-level cycles and depositional response (Lee et al., 2022). Sequence stratigraphy is the study of relationships of sediment facies and stratal architecture within a chronostratigraphic framework of repetitive, genetically related strata bounded by unconforming surfaces of erosion or nondeposition, or their correlative conformities (Wagoner et al., 1988; Vail & Mitchum, 1977; Catuneanu et al., 2009). If factors such as tectonics and sediment supply have minor variations, eustatic changes produce similar depositional sequences globally (Posamentier & Vail, 1988). Interpretation of past responses to eustatic cycles can be applied to projections of future response, as sea level will exert an important fundamental control on coastal evolution. For example, past system response to the last interglacial highstand (HST) 120 thousand years ago (ka) as well as the OIS 1 transgression (~14 ka) can be used to predict a modern response. The NGOM is currently one of the most vulnerable and rapidly changing coastal environments in the United States, and this chapter will examine past evolution of a representative system (Bay St. Louis, Mississippi) in a sequence stratigraphic framework to shed light on its future.

2.1.2 Sea-level Rise

Lisiecki & Raymo, (2005) divided 621 ka of reconstructed eustatic sea level into oxygen isotope stages (OIS) (Figure 2.1). The curve is accurate to about ± 15 m for OIS 5-2 (130-14 ka) and about ± 5 m for OIS 1 (14 ka to modern) (Anderson et al., 2004). Over the last glacioeustatic cycle (~ 120 ka to modern), sea level fluctuated by about 130 m (Labeyrie et al., 1987; Shackleton, 1987) (Figure 2.1) and reached 6 m higher than present during the OIS 5e maximum flooding surface (MFS; ~ 120 ka) in the Gulf of Mexico. During the ~ 20 ka lowstand (LST), when the coastline coincided with the shelf break (Anderson et al., 2004), fluvial valleys extended basinward, depositing slope fans and wedges comprised in part of eroded/ravined previously deposited continental shelf deposits (Anderson et al., 2014; Posamentier & Vail, 1988). Anderson et al. (2004) divided the cycle into three depositional periods: a falling stage from 120 ka to 22 ka, a lowstand (Wisconsin) from 22 ka to 16 ka, and a transgressive stage (TST) from 16 ka to 4 ka (~ 7 mm/yr). During the Holocene, rates in the Gulf of Mexico decreased with time. From 10 to 7 ka, the rise rate averaged about 4.5 mm/yr and then slowed to 2 mm/yr until 4 ka (Figure 2.2). Rise slowed around 4 ka to about 0.5 mm/yr (Figure 2.2).

Sea-level change over the last glacioeustatic cycle had a pivotal role in shaping coastal systems. Following LST, sea-level rise flooded river valleys and created estuaries (Otvos, 1982; Anderson et al., 2014). Since ~ 10 ka, rapid sea-level rise rates in the NGOM produced flooding events manifest as surfaces separating upper estuary sediments from open estuary or marine facies as coastlines transgressed (Figure 2.2) (Milliken et al., 2008; Anderson et al., 2014). The ~ 8.4 to 8.0 ka flooding event was caused by the melting of the Laurentide Ice Sheet, whereas the ~ 7.4 to 6.8 ka event was

caused by ice-sheet retreat in Antarctica (Anderson et al., 2014). As sea level rose, accommodation made available for sediment accumulation (Rodriguez et al., 2008) increased, allowing landward migration of coastal environments in areas of low sediment supply. Some NGOM estuaries moved landward 10s of kilometers, such as Mobile Bay from 8.68 to 8.20 ka, and others increased area by ~ 25% in the span of a few centuries (Milliken et al., 2008). Specific environmental response to sea-level rise was modulated by antecedent topography, sediment supply, and subsidence (Milliken et al., 2008; Anderson et al., 2014).

Relative sea-level (RSL) rise encompasses eustatic rise as well as local elevation changes due to factors such as compaction-driven subsidence and glacial isostatic adjustments (Gonzalez & Törnqvist, 2006). Subsiding areas of the NGOM affected by reduced sediment supply due to human effects are experiencing rapid wetland loss and shoreline erosion (Milliken et al., 2008). Currently, NGOM RSL rise rates range between 2.19–9.65 mm/yr (Figure 2.3), rates that exceed the early Holocene where NGOM estuaries transgressed and increased in area (Milliken et al., 2008; Anderson et al., 2014). In Bay St. Louis, Mississippi, the rate of RSL rise from the Bay Waveland, MS tide station (8747437) was 4.68 mm/yr from 1978 to 2021 (NOAA, 2021). A Pensacola, Florida tide station (8729840), with a rise rate of 2.59 mm/yr (NOAA, 2021), is generally considered to be stable in terms of subsidence (Kolker et al., 2011), indicating Bay St. Louis has a subsidence rate of 2.09 mm/yr over decadal time scales.

Inundation models currently predicting the fate of bay lines and bayhead deltas fail to account for changes in sediment accommodation, accretion, and erosion, factors which will determine if bayhead deltas can backstep or will drown (Anderson et al.,

2014). For example, the Sea Level Rise and Coastal Impacts Viewer (Office for Coastal Management, 2022) and the Coastal Risk Screening Tool (Climate Central, 2022) utilize a bathtub model, subtracting water height from a DEM, although the Sea Level Rise and Coastal Impacts Viewer has a “Marsh Migration” utility that takes subsidence and accretion into account. Also, Sullivan et al. (2020) utilized a high-resolution lidar DEM and numerical simulations of flow and tracer exchange to assess inundation of a Florida river due to 0.2 m and 0.5 m rises in sea level based solely on existing floodplain topography.

Tellingly, instances of Holocene NGOM fluvial systems forming a bay (underfilled valley) indicate sediment supply unable to keep pace with sea-level rise, e.g., Bay St. Louis, Biloxi Bay, and Mobile Bay (Figure 2.4) as well as the Trinity and Sabine systems of Texas (Anderson et al., 2004). Here, coarse sediment is retained in bayhead deltas, and only fine material is transported basinward. NGOM fluvial systems where sediment supply is sufficient to keep pace with sea-level rise (overfilled valley) include the Pearl and Pascagoula River valleys (Figure 2.4) (Meyer-Arendt et al., 1998), as well as the Brazos and Colorado fluvial systems. Fine-grained valley fill compacts leading to subsidence (Siringan & Anderson, 1993).

The last glacioeustatic cycle is well understood with respect to time and sea level and its stratigraphy is shallow enough to explore with core and geophysical methods (Anderson et al., 2004), although resolving flooding events is hampered by dating uncertainty (Anderson et al., 2014). However, the Mississippi coastline, in particular Bay St. Louis, is understudied (Adcock, 2019). A compilation of legacy core and geophysical data from the NGOM was created for the “Mississippi Offshore Sediment Resources

Inventory: Late Quaternary Stratigraphic Evolution of the Inner Shelf’ project, a cooperative agreement between the University of Southern Mississippi (USM) and the Bureau of Ocean Energy Management (BOEM). Existing data sets were organized in an Excel sheet arranged with select metadata as shown in Appendix A. When available, shape files of existing data sets were added to an ArcGIS database and project to identify data gaps. This included geophysical lines, bathymetry, side scan, LiDAR, and core locations and logs. Analyses of these data and gaps was used to inform a plan for collection of new data to support the study of Bay St. Louis. Other researchers may use these data to study NGOM response to sea-level variation.

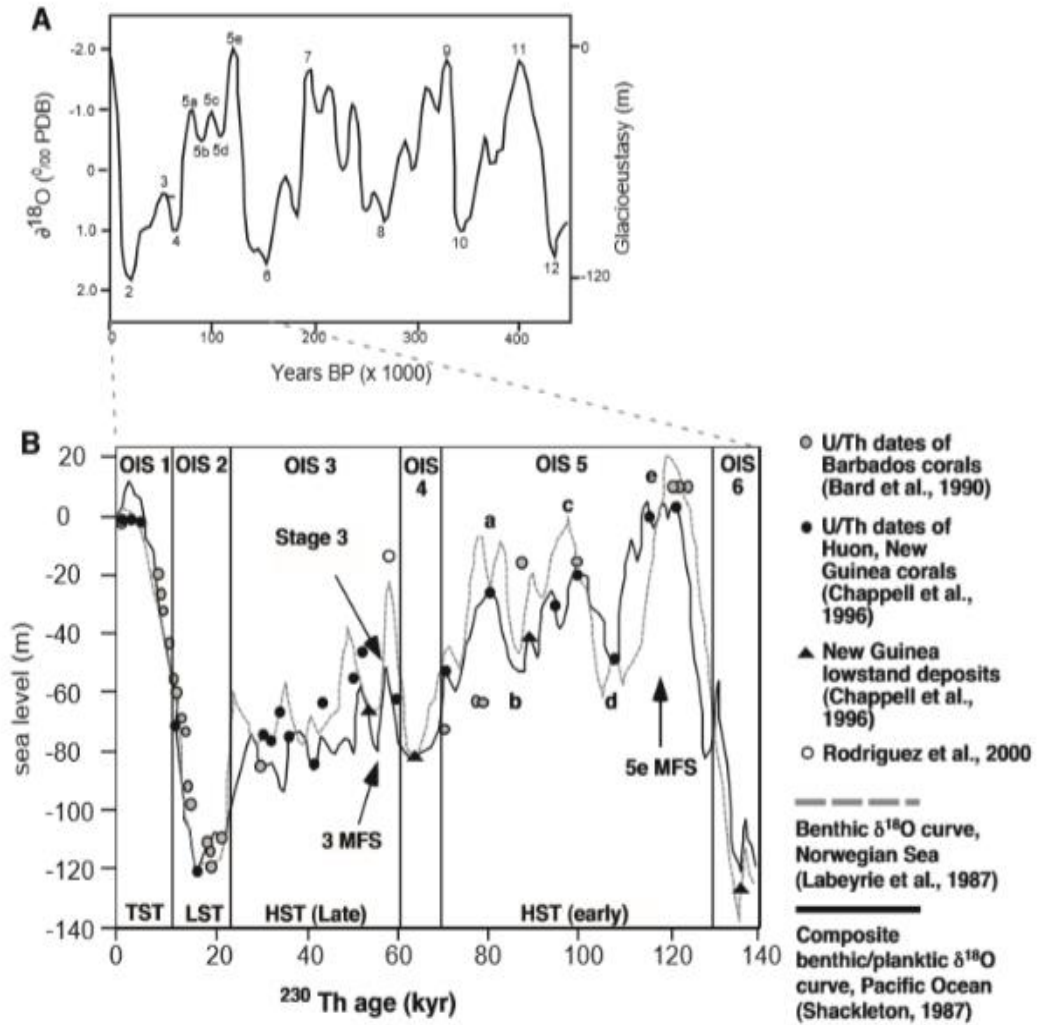
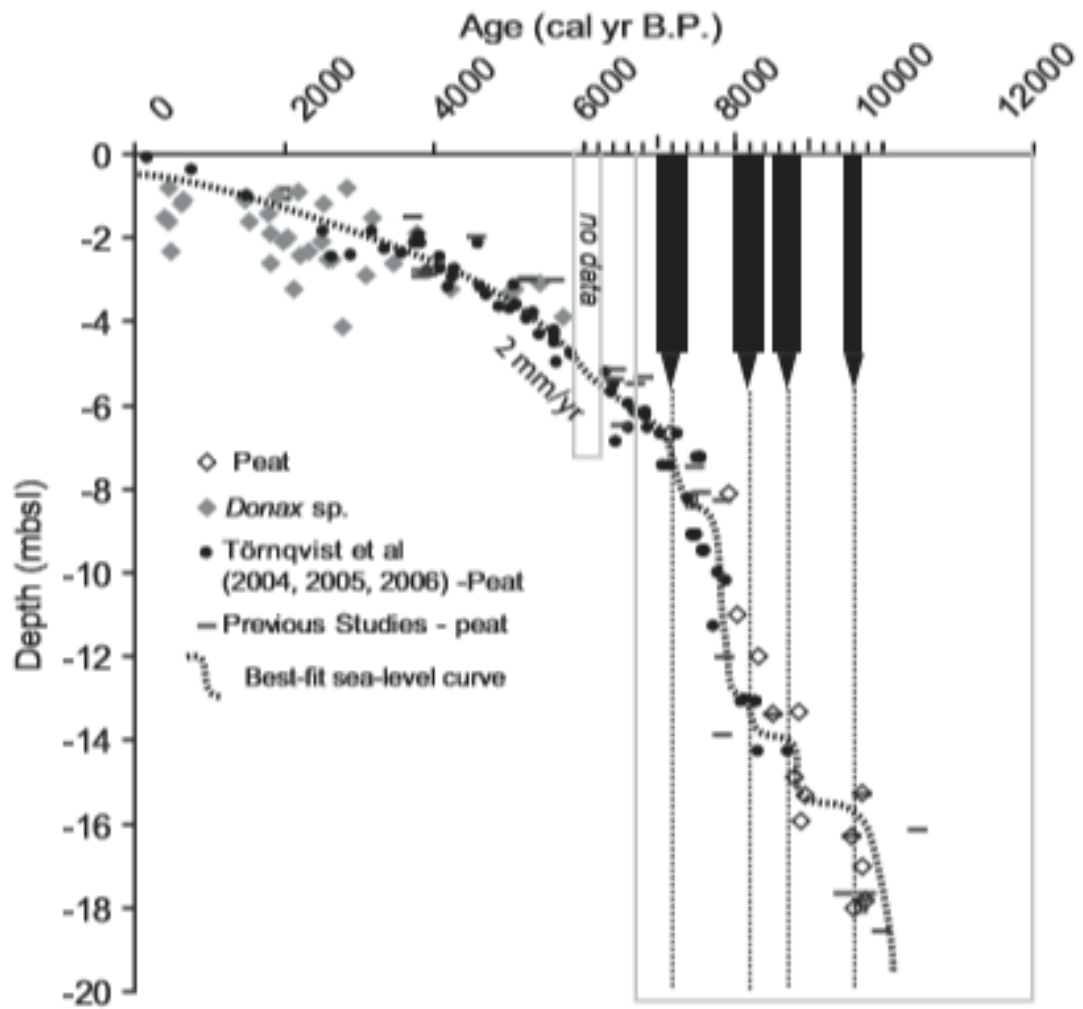


Figure 2.1 *Oxygen Isotope Stages*

A) SPECMAP oxygen isotope curve showing last four glacial cycles (Imbrie et al., 1984) B) OIS (Oxygen Isotope Stages) of the last glacial cycle delineating the early highstand (HST), the late HST, the lowstand (LST), and the transgressive stage (TST) – the OIS 6 sea level was ~ 10 m lower than that of the LST and the ensuing rise of OIS 5e inundated ~ 6 m higher than modern (Anderson et al., 2004).



NoGoM Sea-level record

Figure 2.2 *NGOM Holocene Sea-level Curve*

Northern Gulf of Mexico 10 ka sea-level curve with 9.8–9.5, 8.9–8.5, 8.4–8.0, and 7.4–6.8 ka flooding events (black arrows); rates were 4.5 mm/yr from 10–7 ka, 2 mm/yr from 7–4 ka, and 0.5 mm/yr starting 4 ka (Milliken et al., 2008).

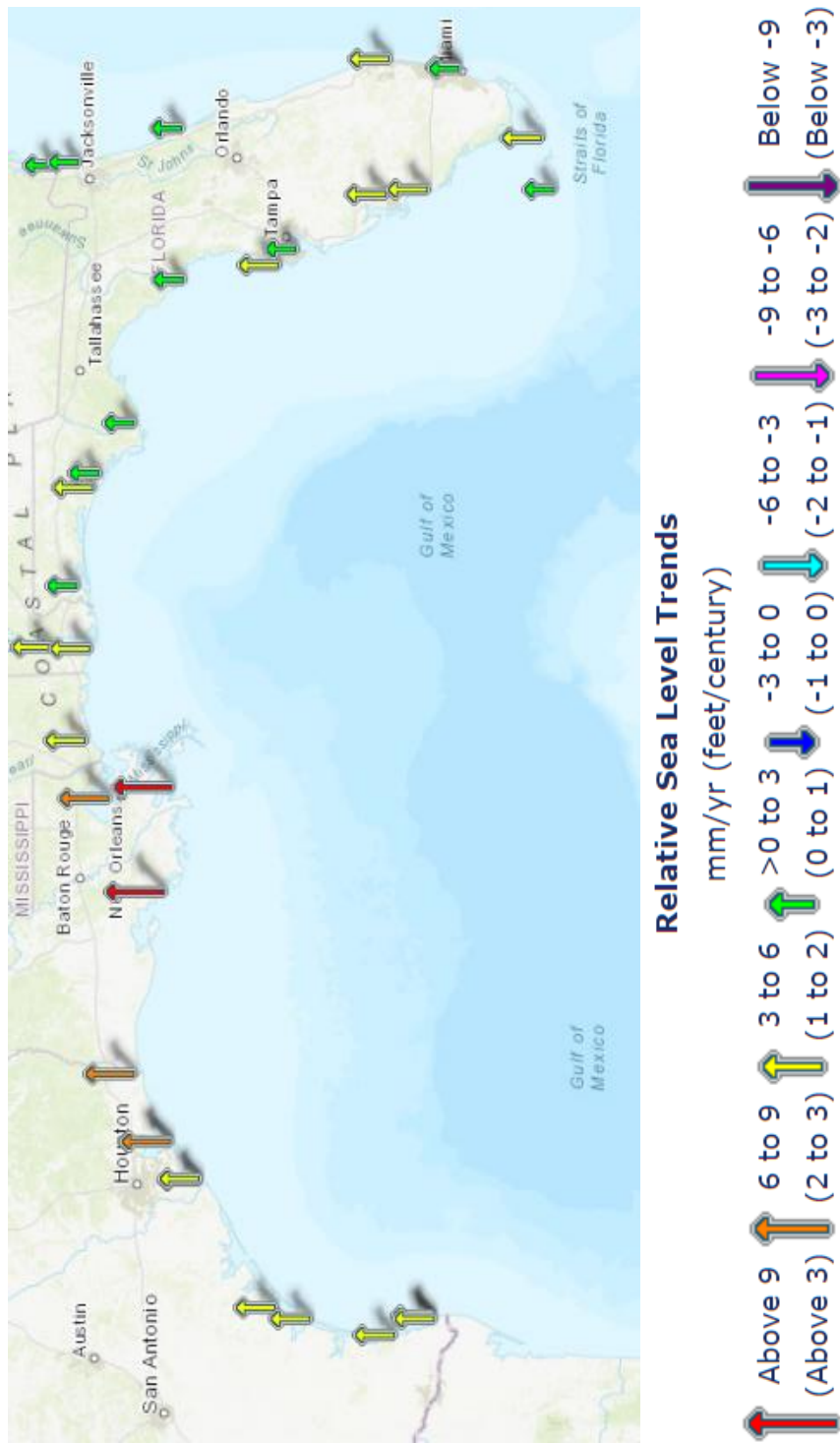


Figure 2.3 *NGOM RSL Trends*

RSL rise rates (a combination of eustatic sea-level rise and vertical land motion) trends of northern Gulf of Mexico measured with respect to local fixed references on land over at least 30 years using NOAA tide gauges, arrows represent magnitude and direction of change (NOAA, 2021); a tide gauge in Bay St. Louis, MS reports a RSL rise rate of 4.68 mm/yr.

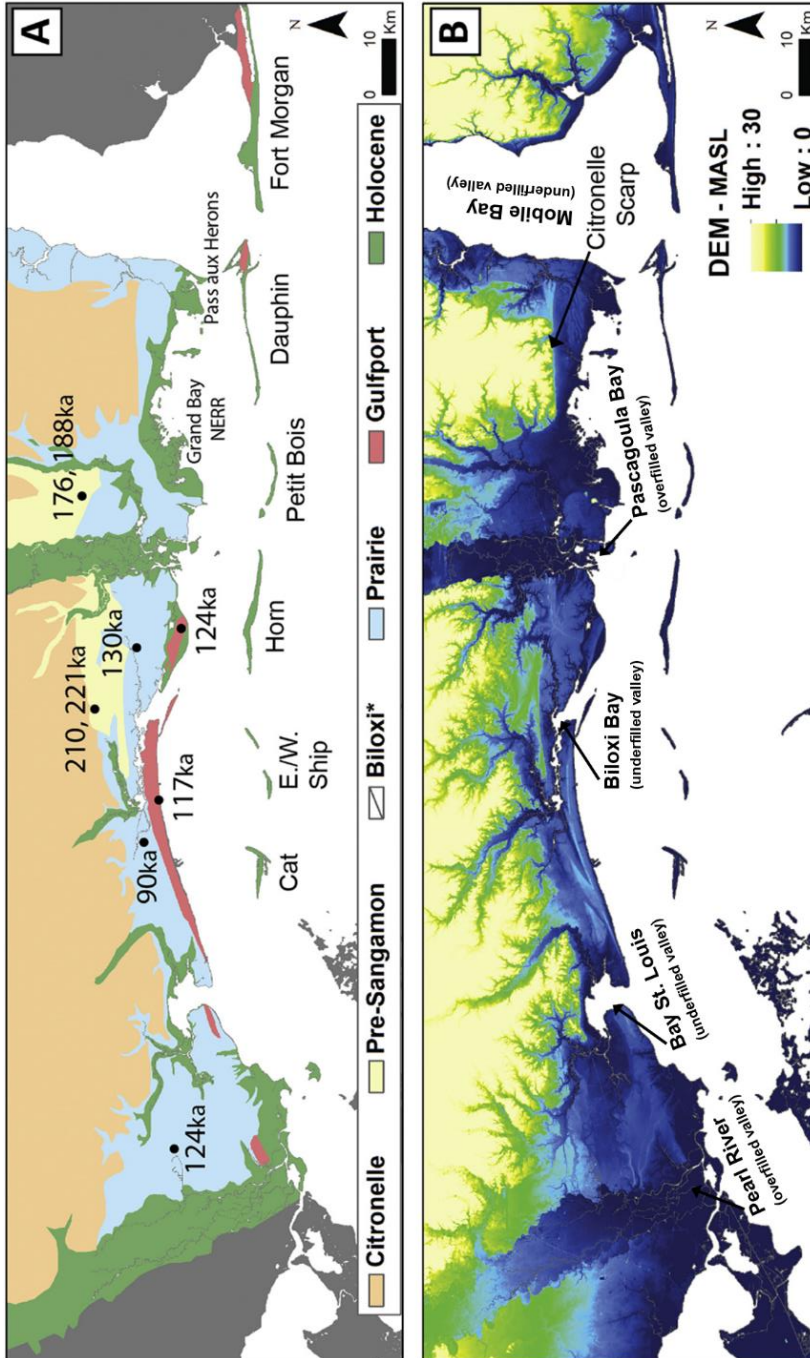


Figure 2.4 *Mississippi Coastal Plain*

(A) South Mississippi coastal plain geologic map with Citronelle Fm. (Pliocene), Pre-Sangamon deposits, Prairie Fm. (late Pleistocene), Gulfport Fm. (late Pleistocene), Biloxi Fm. (* underlies and interfingers with the Prairie Fm. and the Gulfport Fm.), and Holocene deposits (Otvos, 1985; Otvos, 2001). Ages are optically stimulated luminescence dates from Otvos (2005). (B) DEM showing bays of the northern Gulf of Mexico and whether they are over- or underfilled – adapted from (Hollis et al., 2019).

2.1.3 Modern Gulf Coast of Mississippi

The Gulf Coast of Mississippi has a humid-subtropical environment (Anderson et al., 2004; Otvos, 2001), that was cooler and drier during glaciations (Otvos, 2001). Annual precipitation averages 150 cm (Milliken et al., 2008). In the fall to early spring northeasterly and northerly winds create low water levels; however, from March to October east-southeasterly winds dominate (Otvos, 1982) elevating tides. Diurnal tides have about a 0.45 m range (Otvos, 1982). The mainland has lost ~ 12.7 km² between the 1850s and 1986 (Oivanki et al., 1995) due to coastal erosion. Recent studies of Mississippi land area changes are lacking although Morton et al., (2004) reported that land loss rates for the Mississippi mainland coast are low. The South Hancock marshland (Figure 2.4) has intensively eroded due to subsidence as it is on the fringe of an abandoned Mississippi River delta (Otvos, 2001). The Mississippi barrier islands will not keep pace with storm activity and sea-level rise (Gremillion et al., 2020; Eisemann et al., 2018), threatening physical protection of the mainland shoreline.

2.1.3.1 Gulf Coast of Mississippi Geology

The geological units that form the surface of coastal Mississippi range in age from the late Pliocene Epoch to modern (Figure 2.5). The general stratigraphic succession of surface deposits consist of the Upper Pliocene Citronelle Formation (~ 3.4 Ma) found upland separated by pre-Sangamonian (OIS 7 and 6) or Sangamonian (OIS 5) deposits of the Pleistocene Epoch (Otvos, 1982; Heinrich, 2006) (Figure 2.5). OIS 7 through OIS 5e sediment packages along the northeastern Gulf coastal plain are narrow, ranging from 0 to less than 17 km in width (Otvos 1982). Pre-Sangamonian deposits are fragmented coastal surfaces that have been associated with OIS 7 in Mississippi and are intermediate

in elevation to the uplifted Citronelle Formation and lower Sangamonian deposits (Otvos, 2001). The Sangamonian interglacial highstand (OIS 5e) lead to the deposition of the extensive Biloxi, Gulfport, and Prairie Formations (Otvos, 1982; Otvos, 1999) (Figure 2.5). Holocene fluvial and marsh deposits are found near modern rivers or coastlines (Figure 2.5) (Otvos, 1982; Otvos, 2001). Modern fluvial sediment supply is less than that of the Sangamon because rivers had more extensive meander belts on the coastal plain (Anderson et al., 2004) during a climate that was probably like the modern.

2.1.3.1.1 Upper Pliocene

Citronelle deposits underlie ridge and ravine topography of the uplands of the study area (Heinrich, 2006). Primarily fluvial in origin, Citronelle deposits (Figure 2.4 and Figure 2.5) of the Upper Pliocene (~ 3.6-1.7 million years ago) consist of bright-orange-red and brownish-yellow muddy sands with kaolinite being the dominate clay (Otvos, 2001; Matson, 1916). Gravel and coarse sands are also found in this deposit, composed of chert and quartz (Otvos, 2001; Matson, 1916; Hosman, 1996). Eolian ponds on the surface are evidence of dry and windy interglacial climates of the late Pliocene or early Pleistocene (Otvos, 2001; Matson, 1916). The Citronelle deposits were formerly considered part of the Grand Gulf Group (Crider, 2015).

Global Chronostratigraphic Units		Age	Geologic Units	Late Cenozoic Stratigraphic Units in Coastal Mississippi		
Systems	Series/Stages			Updip (North)	Downdip (South)	
Quaternary	Holocene	OIS 1	wetlands, lagoonal, inlet, and delta deposits; mainland and island strand plains, beach complexes and alluvium	alluvium	barrier islands	
		OIS 2	valley fill alluvium	valley fill alluvium		
	Pleistocene	OIS 5e	Prairie Formation (alluvial) Gulfport Formation (barrier complex) Biloxi Formation (neritic to estuarine)	Prairie Formation Gulfport Formation Biloxi Formation		
		OIS 6	Pre-Sangamonian alluvial deposits	Pre-Sangamonian alluvial deposits		
		OIS 7	Pre-Sangamonian units	Pre-Sangamonian units		
	Tertiary	Pliocene	~ 3.6-1.7 million years ago	Citronelle Formation (in uplands only)	Citronelle Formation	

Figure 2.5 Coastal Mississippi Stratigraphic Column

Coastal Mississippi stratigraphic column of Late Tertiary and Quaternary systems – modified from Otvos (2001) and Dockery (1996).

2.1.3.1.2 Sangamon

Stratigraphically, the Sangamon Interglacial (OIS 5e) has been delineated by three formations and valley terraces: Biloxi Formation, Prairie Formation, and Gulfport Formation (Matson, 1916) (Figure 2.5). These formations are slowly subsiding in the study area (Otvos, 2001). They were deposited when rivers of the NGOM had broad alluvial plains that were more extensive than their modern meander belts, supplying more sediment (Anderson et al., 2004).

The Biloxi Formation (Figure 2.4 and Figure 2.5) is a highstand formation overlying Miocene or Pliocene deposits (Otvos, 1982; Otvos, 2001). It was formed during OIS 5e which crested at about six meters above modern sea level (Otvos, 1982; Otvos, 2001). This formation, deposited in marine, brackish, and estuarine conditions like the modern Mississippi Sound (Johnson, 1891; Otvos, 1991; Gohn et al., 2001), underlies or interfingers with the Prairie Formation, Gulfport Formation, and Holocene floodplain deposits (Otvos, 1982; Otvos, 2001). The Biloxi Formation consists of fossiliferous deposits, typically ~15-3 m thick, containing yellowish brown, blue, medium bluish-gray, light gray, medium greenish-gray, and dark greenish-gray muddy or clayey fine sands (13-40 %) and sandy muds with some mud, silt (10-35%) and clay (13-45 %) (Otvos, 1982; Otvos, 1991; Johnson, 1891; Gohn et al., 2001). Gohn et al. (2001) suggested the Biloxi Formation was deposited between the offshore and foreshore zones at Belle Fontaine Point, about 55 km east of the study site.

The Prairie Formation is ~ 12–4.5 m thick and forms a coastal strip 8-11 km wide (Heinrich, 2006) cresting at about 7 meters above modern sea level. It formed a continuous sheet of both Mississippi River and Appalachian sourced material that was

fluvially incised in southern Mississippi (Otvos, 1982; Otvos, 2001). Initial deposition was coeval with Biloxi Formation deposits (OIS 5e). Subsequently fluvial downcutting and floodplain aggradation caused interfingering with the Biloxi Formation. Alluvial deposition of the Prairie Formation initiated before the Gulfport Formation sedimentation yet continued after completion of the Gulfport Formation's barriers (Otvos, 2001). Pearl River migration to the northwest of the modern Bay St. Louis area ravined these alluvial deposits at ~ 40 ka (Heinrich, 2006). The Prairie Formation (Figure 2.4 and Figure 2.5) is predominately muddy and clayey fine sands, moderately silty fine sands, and very fine sands, all alluvial deposits (Otvos, 1982; Otvos, 2001; Heinrich, 2006). Deeper sediments are yellowish-gray, greenish-gray, and gray; however, oxidized surficial sediment is very pale orange, pale yellowish-orange, and medium yellowish-orange and is often found in reddish-brown iron oxide concretions (Otvos, 1982). Dark yellowish-orange or moderate red colors can be found near the Citronelle Formation due to erosion (Otvos, 1982). The Prairie Formation is equivalent with the Beaumont Formation in Texas and the Pamlico Formations on the Atlantic Coast.

The Gulfport Formation (Figure 2.4 and Figure 2.5) is a discontinuous beach ridge formation of the northeastern Gulf formed during the OIS 5e highstand (+ 6 meters above modern sea level) that produced barrier segments currently 9.5–5 m thick (Otvos, 1972; Otvos, 1982; Otvos, 2001) that aggraded above the coeval marine and estuarine Biloxi Formation muds and sandy muds (Otvos, 2001). Subsequent alluvial deposition of the Prairie Formation buried a portion of the Gulfport Formation in the study area (Otvos, 2001). The sediments grade upward from low energy neritic deposits to eolian barrier sands, and the Gulfport Formation is dominated by medium and fine-grained white sand

that is well or well-to-moderately well-sorted, although surficial sands may be oxidized and light orange yellow (Otvos, 1982; Otvos, 2001). Humate from upland plants is found in this formation (Otvos, 1982). The average elevation of a segment of this formation near the study area, English Turn, is 3.7 m (MSL) (Simms, 2021). This barrier trend is found from mainland Texas to Florida (Otvos, 1982; Otvos, 2001). This formation is known as the Ingleside shoreline in Texas and the Pamlico shoreline in Alabama (Simms, 2021).

2.1.3.2 Mississippi Sound

Basinward, Bay St. Louis communicates with the Mississippi Sound, and is partially enclosed by six barrier islands and remnants of the St. Bernard complex of the Mississippi River (Otvos, 1982) (Figure 2.4). During the onset of the Holocene, the low gradient antecedent topography of the Mississippi Sound was between 11 and 10 mbsl, and it was inundated between 8.12-7.84 ka (Rodriguez et al., 2008; Kulp et al., 2002). The sound slopes from ~ 3 to 5 m (depth) basinward and has a Holocene sequence that thickens from ~ 7 to 13 m (Otvos, 1982). Lake Borgne, having salinity influenced by the coastal streams of the Pontchartrain Basin, communicates with the sound to the west, while Mobile Bay, fed by the freshwater rivers Tensaw and Mobile, communicates with the sound to the east. The sound receives freshwater inputs from the Pearl and Pascagoula Rivers; however, smaller tributaries such as the Jourdan, Wolf, and Tchoutacabouffa Rivers (Biloxi Bay) are partly responsible for salinity ranges of 3–24 ppt (January) and 27–35 ppt (July) in the partially and well-mixed microtidal estuary (Otvos, 1982). The Mississippi Sound is frequently impacted by major hurricanes with storm surges up to ~ 8 m (Otvos, 1982; Knabb et al., 2005; Gremillion et al., 2020; Eisemann et al., 2018).

Oyster (*Crassostrea virginica*) reefs, forming from ~ 0-3 mbsl, are common in the sound (Otvos, 1982), although they are rapidly disappearing. Mississippi coastal marshes were reduced from ~ 294 km² to ~ 272 km² from 1956 to 1978 by land filling and erosion (Meyer-Arendt & Gazzier, 1990), and despite the Wetland Protections Law of 1973 being enacted, mainland coastal marshes continued to erode, having been reduced to ~ 237 km² in 1992 (Meyer-Arendt et al., 1998). From 1947 to 2007, the state lost over 40 km² of coastal wetlands (Mississippi Department of Environmental Quality, 2016). Marsh grasses found throughout the estuaries and barrier islands include *Spartina alterniflora* (smooth cordgrass), *Spartina patens* (salt meadow cordgrass), *Juncus roemarianus* (black rush), *Distichlis spicata* (seashore salt grass), and *Schoenoplectus americanus* (Olney's three-square bulrush) (Eleuterius & Caldwell, 1985). Mississippi Sound shorelines are currently eroding at an average of 2.1 m/yr (Morton et al., 2004).

2.1.3.3 Bay St. Louis

Bay St. Louis is an estuary located on the Mississippi coast and is fed by two blackwater rivers, the Jourdan, and the Wolf (Figure 2.6). Blackwater rivers are defined as slow-moving rivers traversing Southern forested swamps and wetlands allowing decaying vegetation to leech tannins, acidifying, and staining the water. The upper bay consists of bayhead deltas and the river mouths. The lower bay consists of a narrow throat and an expanding mouth. These two rivers travel through and incise the Pliocene Citronelle Formation before entering the bay which is mostly surrounded by the Sangamon Prairie formation (Otvos, 1982) (Figure 2.7). However, little is known about the Holocene history of Bay St. Louis. The bayhead deltas of both rivers had been heavily modified in the 1950s and 1960s as canals were dug for residential neighborhoods (Meyer-Arendt, 1995) causing a loss of $\sim 1.5 \text{ km}^2$ of wetlands (Meyer-Arendt et al., 1998). Comparison of historical charts dating back to 1852 of the modern bay line shows a general trend of bayhead delta erosion, although delineation of the landward delta edge has been too recent to provide transgression data. The Jourdan River watershed is 378 km^2 , whereas the Wolf River watershed is 421 km^2 (Wilson et al., 2009). The bay mouth is in the Sangamon Biloxi Formation, which underlies Prairie and Gulfport formations (Otvos, 1982) (Figure 2.7). The average depth of the bay is 1.5 m, and the average salinity is less than 20 ppt. The semi-enclosed bay, $\sim 30 \text{ km}^2$ in area, has highly brackish, muddy-sandy deposits (Otvos, 1982). The RSL trend is 4.68 mm/yr based on data from 1978 to 2021 at tide station Bay Waveland (8747437) (NOAA, 2021).



Figure 2.6 *Bay St. Louis*

Bay St. Louis with the mouths of the Jourdan River and the Wolf River and modern bayhead delta. The bay communicates with the Mississippi Sound.

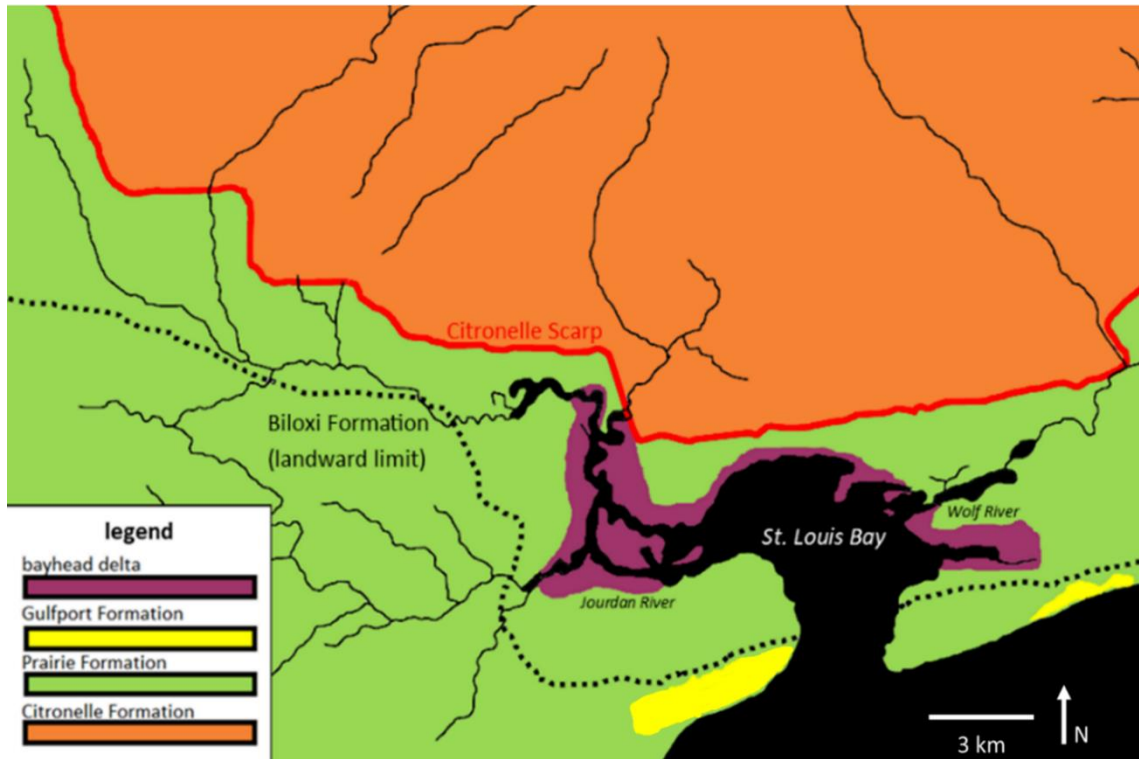


Figure 2.7 *Geology of Bay St. Louis Environments*

Geology of Bay St. Louis environments showing areas of Pliocene deposition (Citronelle Formation), Sangamon deposits (Biloxi Formation overlaid by Prairie and Gulfport Formations), and modern bayhead delta - adapted from Otvos (1982) and Simms (2021).

2.2 Hypotheses

(H1) The morphology of the modern bay was constrained by the location of OIS 5e deposits (the Biloxi and Prairie Formations). The bay mouth was channelized between the Gulfport Formation on either side. This hypothesis will be assessed by creating a sequence boundary surface from interpreted paleo channels and paleo valleys from HST to LST to determine if OIS 5e deposits had more morphological influence than earlier incision (OIS 6 or earlier).

(H2) A single bayhead delta formed before the embayment of Bay St. Louis was drowned during the Holocene, where it subsequently backstepped to form the two modern deltas observed today by the mouths of the Jourdan River and the Wolf River. This hypothesis will be assessed by examining geophysics, sediment cores, and radiocarbon ages within Bay St. Louis to determine if there are remnant Holocene delta deposits.

2.3 Methods

To reconstruct Bay St. Louis's geologic history, seismic and core data were interpreted to construct facies interpretations in a sequence stratigraphic framework from OIS 6 to present.

2.3.1 Data

2.3.1.1 Core Data

Geotechnical borings were collected by Mississippi Department of Transportation (MDOT) in 2006 to inform engineering and design of a highway bridge across Bay St. Louis following its collapse during Hurricane Katrina. Fourteen borings were used for this study that ranged in sub seafloor penetration of over 30 m to ~ 10 m deep.

Geotechnical descriptions were provided to MDOT by Burns, Cooley, Dennis, Inc., (2009) (Figure 2.8). Sediment characteristics and lithological interpretations from these borings were digitized and integrated with seismic data in SonarWiz, changing the descriptor “clay” to “mud” (Figure 2.9). USM also extracted three piston cores from three different intersections of seismic survey lines in the central basin where major changes were observed in the subsurface stratigraphy. Radiocarbon dating using accelerator mass spectrometry (AMS) of plant and wood material was performed by the Woods Hole Oceanographic Institution, and dates were calibrated using IntCal20 (Reimer et al., 2020) in the CALIB 8.2 software (Stuiver et al., 2022).

2.3.1.2 Geophysical Data

Both legacy and newly acquired boomer data were coupled with core data for interpretations. These data were imported into SonarWiz. To convert two-way travel times to depth, sound velocities of 1500 m/s in water and 1600 m/s in sediment were used. Legacy data were provided by U.S. Geological Survey (USGS) of which ~ 29 km of line-kilometers were used. These data were collected aboard Research Vessel (R/V) *E. Coli* using a boomer seismic system (Bosse et al., 2018) (Figure 2.10). They were filtered from 700 Hz to 5000 Hz. These data were post processed in SonarWiz with bottom tracking and water column blanking. About 42 km of data collected by USM using an Applied Acoustic Engineering CSP 1000 (1.5 kHz) were also used. These data were post processed in SonarWiz with a band pass filter to filter out noise, automatic gain control (AGC) to amplify signals weakened by attenuation, stacking to enhance reflectors, bottom tracking to allow water column blanking, and water column blanking to make images for presentation. The Hamming band pass filter had a low-cut frequency of 250

Hz, a high-cut frequency of 2500 Hz, and 50 taps. AGC had a window size of 30 % of maximum samples and an intensity of 25 % of maximum. Stacking utilized the average value of 2 shots.

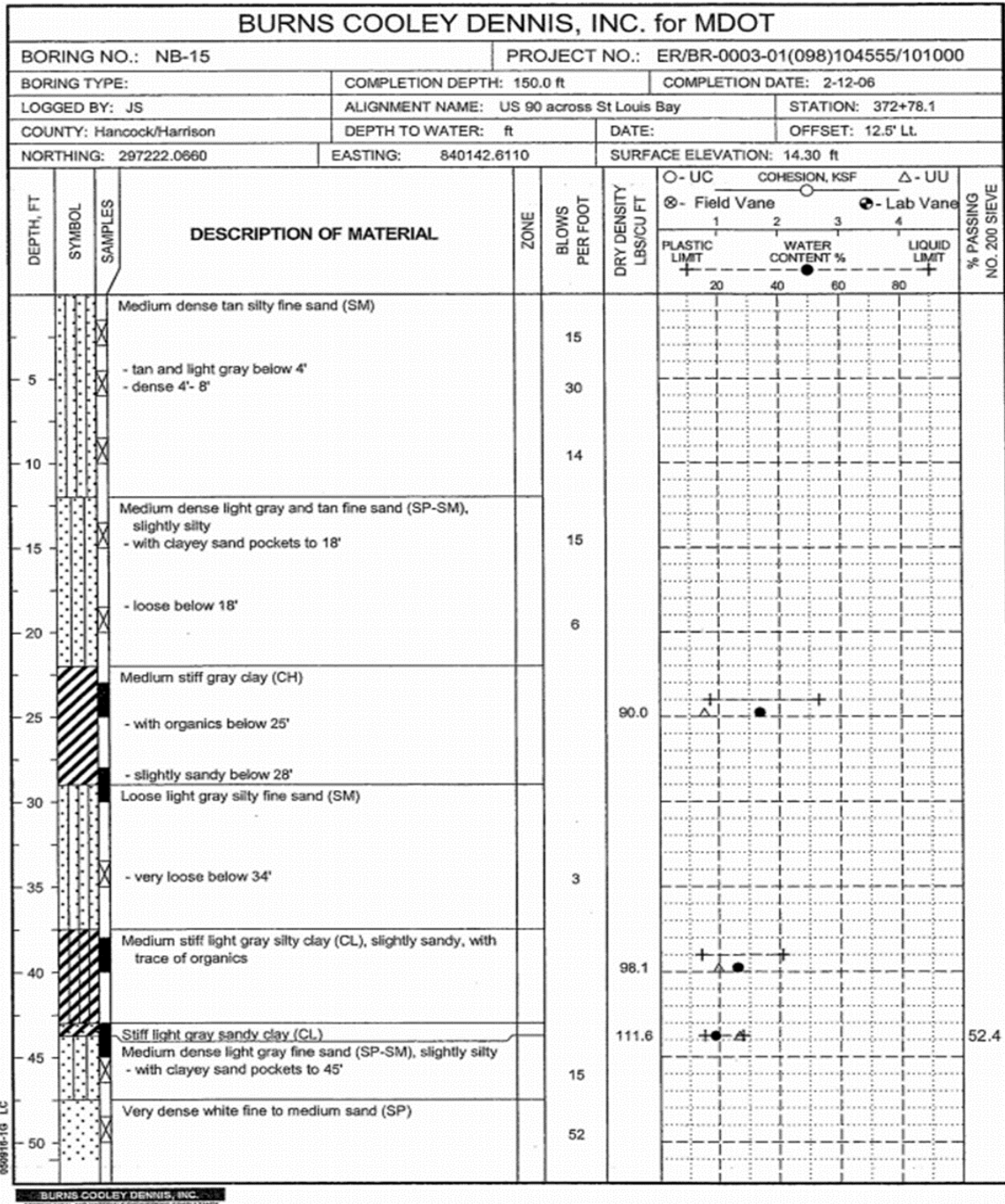


Figure 2.8 MDOT Geotechnical Report

Example of MDOT engineering boring description by (Burns, Cooley, Dennis, Inc., 2009) for preparation of building a US 90 bridge across Bay St. Louis; descriptions were used to digitize cores with seismic data in SonarWiz (the descriptor “clay” was changed to “mud”).

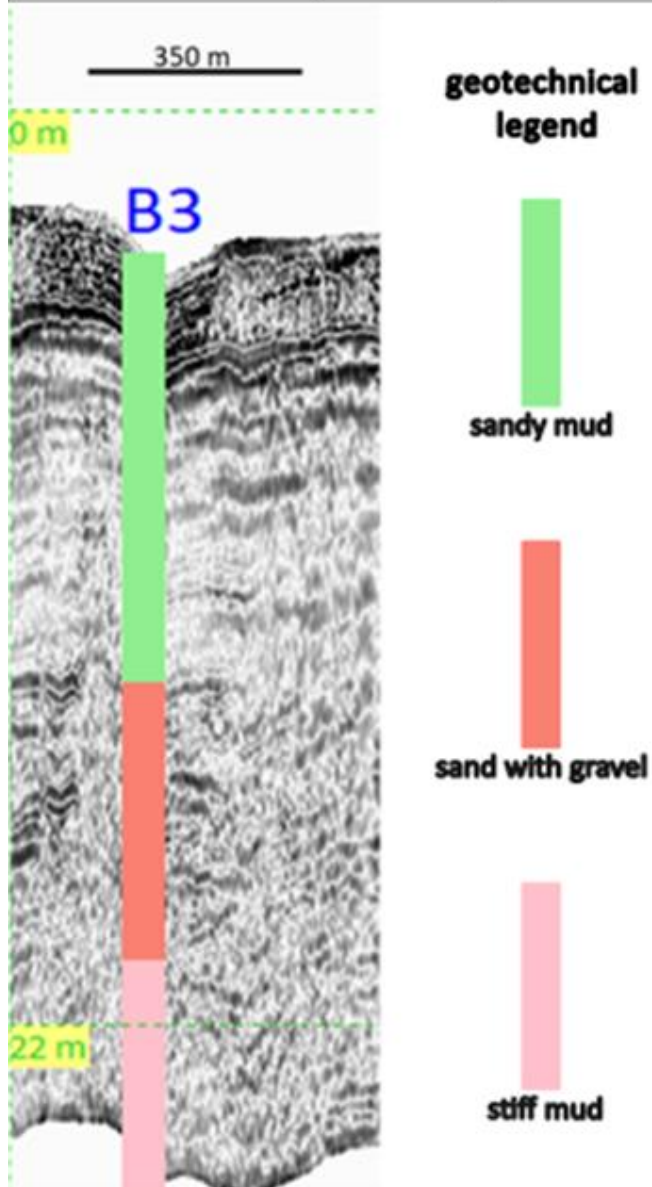
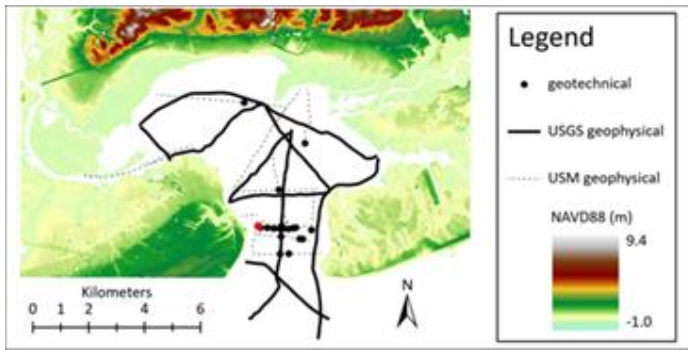


Figure 2.9 *Geotechnical and Geophysical Integration*

Example of an MDOT core (B3 - red dot) digitized into seismic data (USM) using SonarWiz.

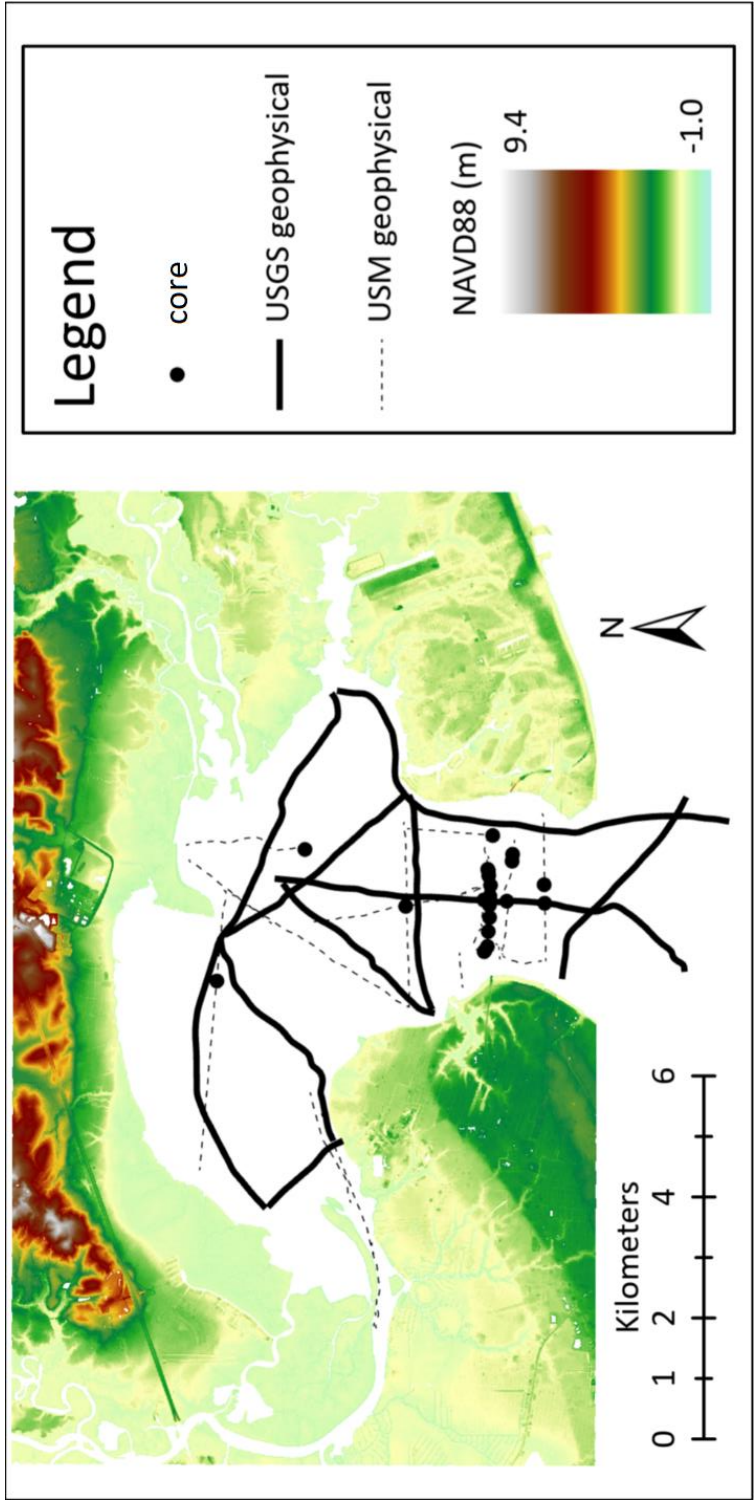


Figure 2.10 *Data Location*

Locations of core and geophysical data used in this study - DEM is from LiDAR collected in 2015 (from U.S. Geological Survey, 2018 accessed through the Open Topography Facility).

2.3.1.3 Stratigraphic Bounding Surface Interpretation

Core data aided in the interpretation of seismic reflectors. All reflectors were snapped to a bathymetric grid. As the sea-level curve has been well studied over the period of this study, reflectors were associated with an OIS date using fundamentals of sequence stratigraphy (Vail & Mitchum, 1977; Posamentier & Vail, 1988). The gridded reflectors were:

- 1) OIS 7 (Pre-Sangamon Unit)
- 2) OIS 6 and OIS 5 (valley and/or channel incisions)
- 3) OIS 5e (Sangamon Unit)
- 4) undifferentiated Pleistocene subaerial surface
- 5) OIS 2 and OIS 1 (valley and/or channel incisions)
- 6) OIS 1 (bayhead delta, bay ravinement surface, and bay sedimentation).

Reflectors were converted to XYZ files and were gridded using the Kriging Gridding Method in Surfer® to produce surfaces with horizontal components in World Geodetic System 1984 (not projected) and the Z component in mbsl.

2.4 Results

2.4.1 OIS 6

During OIS 6, incised valleys down cut basinward due to the ~ 130 mbsl eustatic sea level. The fluvial extensions of OIS 6 were interpreted from downward sloping reflectors along the valley and channel walls with planar or sloping parallel reflectors within the incisions. The deepest excavation found was forty-four mbsl in the valley bend in the lower bay. The shallowest OIS 6 reflectors are valley shoulders about four mbsl in the upper bay (Figure 2.16). Sediment coinciding with these OIS 6 reflectors from

penetrating geotechnical data included stiff mud and dense sand (Figure 2.12), and sand, sand with gravel, and oxidized sediment (Figure 2.14). Chaotic and transparent reflectors underlie dipping oblique reflectors, and the geometries are indicative of channel fill (Goff, 2014; Thomas & Anderson, 1994; Hollis et al., 2019). These latter geophysical reflectors coincide with dense sand as described in MDOT borings (Figure 2.12). Strong impedance contrasts in seismic reflectors coincide with truncations bounding the top of the OIS 6 valley. These truncations are interpreted as having occurred during OIS 5 (Figure 2.11 and Figure 2.15) or OIS 2 (Figure 2.12 and Figure 2.14), as discussed below.

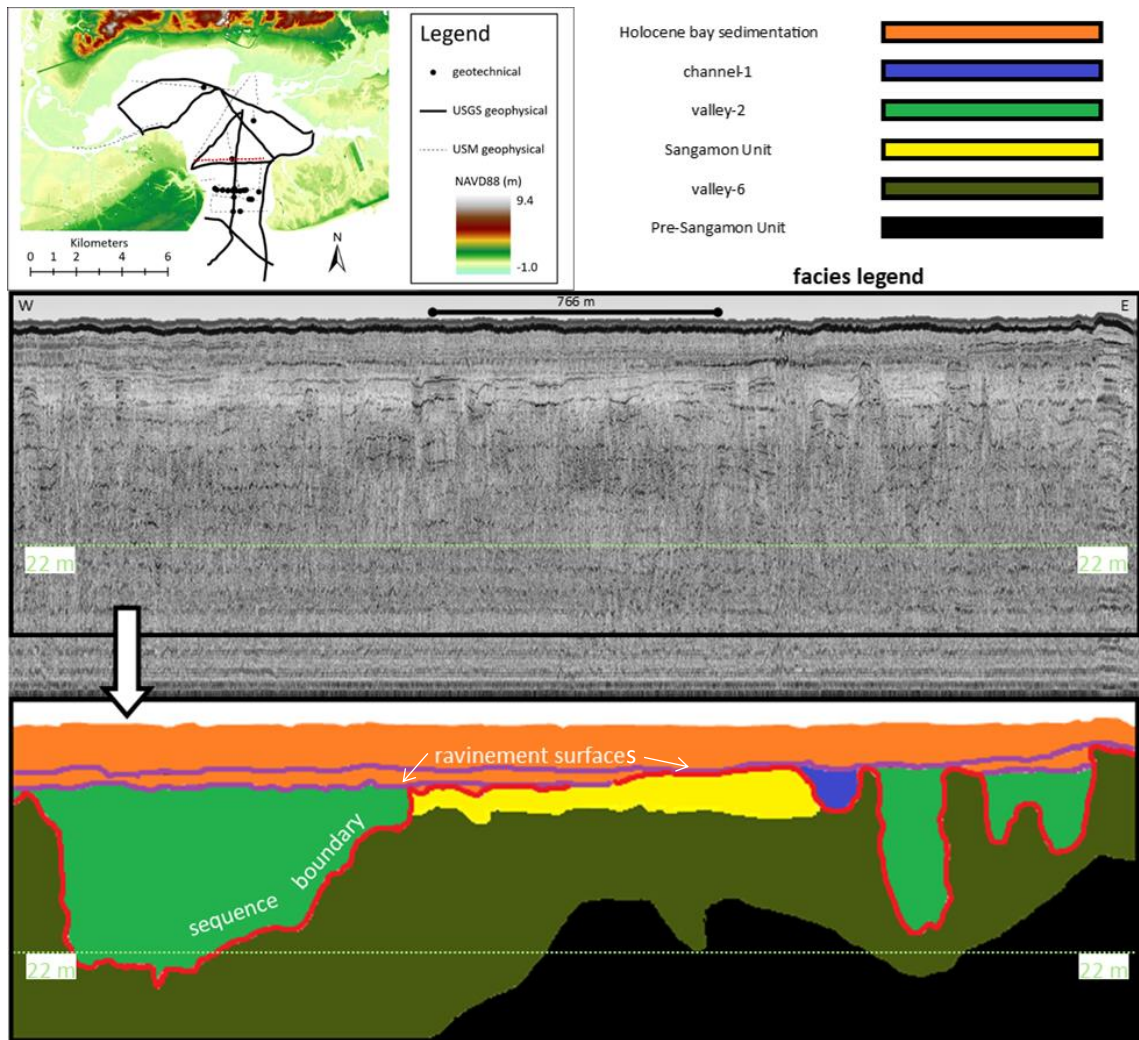


Figure 2.11 *USM Seismic Line Striking the Top of the Lower Bay*

USM geophysical line striking across the top of the lower bay (red dashed line in map inset) with geophysical interpretations at bottom demonstrating revisitation of an OIS 6 valley by OIS 2 and OIS 1 excavations, with some Sangamon deposits intact. Note two ravinement surfaces are interpreted.

2.4.2 Undifferentiated Pleistocene

The undifferentiated Pleistocene surface is a time transgressive surface consisting of heavily oxidized Pleistocene sediment that was found to range in depth from ~ 7 to 0 mbsl. The surface was interpreted as the top of high amplitude reflectors overlain by either valley fill (Figure 2.14), or wavy parallel reflectors of low amplitude (Figure 2.15), as found in Mobile Bay (Rodriguez et al., 2008). This reflector coincided with oxidized, orange, mottled, dewatered clay layers in cores (Figure 2.14), like those described by McBride et al. (1991).

2.4.3 OIS 2

During OIS 2, incised valleys down cut basinward due to the ~ 120 mbsl eustatic sea level. The fluvial extensions of OIS 2 were interpreted from downward sloping reflectors along the valley and channel walls with planar or sloping parallel reflectors that truncate OIS 6 (Figure 2.11, Figure 2.12, and Figure 2.14), Sangamon (OIS 5e) (Figure 2.13), and/or undifferentiated Pleistocene reflectors. OIS 2 reflectors were subsequently truncated by OIS 1 channels in some instances (Figure 2.12). The OIS 2 surface ranged in depth from ~ 30 to 0 mbsl. Due to the fact OIS 2 reflectors coincided with a subaerial surface identified in cores, we consider this a sequence boundary. The sequence boundary is the surface upon which subsequent Holocene deposition occurred.

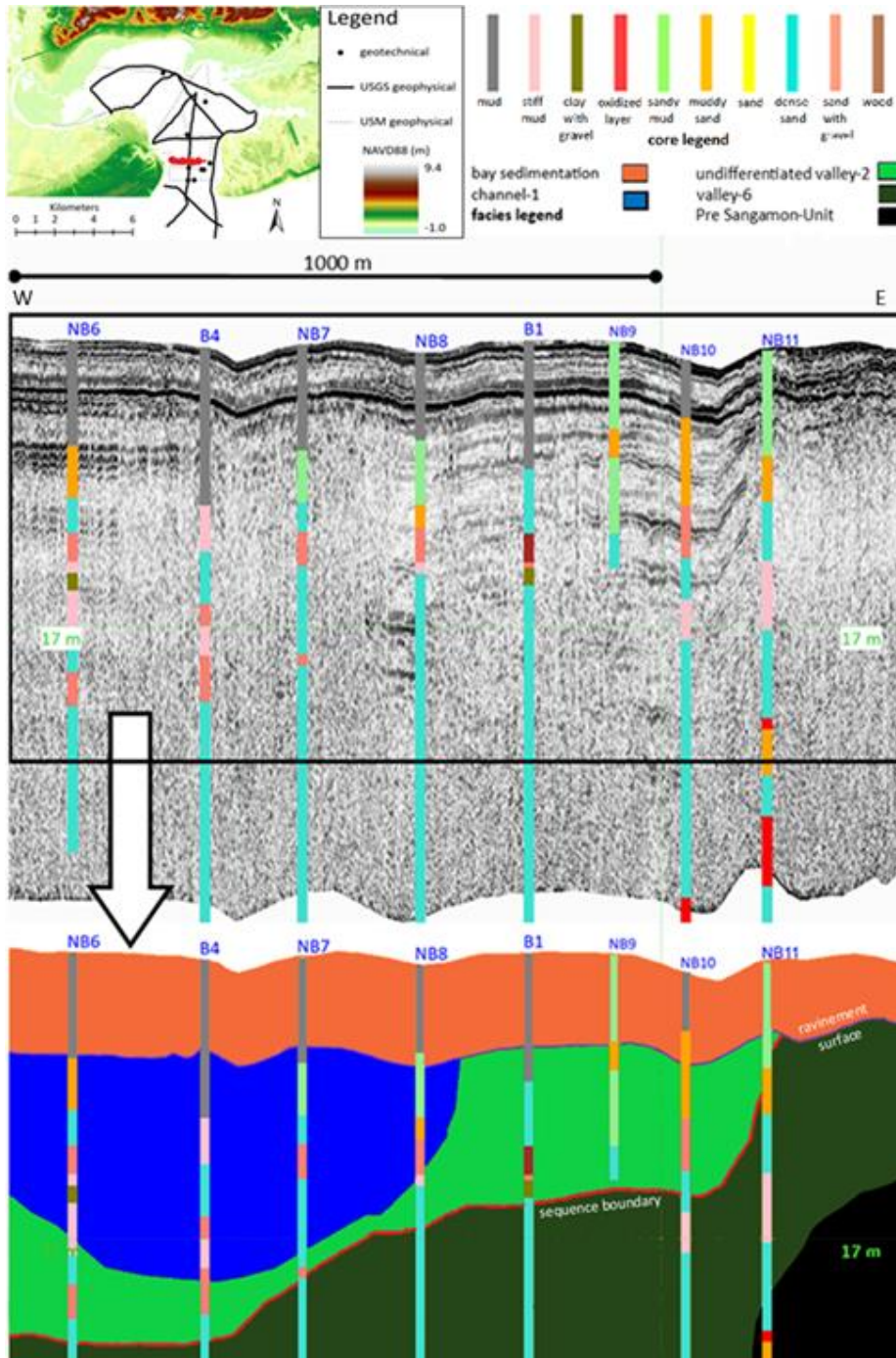


Figure 2.12 *USM Seismic Line Striking the Lower Bay with MDOT Cores*

USM geophysical strike line (red dashed line in map inset) and MDOT geotechnical data (red circles in map inset) from the lower bay with interpretation of Pre-Sangamon Unit, OIS 6 valley, revisitation of an OIS 2 valley with OIS 1 channelization, and Holocene Bay sedimentation (color keys for geotechnical lithography and geophysical interpretations shown in core and facies legends).

2.4.4 Holocene Bayhead Delta

An OIS 1 delta, above the OIS 2 reflector (sequence boundary), was interpreted from wavy parallel reflectors often interrupted by low amplitude planar parallel reflectors (Figure 2.13-Figure 2.15). The deltaic reflectors correlated with gray sandy mud, organics, and wood layers (Figure 2.13) in the cores like those facies described by (Siringan & Anderson, 1993). These deltaic reflectors were truncated by a ravinement surface (Figure 2.13 and Figure 2.14). The delta remnants were found from ~ 10 to ~ 2 mbsl. Three plant or wood samples from this buried delta in the modern bay throat were dated from piston core SLB3 (Table 2.1 and Figure 2.13). The deepest radiocarbon-dated sample (8.61 mbsl) has a median probability age of 6,886 yr B.P. At 8.46 mbsl a sample has a median probability of 32,081 yr B.P. and is reworked material, whereas the upper most sample (8.07 mbsl) has a median probability of 6,291 yr B.P.

Table 2.1

Samples Processed at the National Ocean Sciences AMS Laboratory at the Woods Hole Oceanographic Institution and Calibrated Using IntCal20 (Reimer et al., 2020)

Lab code	Sample name Depth (mbsl)	Material	Conventional ¹⁴ C age (yr B.P., 1σ)	Calibrated ¹⁴ C age (yr B.P., 2σ)	Median probability (yr B.P.)
OS-160710	SLB3 (8.61)	Plant or wood	6,040 ± 45	7,147-6,748	6,886
OS-160711	SLB3 (8.07)	Plant or wood	5,490 ± 35	6,392-6,204	6,291
OS-160712	SLB3 (8.46) *	Plant or wood	27,900 ± 590	33,650-31,040	32,081

Note: *rejected due to reworking

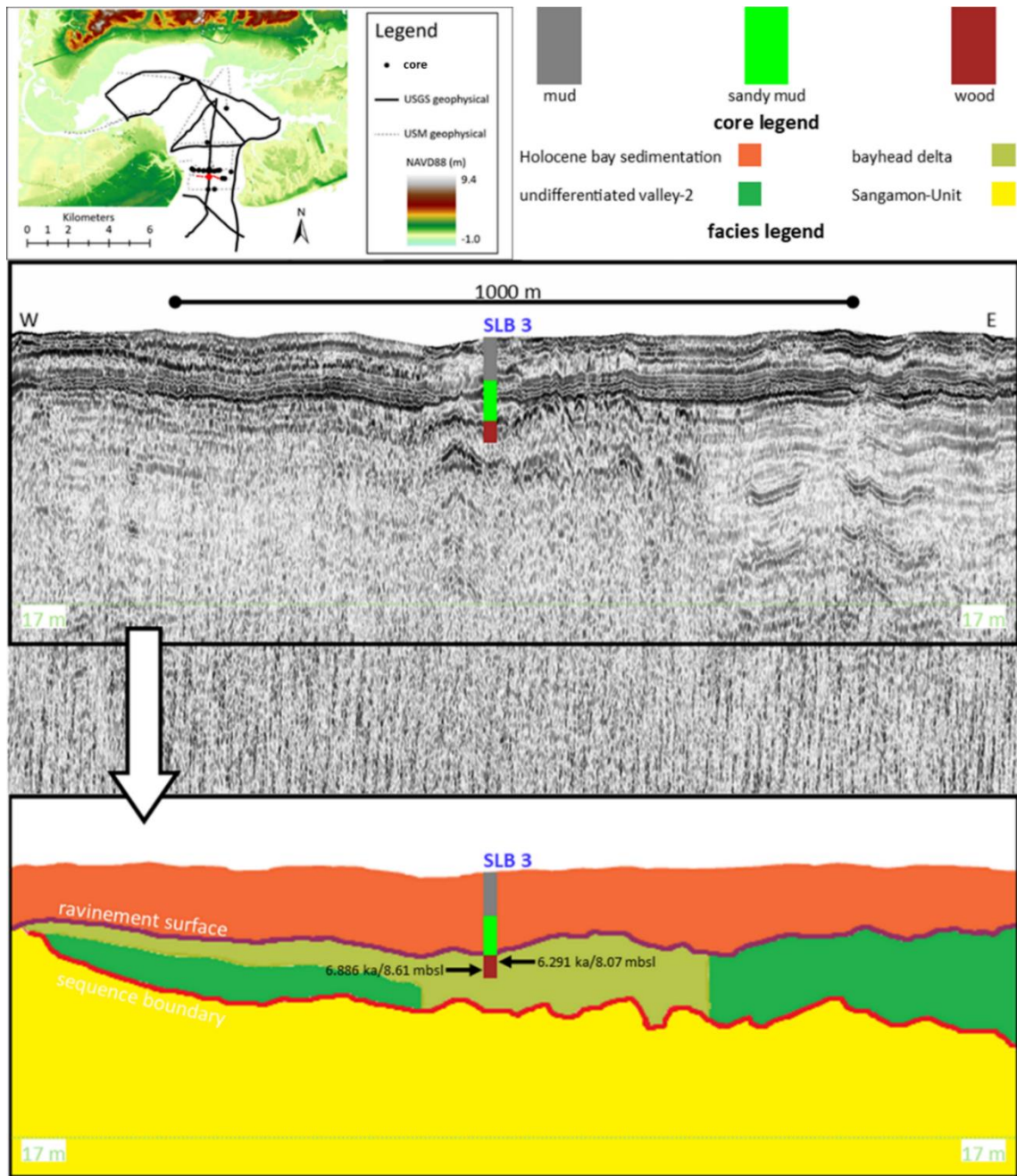


Figure 2.13 *USM Seismic Line Striking the Lower Bay with USM Core*

USM seismic line (red dashed line in map inset) with USM piston core SLB3 (red dot in map inset) showing Sangamon deposits underneath a drowned delta (with dates of plant or wood samples) fringing an OIS 2 valley (color keys for geotechnical lithography and geophysical interpretations shown in core and facies legends).

2.4.5 Ravinement Surfaces

A transgressive ravinement surface (unconformity) is a Holocene erosive flooding surface (Rodriguez et al., 2008) and was found in the lower bay beneath low amplitude reflectors interpreted as modern bay sedimentation. This disconformable surface was found above OIS 6 (Figure 2.11), OIS 2 (Figure 2.11-Figure 2.14), Holocene bayhead delta (Figure 2.13 and Figure 2.14), and OIS 1 (Figure 2.12) reflectors. In some cases, a separate shallower ravinement surface was found within Holocene Bay reflectors in seismic lines with higher resolution (Figure 2.11 and Figure 2.14).

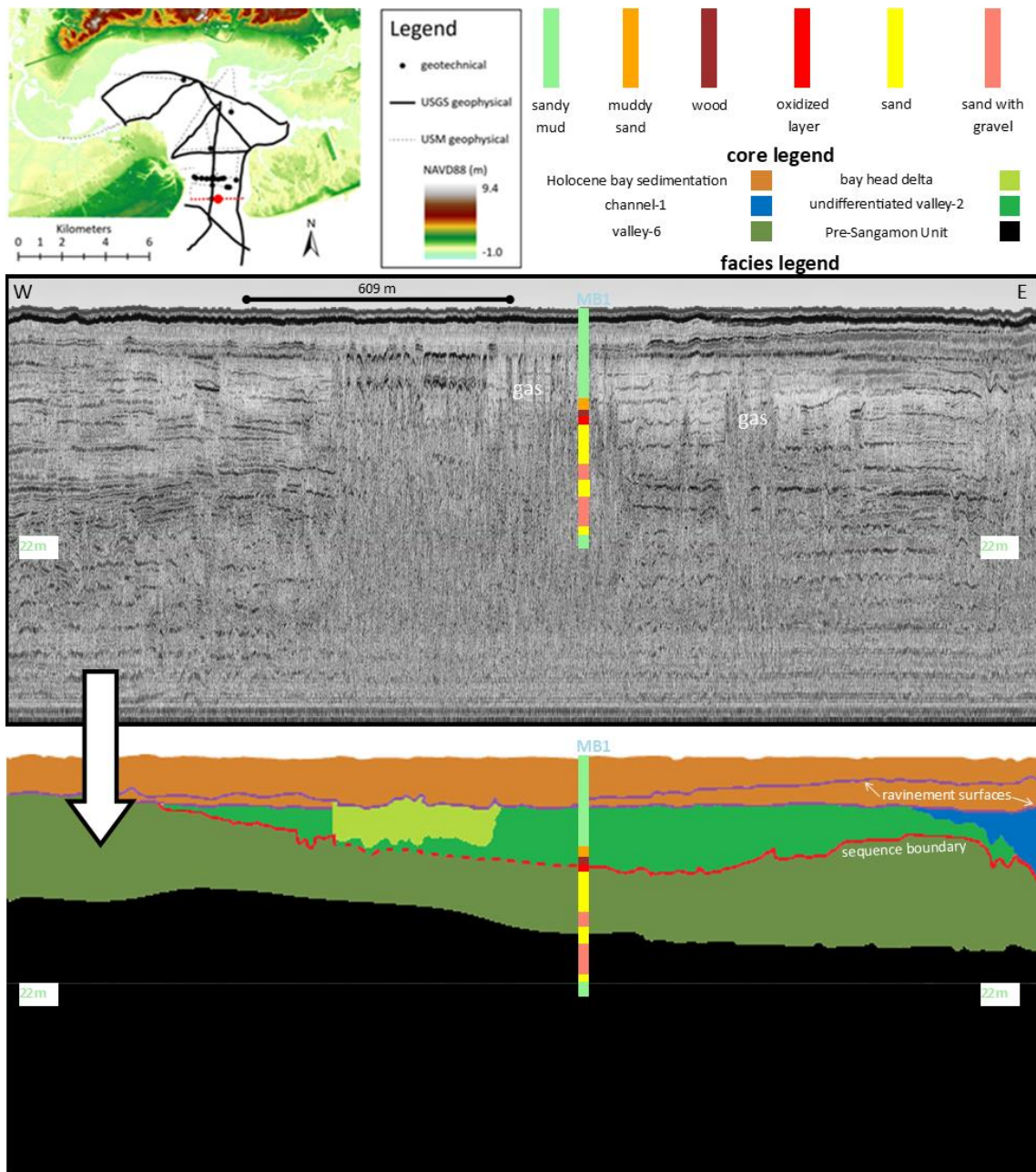


Figure 2.14 *USGS Seismic Striking the Lower Bay with Core*

USM seismic line (red dashed line on map inset) striking across the lower bay with core MB1 (red dot on map inset) showing a basement of Pre-Sangamon Unit underlying OIS 6 valley fill revisited by an OIS 2 valley fringed by bayhead delta which was topped by Holocene Bay sedimentation after ravinement (color keys for core lithography and geophysical interpretations shown in core and facies legends). Note two ravinement surfaces are interpreted.

2.4.6 Holocene Bay Sedimentation

Above the deeper ravinement surface, dark greenish-gray mud and sandy mud was found in geotechnical data and cores which correlated with even to wavy low amplitude planar parallel reflectors rising to the seafloor from ~ 2 to ~ 6 mbsl (Figure 2.12-Figure 2.14). These facies, like bay sedimentation in Galveston Bay described by (Siringan & Anderson, 1993), were interpreted as Holocene Bay sedimentation.

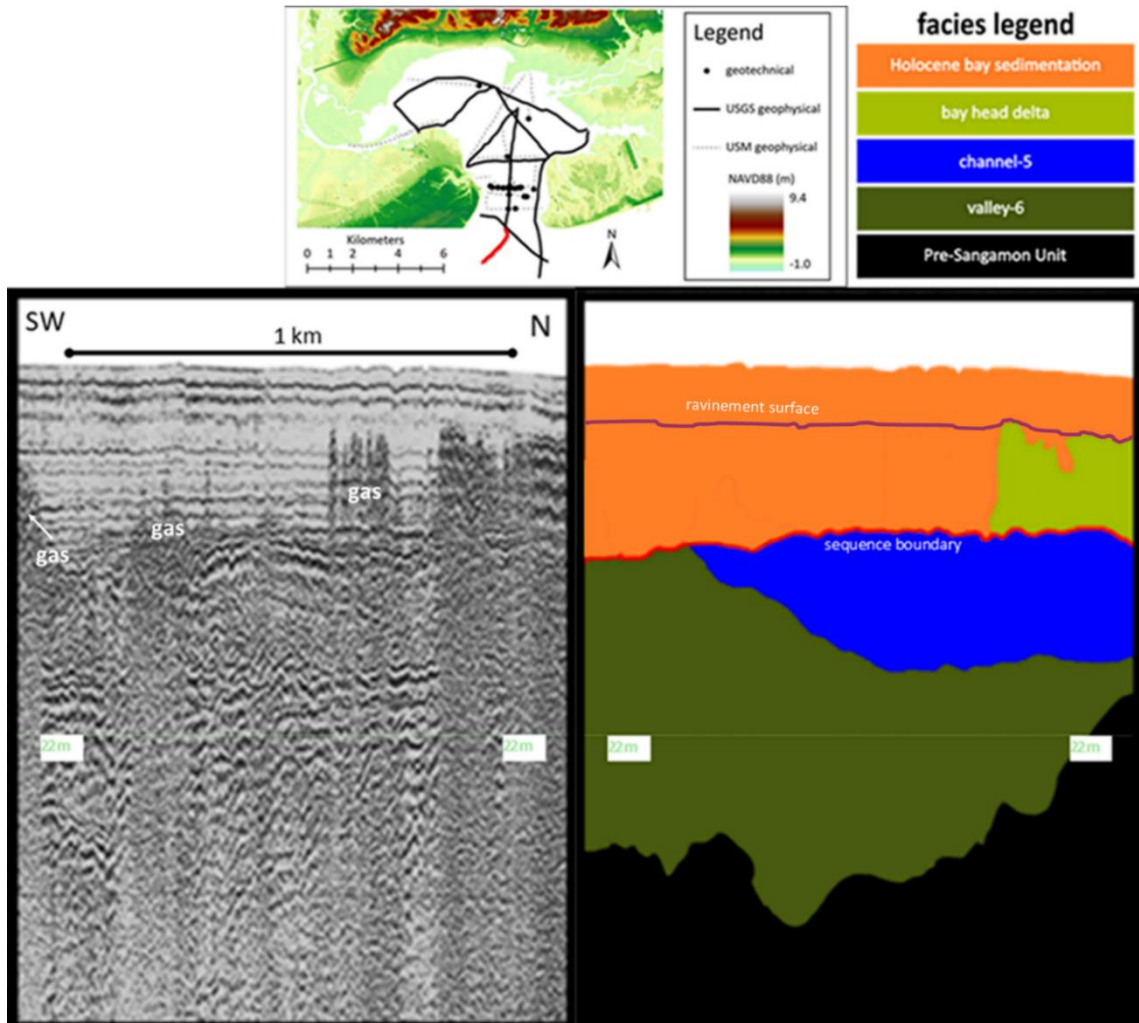


Figure 2.15 *USGS Seismic Line Dipping at the Bay Mouth*

USGS seismic line (red line on map inset) that dipped from the mouth of Bay St. Louis to the Mississippi Sound with the basement of Pre-Sangamon Unit, a paleo valley from OIS 6 underlying a paleo channel from OIS 5 capped by an oxidized surface providing the antecedent geology for bayhead delta deposition (color key for core interpretations shown in facies legend).

2.5 Discussion

2.5.1 OIS 6 and OIS 5

During late OIS 6 and early OIS 5, the ancestors of the Jourdan and Wolf River flowed to an area of confluence with less sinuosity than during OIS 2, indicating a steeper gradient during OIS 6, possibly due to a lower eustatic position described by Labeyrie et al. (1987) (Figure 2.1 and Figure 2.16). A pre-Sangamon high (~ 2 mbsl) presents itself in the modern upper middle bay (Figure 2.16). Valley depths of OIS 6, ranging from ~ 44-22 mbsl, were about 15 m deeper than those of OIS 2 (Figure 2.16 and Figure 2.17). At the modern bay mouth, the OIS 6 valley spans ~ 4 km, consisting of both river ancestors at this point. Upon reaching the area of the modern eastern side of the bay mouth, the OIS 6 valley took an abrupt bend to the east, incising to 44 mbsl (Figure 2.16).

2.5.2 OIS 2

The OIS 2 incisions reoccupied the OIS 6 valleys to a considerable extent (Figure 2.16 and Figure 2.17). Valley reoccupation of smaller rivers, such as the Lavaca and Nueces Rivers of the northwestern Gulf of Mexico, over eustatic cycles has caused deepening comparable to that of larger rivers that abandoned their valleys (Anderson et al., 2014). The ancestor of the Jourdan River was located near a modern bayou (Bayou Cut-Off) that cuts through the bayhead delta and connects the river with the bay (Figure 2.17). The Wolf River ancestor formed the eastern tributary and directly fed the area of confluence (Figure 2.17). The OIS 2 valley thalweg spanning ~ 1 km wide is located on the eastern side of the modern throat of the bay, where the Pleistocene surface was found at about 9 mbsl (Figure 2.17). The OIS 2 valley did not reoccupy the previous OIS 6 bend

to the east. The incision depth of the combined fluvial systems (799 km² modern watershed) of about 22 m at the mouth is 33 m shallower than the Trinity River (44,000 km² modern watershed) valley's excavation at the modern shoreline in Texas (Siringan & Anderson, 1993; Anderson et al., 2004).

2.5.3 OIS 1

During OIS 1, fluvial meandering occurred, resulting in three fluvial incisions in the upper bay: two in the north and one in the northeast. These incisions all converged upstream of an area of confluence located at the top of the lower bay (Figure 2.17). These incisions were probably created after 4 ka by channelization within the respective Jourdan and Wolf River valleys after the bay was created and elevated the base level of both fluvial systems. These OIS 1 channels are responsible for incising the Sangamon Prairie Formation forming the general outline of the modern upper (northern) bay.

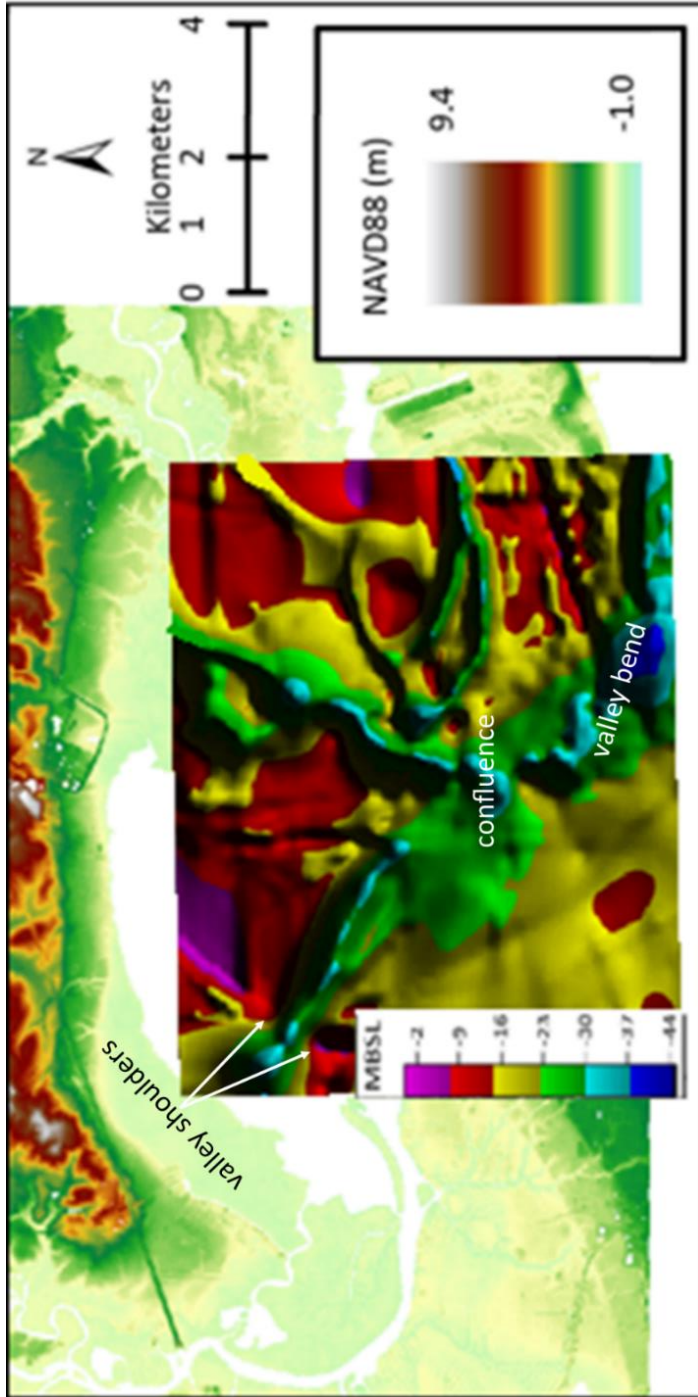


Figure 2.16 *OIS 6 and OIS 5 Fluvial Extensions*

OIS 6 and OIS 5 fluvial extensions of ancestral Jourdan and Wolf Rivers in relation to modern Bay St. Louis area, topography showing less fluvial sinuosity of discrete rivers than the modern-day rivers and wide outflow in relation to the width of the modern bay throat; valley shoulders are as shallow as 4 mbsl and the valley bend of the modern bay mouth is 44 mbsl at the deepest point. Modern topography is shown in the background.

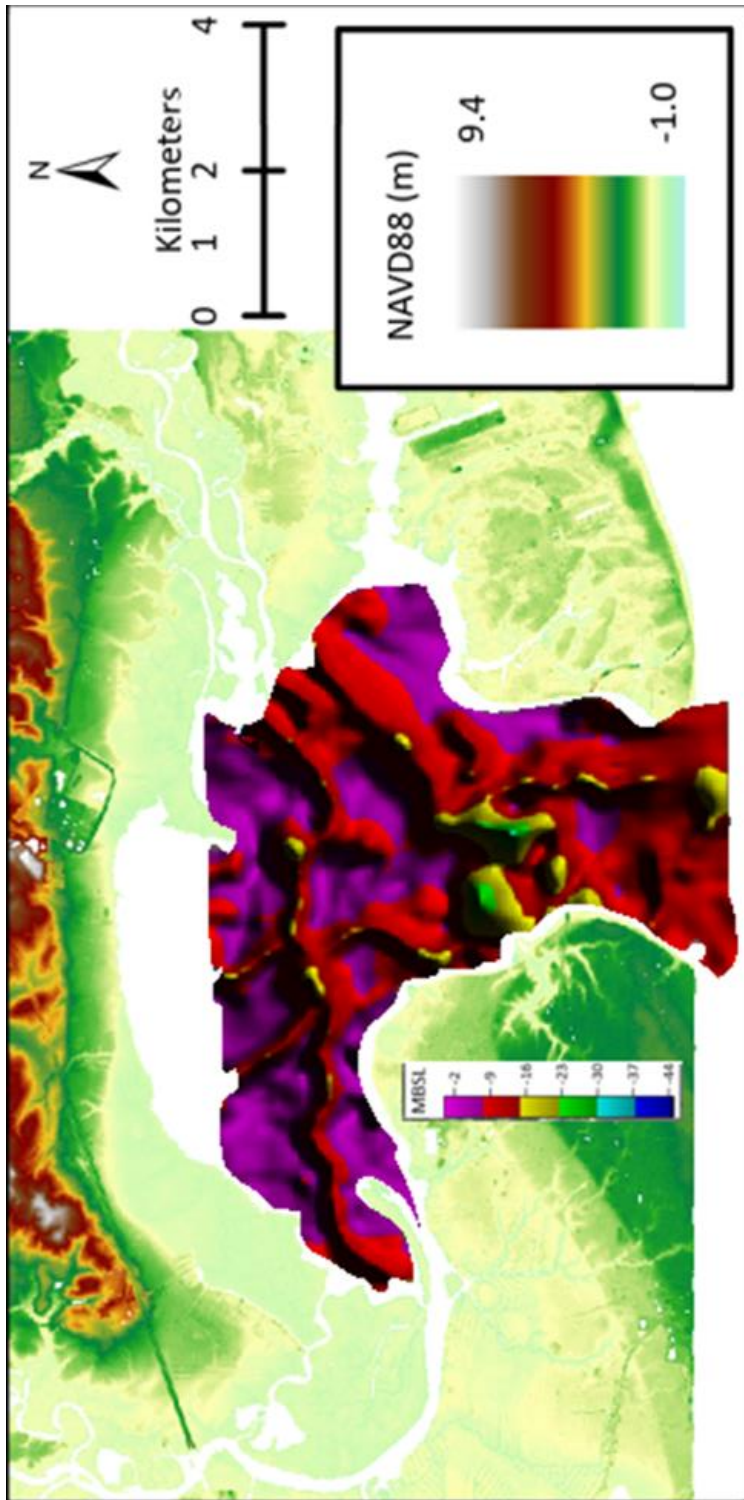


Figure 2.17 *Sequence Boundary*

Sequence boundary (OIS 2) underneath Bay St. Louis including Pleistocene subaerial surface and LST valleys and channels associated with the Jourdan and Wolf Rivers that merge at the top of the modern bay throat. Modern topography is shown in the background.

2.5.4 Bayhead Delta

The OIS 1 bayhead delta remnants are mostly within or adjacent to the OIS 2 valley in the lower bay (Figure 2.18). The presence of bayhead delta deposits southwest of the mapped OIS 2 valley suggests the valley trends to the west toward the modern bay shoreline (Figure 2.19). Due to transgressive and bay ravinement, much of this Holocene delta is not preserved. Given the basal depths of these remnants of ~ 10 to ~ 8 mbsl, they likely formed 8 to 7 ka, when the average sea-level rise rate was ~ 4.5 mm/yr (Milliken et al., 2008) (Figure 2.2). The delta tops were found at ~ 6 mbsl, and our radiocarbon data indicate they were ravined following the 7.4 to 6.8 ka flooding event that is likely also responsible for creating the upper bay. Given the dates and depths of the two Holocene samples, the sedimentation rate equated to about 1 mm/yr and could not keep pace with the 2 mm/yr sea-level rise rate at the time of deposition. The delta initially backstepped up the fluvial incisions only, until 4 ka when the sea-level rise rate decreased to 0.5 mm/yr. The downdip range of the Holocene bayhead delta was not determined due to lack of data; however, the minimum distance transgressed was 5 km, averaging 2.5 m/yr. Therefore, another kilometer of transgression to the Citronelle Scarp under similar sea-level rise without change in sedimentation rates would take ~ 400 yrs. The 7.4 to 6.8 ka flooding event also caused bayhead delta backstepping in Calcasieu and Sabine lakes, as well as Galveston and Matagorda Bays (Anderson et al., 2014). The remarkable coeval nature of these changes and responses to rapid sea-level rise rates points to the sensitivity of the NGOM system.

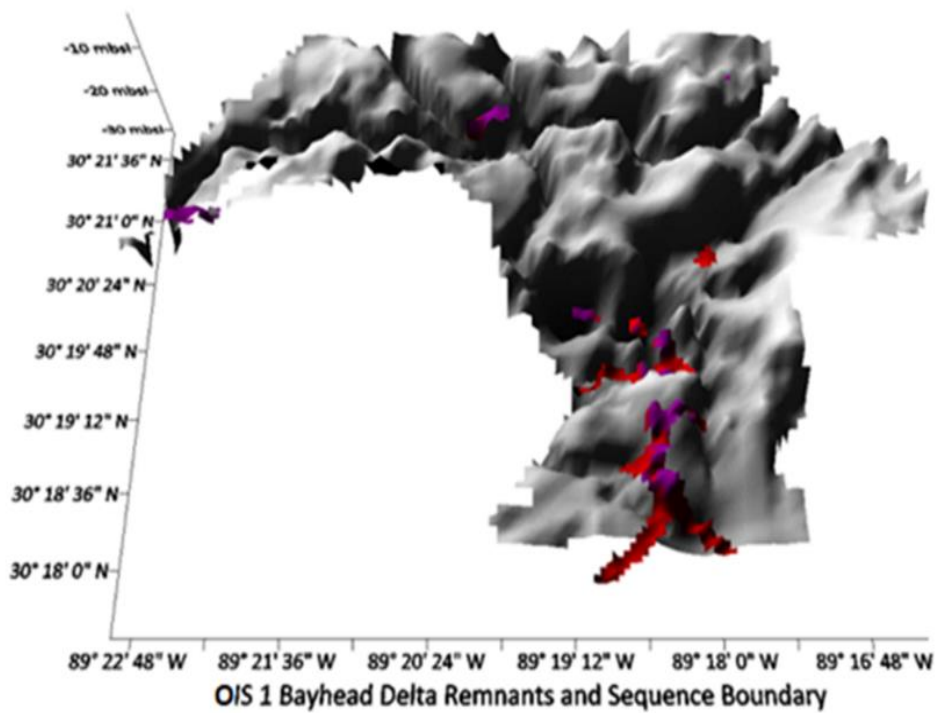


Figure 2.18 *OIS 1 Bayhead Delta Remnants and Sequence Boundary*

OIS 1 bayhead delta remnants fringing OIS 2 valley superimposed on sequence boundary; the remnant at the southwest of the bay mouth indicates a valley or channel existed that was not identified through geophysical interpretation due to lack of coverage (possibly an avulsion or bifurcation of the OIS 2 valley to the east).

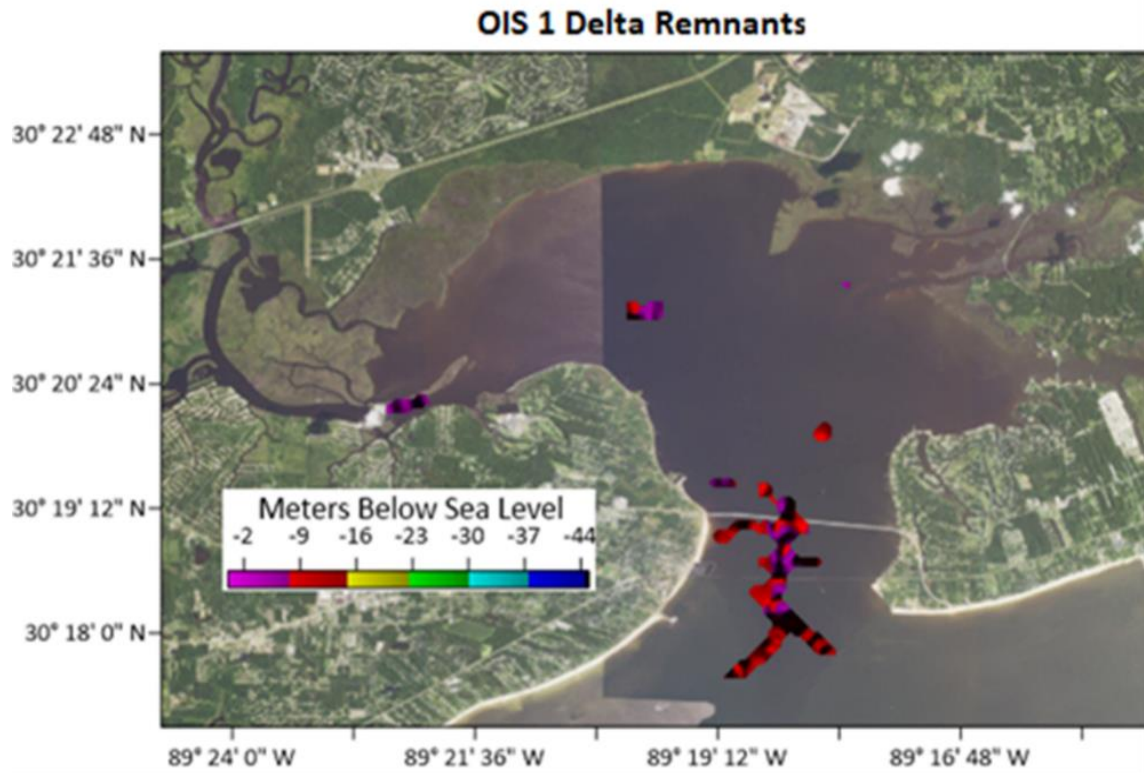


Figure 2.19 *OIS 1 Bayhead Delta Remnants and Bay St. Louis*

Remnants of OIS 1 bayhead delta with basal depths of ~ 10–8 mbsl superimposed on the modern bay; due to bay ravinement and incomplete geophysical coverage, much of the remnant delta is probably not depicted in this figure especially in the upper bay where bay ravinement may have been extensive due to the shallower bathymetry.

2.6 Conclusion

2.6.1 Morphology

The geologic evolution Bay of St. Louis, Mississippi, is profoundly influenced by antecedent geology. During OIS 6 time a wide deep valley was incised throughout the study area. Subsequently, during the OIS 5e highstand deposition occurred on valley shoulders and interfluves. Fluvial deposition and erosion shifted significantly basinward of the study between OIS 5e to OIS 3. During OIS 2, the study area experienced reoccupation of the OIS 6 valley. During OIS 1, the Jourdan and Wolf Rivers were avulsing during Holocene sea-level rise.

The width and the depth of the OIS 6 valley downstream of confluence exerted a first order control of the modern geomorphology of the lower bay. The upper bay, however, was initially shaped in OIS 2 by fluvial incision followed by OIS 1 paleo channel avulsions of the Jourdan River and Wolf Rivers. Hence, the mouth of the bay was shaped during the Illinoian glacial period, whereas the body of the bay was shaped during the Wisconsin glacial period (Figure 2.20).

2.6.2 Bayhead Delta Backstepping and Ravinement

The Holocene delta remnants preserved underlying the modern lower bay formed over the sequence boundary 8 to 10 mbsl sometime after the 8.4–8.0 ka flooding event but before the 7.4–6.8 ka flooding event, when the sea-level rise rate was 4.5 mm/yr. The delta tops were ravined by the 7.4–6.8 ka flooding event as rapid flooding occurred landwards. Following this transgression, a single bayhead delta downdip of the valley confluence separated into two deltas up dip, one fringing each river valley (Figure 2.20). These remnants quickly drowned and were protected from further erosion. Around 7.0

ka, sea-level rise then slowed to 2 mm/yr, allowing a slow retreat of the bayhead delta followed by bay ravinement. Bayhead delta backstepping/erosion in response to the 7.4 to 6.8 ka flooding event is consistent with other areas such as Calcasieu (LA) and Sabine (TX) lakes, as well as Galveston (TX) and Matagorda Bays (TX) (Anderson et al., 2014). This highlights the remarkably consistent response of Gulf of Mexico bayhead deltas to rapid Holocene sea-level rise rates. With future accelerated rise in sea level from the current rate of 4.68 mm/yr and with no increase in sedimentation, the bayhead delta of Bay St. Louis will likely migrate approximately a kilometer to the Citronelle Scarp in ~ 400 years.

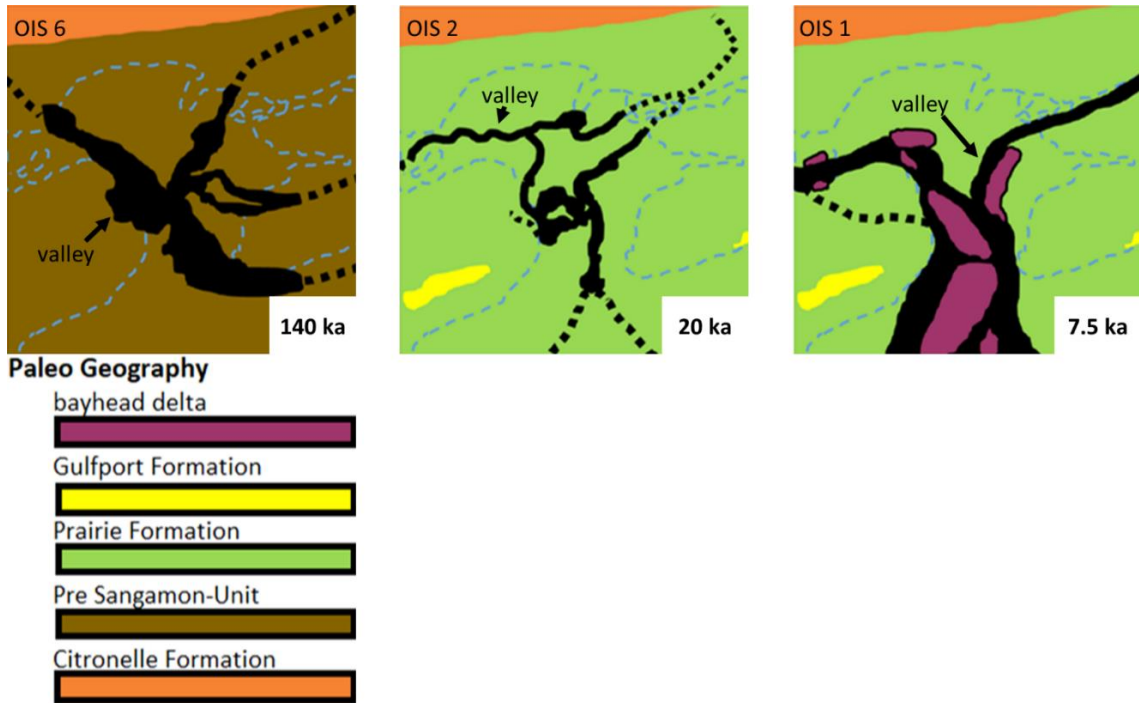


Figure 2.20 *Bay St. Louis Paleogeology*

(OIS 6) paleogeology of Bay St. Louis showing OIS 6 channels converging at the modern bay (blue dotted line) throat and making an abrupt stream course change to the east incising the Pre-Sangamon Unit, (OIS 2) channels with avulsion in the Prairie Formation at the location of the modern upper bay, suggesting low gradient topography, and confluence in the modern bay throat followed by valley extension either to the south southwest and/or to the south southeast, and (OIS 1) transgressing bayhead delta due to Holocene sea-level rise (note valley widening due to flooding in black).

2.7 References

- Adcock, D, 2019. Stratigraphic Characterization of the Pleistocene Paleodrainage Network in the Western Mississippi Sound. *Theses and Dissertations*. 4073.
<https://scholarsjunction.msstate.edu/td/4073>
- Anderson, J. B. et al., 2004. Late Quaternary Stratigraphic Evolution of the Northern Gulf of Mexico Margin: A Synthesis. In: *Late Quaternary Stratigraphic Evolution of the Northern Gulf of Mexico Margin*. Tulsa: SEPM, pp. 1-23.
- Anderson, J. B. et al., 2022. Holocene Evolution of the Western Louisiana-Texas Coast, USA: Response to Sea-Level Rise and Climate Change. *Geological Society of America Memoir 221*, pp. 1-81.
- Anderson, J. B. et al., 2014. Variable response of the coastal environments of the northwestern Gulf of Mexico to sea level rise and climate change: Implications for future change. *Marine Geology*, Volume 352, pp. 348-366.
- Bosse, S. T., Flocks, J. G. & Forde, A. S., 2018. Archive of digitized analog boomer seismic reflection data collected during USGS cruise USFHC in Mississippi Sound and Bay St. Louis, September 1989. St. Petersburg(Florida): USGS.
- Burns, Cooley, Dennis, Inc., 2009. Engineering Boring Reports.
- Catuneanu, O. et al., 2009. Towards the standardization of sequence stratigraphy. *Earth-Science Reviews*, 92(1), pp. 1-33.
- Climate Central, 2022. *Coastal Risk Screening Tool*. [Online]
Available at: <https://coastal.climatecentral.org/>
[Accessed 5 May 2022].

- Crider, A. F., 2015. *Geology and Mineral Resources of Mississippi*. [Online]
Available at: <https://pubs.usgs.gov/bul/0283/report.pdf>
[Accessed 25 4 2022].
- Dockery, D. T., 1996. Toward a Revision of the Generalized Stratigraphic Column of Mississippi. *Mississippi Geology*, March, 17(1), pp. 1-9.
- Eisemann, E. R., Wallace, D. J., Buijsman, M. C. & Pierce, T., 2018. Response of a Vulnerable Barrier Island to Multi-Year Storm Impacts: LiDAR-Data-Inferred Morphodynamic Changes on Ship Island, Mississippi, USA. *Geomorphology*, Volume 313, pp. 58-71.
- Eleuterius, L. N. & Caldwell, J. D., 1985. Soil Characteristics of *Spartina alterniflora*, *Spartina patens*, *Juncus roemerianus*, *Scirpus olneyi*, and *Distichlis spicata* Populations at One Locality in Mississippi. *Gulf Research Reports*, January, 8(1), pp. 27-33.
- Goff, J. A., 2014. Seismic and core investigation off Panama city, Florida, reveals sand ridge influence on formation of the shoreface ravinement. *Continental Shelf Research*, 1 October, Volume 88, pp. 34-46.
- Gohn, G. S. et al., 2001. B. Physical Stratigraphy, Calcareous Nannofossil Biostratigraphy, and Depositional History of the Quaternary Sediments in the USGS Belle Fontaine No. 1 Core, Jackson County, Mississippi. U.S. Geological Survey.
- Gonzalez, J. L. & Törnqvist, T. E., 2006. Coastal Louisiana in Crisis: Subsidence or Sea Level Rise?. *Eos*, 7 November, 87(45), pp. 493-508.

- Gremillion, S. L., Wallace, D. J., Wright, S. L. & Buijsman, M. C., 2020. Response and Recovery of Horn and Petit Bois Islands, Mississippi, USA to Tropical Cyclone Impacts: 2004 - 2016. *Geomorphology*, Volume 360.
- Heinrich, P. V., 2006. Pleistocene and Holocene Fluvial Systems of the Lower Pearl River, Mississippi and Louisiana, USA. *Gulf Coast Association of Geological Societies Transactions*, Volume 56, pp. 267-278.
- Hollis, R. J. et al., 2019. Late Quaternary evolution and stratigraphic framework influence on coastal systems along the north-central Gulf of Mexico, USA. *Quaternary Science Reviews*, Volume 223.
- Hosman, R. L., 1996. Regional Stratigraphy and Subsurface Geology of Cenozoic Deposits, Gulf Coastal Plain, South-Central United States. U.S. Geological Survey.
- Imbrie, J. D. et al., 1984. Stacked and smoothed oxygen-isotope record as a function of age in the SPECMAP time scale (SPECMAPStack). *PANGAEA*.
- Johnson, L. C., 1891. The Nita crevasse [Louisiana]. Issue 2, pp. 20-25.
- Knabb, R. D., Rhome, J. R. & Brown, D. P., 2005. Tropical Cyclone Report Hurricane Katrina 23-30 August 2005.
- Kolker, A. S., Allison, M. A. & Hameed, S., 2011. An evaluation of subsidence rates and sea-level variability in the northern Gulf of Mexico. *Geophysical Research Letters*, Volume 38(21).
- Kulp, M. et al., 2002. Latest Quaternary Stratigraphic Framework of the Mississippi River Delta Region. *Gulf Coast Association of Geological Societies Transactions*, Volume 52, pp. 573-582.

- Labeyrie, L. D., Duplessy, J. C. & Blanc, P. L., 1987. Variations in mode of formation and temperature of oceanic deep waters over the past 125,000 years. *Nature*, Volume 327, pp. 477-481.
- Lee, B.-R., Yoo, D.-G. & Lee, G.-S., 2022. High-resolution sequence stratigraphy and evolution of the Jeju Strait shelf, Korea, since the Last Glacial Maximum. *Marine and Petroleum Geology*, Volume 135.
- Lisiecki, L. E. & Raymo, M. E., 2005. A Pliocene-Pleistocene stack of 57 globally distributed benthic $\delta^{18}O$ records. *Paleoceanography*, I(20).
- Matson, G. C., 1916. *The Pliocene Citronelle Formation of the Gulf Coastal Plain*.
[Online]
Available at: <https://pubs.usgs.gov/pp/00981/report.pdf>
[Accessed 25 4 2022].
- McBride, R. A. et al., 1991. Geomorphic History, Geologic Framework, and Hard Mineral Resources of the Petit Bois Pass Area, Mississippi-Alabama. In: *Coastal Depositional Systems in the Gulf of Mexico: Quaternary Framework and Environmental Issues*.
- Meyer-Arendt, K. J., 1995. Historical Human Modification of Mississippi's Mainland Shoreline. Jackson: Mississippi Office of Geology.
- Meyer-Arendt, K. J. & Gazzier, C. A., 1990. *Abstract: Shoreline Erosion and Wetland Loss in Mississippi*. [Online]
Available at:
<http://archives.datapages.com/data/gcags/data/040/040001/pdfs/0599.pdf>
[Accessed 27 4 2022].

- Meyer-Arendt, K. J., Oivanki, S. M. & Yassin, B., 1998. Wetland changes in coastal Mississippi, 1950 to 1992. *Marine Resources and History of the Mississippi Gulf Coast*, Volume 2, pp. 377-399.
- Milliken, K. T., Anderson, J. B. & Rodriguez, A. B., 2008. A new composite sea-level curve for the northern Gulf of Mexico. In: J. B. Anderson & A. B. Rodriguez, eds. *Response of Upper Gulf Coast Estuaries to Holocene Climate Change and Sea-Level Rise*. Boulder: The Geologic Society of America, pp. 1-12.
- Mississippi Department of Environmental Quality, 2016. A Path Toward Sustainable Ecosystem Restoration. National Fish and Wildlife Foundation.
- Morton, R. A., Miller, T. L. & Moore, L. J., 2004. National Assessment of Shoreline Change: Part 1 Historical Shoreline Changes and Associated Coastal Land Loss along the U.S. Gulf of Mexico, St. Petersburg: U.S. Geological Survey.
- NOAA, 2021. National Oceanic and Atmospheric Administration (NOAA) Digital Coast Data Access Viewer. Charlestown(South Carolina): NOAA Office for Coastal Management.
- NOAA, 2021. *Sea Level Trends*. [Online]
Available at: <https://tidesandcurrents.noaa.gov/sltrends/sltrends.html>
[Accessed 25 March 2022].
- Office for Coastal Management, 2022. *NOAA Coastal Inundation Digital Elevation Mode: Mississippi from 2010-06-15 to 2010-08-15*. [Online]
Available at: <https://www.fisheries.noaa.gov/inport/item/48087>
- Oivanki, S. M., Meyer-Arendt, K. J. & Yassin, B., 1995. *Analysis of Land Use and Land Cover Changes on the Mississippi Coast: 1950s-1992*. [Online]

Available at: <http://archives.datapages.com/data/gcags/data/045/045001/0467.htm>
[Accessed 29 3 2022].

- Otvos, E. G., 1972. Pre-Sangamon beach ridges along the northeastern Gulf Coast; fact or fiction?. *Gulf Coast Association of Geological Societies Transactions*, Issue 22, pp. 223-228.
- Otvos, E. G., 1982. Coastal Geology of Mississippi, Alabama and Adjacent Areas. The New Orleans Geological Society.
- Otvos, E. G., 1985. Coastal Evolution - Louisiana to Northwest Florida. New Orleans, The New Orleans Geological Society.
- Otvos, E. G., 1991. Northeastern Gulf Coast Quaternary. In: R. B. Morrison, ed. *Quaternary nonglacial geology; conterminous United States*. Geological Society of America, pp. 588-594.
- Otvos, E. G., 1999. Quaternary Coastal History, Basin Geometry and Assumed Evidence for Hurricane Activity, Northeastern Gulf of Mexico Coastal Plain. *Journal of Coastal Research*, 15(2), pp. 438-443.
- Otvos, E. G., 2001. H. Mississippi Coast: Stratigraphy and Quaternary Evolution in the Northern Gulf Coastal Plain Framework, USGS.
- Otvos, E. G., 2005. Numerical chronology of Pleistocene coastal plain and valley development; extensive aggradation during glacial low sea-levels. *Quaternary International*, 135(1), pp. 91-113.
- Posamentier, H. W. & Vail, P. R., 1988. *Eustatic Controls on Clastic Deposition II—sequence and Systems Tract Models*. [Online]
Available at:

http://archives.datapages.com/data/sepm_sp/sp42/eustatic_controls_on_clastic_deposition_ii.htm

[Accessed 26 3 2022].

- Reimer, P. J. et al., 2020. The IntCal20 Northern Hemisphere Radiocarbon Age Calibration Curve (0-55 cal kBP). *Radiocarbon*, Volume 62, pp. 725-757.
- Rodriguez, A. B., Greene, D. L., Anderson, J. B. & Simms, A. R., 2008. Response of Mobile Bay and eastern Mississippi Sound, Alabama, to changes in sediment accommodation and accumulation. In: *Response of Upper Gulf Coast Estuaries to Holocene Climate Change and Sea-Level Rise*. Boulder: The Geological Society of America, pp. 13-30.
- Shackleton, N. J., 1987. Oxygen isotopes, ice volume and sea level. *Quaternary Science Reviews*, Volume 6, pp. 183-190.
- Simms, A. R., 2021. Last Interglacial Sea Levels within the Gulf of Mexico and Northwestern Caribbean Sea. *Earth System Science Data*, 13(3), pp. 1419-1439.
- Siringan, F. P. & Anderson, J. B., 1993. Seismic Facies, Architecture, and Evolution of the Bolivar Roads Tidal Inlet/Delta Complex, East Texas Gulf Coast. *Journal of Sedimentary Petrology*, 63(5), pp. 794-808.
- Stuiver, M., Reimer, P. J. & Reimer, R. W., 2022. *CALIB 8.2* [WWW program].
- Sullivan, J. C., Wan, Y. & Willis, R. A., 2020. Modeling Floodplain Inundation, Circulation, and Residence Time Under Changing Tide and Sea Levels. *Estuaries and Coasts*, Volume 43, pp. 693-707.
- Thomas, M. A. & Anderson, J. B., 1994. Sea-Level Controls on the Facies Architecture of the Trinity/Sabine Incised-Valley System, Texas Continental Shelf. In: *Incised-*

Valley Systems: Origin and Sedimentary Sequences. SEPM Society for Sedimentary Geology.

U.S. Geological Survey, 2018. USGS Lidar Point Cloud MS Coastal-3DEPEExt-Coastal-AOI 2015 790325 LAS 2018. U.S. Geological Survey.

Vail, P. R. & Mitchum, R. M., 1977. Seismic Stratigraphy and Global Changes of Sea Level, Part 1: Overview. In: C. E. Clayton, ed. *Seismic Stratigraphy -- Applications to Hydrocarbon Exploration*. Tulsa(Oklahoma): American Association of Petroleum Geologists, pp. 83-97.

Wagoner, J. C. V. et al., 1988. *An Overview of the Fundamentals of Sequence Stratigraphy and Key Definitions*. [Online]

Available at:

http://archives.datapages.com/data/sepm_sp/sp42/an_overview_of_the_fundamentals.htm

[Accessed 2 5 2022].

Wilson, K. V., Clair, M. G., Turnispeed, D. P. & Rebich, R. A., 2009. Development of a Watershed Boundary Dataset for Mississippi: U.S. Geological Survey Open-File Report 2008-1198, St. Petersburg: U.S. Geological Survey.

CHAPTER III - SEDIMENTOLOGICAL EFFECTS OF HURRICANE NATE
(CATEGORY 1) ON SHIP ISLAND

3.1 Introduction

Tropical cyclone impacts cause loss of life, devastating damage to infrastructure, and adversely affect natural resources and the economy (Morton et al., 2005). The growing population of coastal communities are therefore at great risk in the future. There are four classes of tropical cyclones defined by maximum sustained winds: tropical depression – ~ 61 km/h or less, tropical storm – ~ 63 to 117 km/h, hurricane – 119 km/h or higher, and major hurricane (category 3-5) – ~ 179 km/h or higher. Tropical cyclones elevate sea level with storm surge generally increasing with category, although there are many other compounding factors controlling surge height. Storm surge is a combination of water build up due to wind stress and water level rise due to low atmospheric pressure, producing larger waves that attack shorelines (Davis & Dolan, 1993). It is often, along with flooding, the biggest cause of lives lost in hurricanes (Erdman, 2020). Storm surge exacerbates the effects of sea-level rise (Fleming et al., 2018) and the astronomical tidal cycle by amplifying water levels. According to Intergovernmental Panel on Climate Change (IPCC), Representative Concentration Pathways (RCP) of 2.6 and 8.5 W/m² of increased radiative forcing, sea level is likely to rise 0.29 m to 1.10 m by 2100 (Oppenheimer et al., 2019), causing storm surges from tropical cyclones to flow farther inland, making minor storms more impactful in terms of coastal flooding. Additionally, the intensity of major hurricanes is predicted to increase (Emanuel, 2013).

Barrier islands are important coastal landscapes which provide habitats and protect mainland areas from tropical cyclone wave energy. The response of barrier

islands to sea-level rise and storm-induced erosion will be modulated by sediment supply (Anderson et al., 2014). Barriers reduce storm effects by causing waves to break before reaching the mainland (Fleming et al., 2018). Thus, understanding the timescale of their geomorphological change is important for the coastal communities they protect (Mellet & Plater, 2018). Storm surge inundation creates overwash, shallow overland flow transporting sediment from the open-coastal barrier to the backbarrier (Morton & Sallenger, 2003). Swift & Moslow (1982) propose that barrier islands may shed more sand offshore, forming shelf sand-sheets, than can return to the littoral system through shoreface erosion. If sediment supply is constant and there are no topographic restraints, landward translation from storm impacts will keep pace with sea-level rise (barrier rollover) (Mellet & Plater, 2018) as was the case with Follet's Island, TX (Anderson et al., 2014; Odezulu et al., 2018). If a barrier island is resistant to landward translation, for example due to steep antecedent topography or coarse grain sizes, it may be overstepped (Mellet & Plater, 2018), which exposes the mainland shoreline to open ocean wave attack. In some cases, as sea-level rise slows or sediment supply increases, the barrier could reemerge in a more landward location. If sediment supply is cut off in a transgressive regime, such as in the case of barrier islands associated with headlands of abandoned Gulf of Mexico Mississippi River deltas, islands may be reduced to marine sand bodies (Penland et al., 1988) and never reemerge. To determine a barrier island's response to tropical cyclone impacts, site specific sediment budgets, antecedent topography, and RSL rise need to be quantified.

Storm erosion has been shown to cause shoreline to retreat an order of magnitude larger than fair weather retreat (Anderson et al., 2014) and large storms have enough

energy to mobilize sediment below the depth of closure and to erode shorefaces, e.g. (Schwab, 2017), removing sediment permanently (Morton, 2008). Eroded sediments within the depth of closure may subsequently be returned by fair-weather waves (Dupre, 1985), and tropical cyclone energy can mobilize sediment below the fair-weather base constructively (Otvos & Carter, 2008; Eisemann et al., 2018). For example, Hurricane Camille created depositional morphologic changes on Dauphin Island (Morton, 2010). Beach ridges in northern Australia above fair-weather waves may be constructed by cyclones that will also overtop these ridges depositing sand sheets inland (Nott, 2006). Studying the sedimentology of the sediments mobilized during hurricanes will allow coastal communities to implement better mitigation strategies as the fate of barrier protection and shoreline defense can be better predicted (Morton, 2008). Any coastal erosion mitigation program should incorporate an understanding of sediment sources and sinks, influenced by storms on a time scale relevant to mitigation (Schwab, 2017).

Along the low-lying Gulf of Mexico coastlines, tropical storms provide about 15 % of monthly wave energies during less than 1 % of time (Eisemann et al., 2018). Ship Island, Mississippi, an uninhabited barrier island fronting the Mississippi Sound, is vulnerable due to a history of major storm impacts and low sediment supply. It protects a portion of the mainland Mississippi coast and was recently the site of a nourishment project of unprecedented scale that healed a major breach caused by Hurricane Camille (Oivanki et al., 1995; US Army Corps of Engineers, 2020). The geomorphology of Ship Island has been heavily influenced by major hurricanes (categories 3–5) during the historical record (Eisemann et al., 2018), yet minor tropical cyclones hurricanes are more prevalent as the study area has historically been impacted by a tropical storm or minor

hurricane (categories 1 and 2) every 3 to 4 years (Byrnes et al., 2013). Accelerated sea-level rise, decreased rates of sediment delivery due to anthropogenic activity, and decreased vegetation due to greater overwash, necessitates the study of minor hurricane impacts. As the barriers become increasingly vulnerable, minor hurricane impacts may have an enhanced effect. Analyzing the grain size, sediment volume, and sediment flux transported by a minor hurricane provides insight into geomorphologic changes, including the losses or gains an island platform incurs, that might not be as apparent as the effect of larger storms. The analyses can also be used to predict the effectiveness of artificial projects on the shoreline such as beach nourishment and seawall defenses.

One such minor storm was Hurricane Nate, which made landfall near Ship Island, Mississippi on October 8, 2017, with maximum winds of 140 km/h (Cangialosi & Avila, 2017). The purpose of this study is to quantify sediment transport of Hurricane Nate deposits and to determine if the minor hurricane was destructive or constructive to Ship Island. This is achieved through field surveys, trenching, grain-size analyze analysis, and imagery analysis. In addition, this study will compare the effects of Hurricane Nate with those of Hurricane Katrina.

3.2 Study Area

3.2.1 Regional Setting

The Mississippi-Alabama (MS-AL) barrier chain consists of five islands (Dauphin, Petit Bois, Horn, Ship and Cat) (Figure 3.1). The sediment budget is predominately driven by westward littoral transport (Otvos & Carter, 2013) leading to downdrift migration of tidal inlets coupled with spit accretion (Morton, 2007). This barrier chain has a 0.5 m diurnal tidal range, 0.6 m and 0.4 m mean significant wave

height in the winter and summer, respectively, and 148-degree mean wave direction (Twichell et al., 2013; Rosati et al., 2007). The MS-AL barrier islands are rapidly eroding and migrating laterally (westward) (Morton et al., 2005). From the 1840s to 2005, the average land area loss for Petit Bois Island and Cat Island was 30,000 m²/yr and for Horn Island and Ship Island was 25,000 m²/yr (Morton, 2007) primarily due to low sediment supply, storm impacts, and sea-level rise.

Meyer-Arendt (1995) reports Mississippi mainland coastal erosion of 2–3 m/yr due to storm activity across the state. From 1851 to 2010, the Mississippi coast has been hit by at least nineteen hurricanes, nine of them having been major (category 3-5) (Blake & Gibney, 2011). Biloxi, a city ~ 20 km north of East Ship Island, has a 26 yr return period of major hurricanes and a 11 yr period of all hurricanes (Blake & Gibney, 2011). From 1851-2010, four of the United States mainland's thirty most intense hurricanes impacted Mississippi: Fort Lauderdale Hurricane (1947), Camille (1969), Frederic (1979), and Katrina (2005). The Fort Lauderdale Hurricane (1947), a category 4, breached Ship Island (Otvos, 1970) which healed by 1960 (Rucker & Snowden, 1990). Hurricane Camille made landfall as a category 5 with a minimum pressure of 909 millibars (Blake & Gibney, 2011) and ~ 7.6 m storm surge (Romano, 2010; Pielke et al., 1999). Hurricane Ivan, making landfall in Alabama as a category three, affected the Gulf Coast in September 2004, creating a 3.2 m storm surge and 126 k/h gusts at or near Biloxi (Stewart, 2004). In 2005 Hurricane Katrina (category 3) created a 10 m storm surge on Ship Island causing catastrophic erosion (Eisemann et al., 2018). In 2008 Hurricane Ike, a category two in NGOM, followed on the heels of Hurricane Gustav, a category two, damaging Mississippi, and Alabama barrier islands (Dean, 2008). Two

days after Hurricane Ike, East Ship Island was observed to be mostly subaqueous (Dean, 2008). Major hurricanes cause barrier island erosion (Dean, 2008; Byrnes et al., 2013; Carter et al., 2018; Gremillion et al., 2020), and only minimal post storm recovery has been observed in the 21st century (Eisemann et al., 2018; Gremillion et al., 2020). However, there have been few studies on sediment dynamics due to minor hurricanes e.g., (Martin & Muller, 2021; Eisemann et al., 2018; Gremillion et al., 2020). While major storms may cause irrecoverable erosion, minor storms may be constructive to barrier island systems.

3.2.1.1 Ship Island

Ship Island, MS (Figure 3.1), is a 13 km long, 0.8 km wide (Twichell et al., 2013) barrier island located in the Mississippi-Alabama barrier chain that separates the Gulf of Mexico from the Mississippi Sound. As part of the Gulf Islands National Seashore, the island has seen little human impacts. Mostly unvegetated, Ship Island supports shrubs and grasses, although there were two small sets of wooded ridges to the east (Rucker & Snowden, 1990) that are no longer present due to Hurricane Katrina (Carter et al., 2018). It represents one of the most vulnerable barrier islands along the NGOM because it is located at the western terminus of the littoral transport, where sediment supply is low as the littoral transport is interrupted by dredged channels and wave sheltering by the Chandeleur Islands (Byrnes et al., 2013). The island is situated between two tidal inlets; Ship Island pass to the west and Little Dog Keys Pass to the east. Ship Island Pass, a natural tidal inlet, has been maintained for navigation as part of the Gulfport Ship Channel frequently since the early 1900s (Byrnes et al., 2013). The authorized navigation channel was moved ~ 0.5 km to the west in the 1990s to prevent infilling (Byrnes et al.,

2013) and is now at least 15 m deep, excavated into Pleistocene deposits. This channel prevents downdrift inlet migration and spit accretion that occurs with the updrift barriers of the chain and is a sediment sink for the chain's littoral transport. Little Dog Keys Pass and Dog Keys Pass are tidal inlets ~ 8 m deep (Byrnes et al., 2013) situated east of Ship Island, Dog Keys Pass being farther east. Little Dog Keys Pass has an expanding ebb shoal delta that is currently a sediment sink, partly depriving the eastern end of Ship Island from updrift sediment (Byrnes et al., 2013).

Ship Island is a Holocene barrier platform consisting of quartz sand (Cipriani & Stone, 2001) interfingered bay muds in Mississippi Sound and shoreface sands that extend about 2 km into the Gulf of Mexico (Twichell et al., 2013). The abandoned St. Bernard delta of the Mississippi River interfingered with the shoreface in the late Holocene (Twichell et al., 2013). A paleo tidal channel exists under the location of Camille Cut that is about 1 m below the seafloor 1 km south of the island (Twichell et al., 2013).

The island is frequently impacted by hurricanes resulting in major geomorphic changes. In 1969, Hurricane Camille breached the island (Camille Cut) to form East and West Ship Island. The 3.86-kilometer Camille Cut had healed to within one-half kilometer through spit accretion when in 2005 Hurricane Katrina (category 3) widened the cut to 5.6 kilometers (Perez, 2019). As a part of the Gulf Islands National Seashore managed by the National Park Service, it was in a mostly natural state until a recent nourishment project (US Army Corps of Engineers, 2020). The U.S. Army Corps of Engineers dredged sand 32-56 km away and placed it in Camille Cut (Figure 3.1) to create a ~ 150 m wide berm ~ 1.5 m above sea level (Perez, 2019). A second phase

widened the berm an additional ~ 150 m and raised it another ~ 0.60 m, and dune vegetation was added (Hrvacevic, 2020). Sand was also added to the north side of the Camille Cut area and to East Ship Island (Hrvacevic, 2020). The response of this nourishment project to future storm impacts remains unclear.



Figure 3.1 *Mississippi-Alabama Barrier Chain*

Mississippi-Alabama barrier chain with Ship Island, and Ship Island Pass, Camille Cut (now filled in), Little Dog Keys Pass, and Dog Keys Pass.

3.2.1.2 Hurricane Nate

On October 8, 2017, 0520 UTC, Hurricane Nate made landfall near Biloxi, MS (30.4 ° N 89.0 ° W) with 120 k/h winds (Figure 3.2) (Beven & Berg, 2018). A Weather Flow station on Ship Island recorded 94 k/h sustained winds and gusts up to 117 k/h at 0319 UTC about two hours before landfall (Beven & Berg, 2018). Inundation was 2.7 m in Biloxi (Beven & Berg, 2018). While the inundation on Ship Island approached 8 m during Hurricane Katrina, resulting in subaerial land loss of ~ 1.1 km² (Eisemann et al., 2018), inundation on Ship Island was less than 3 m during Hurricane Nate (Figure 3.3).

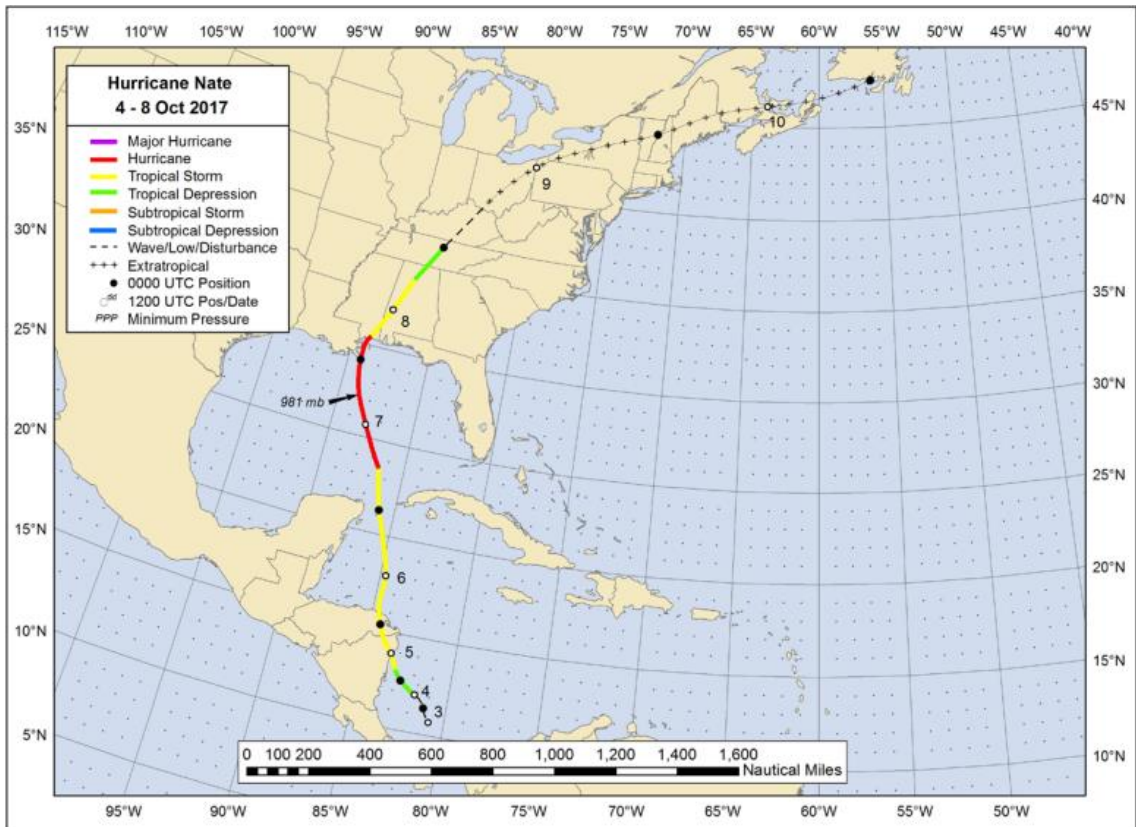
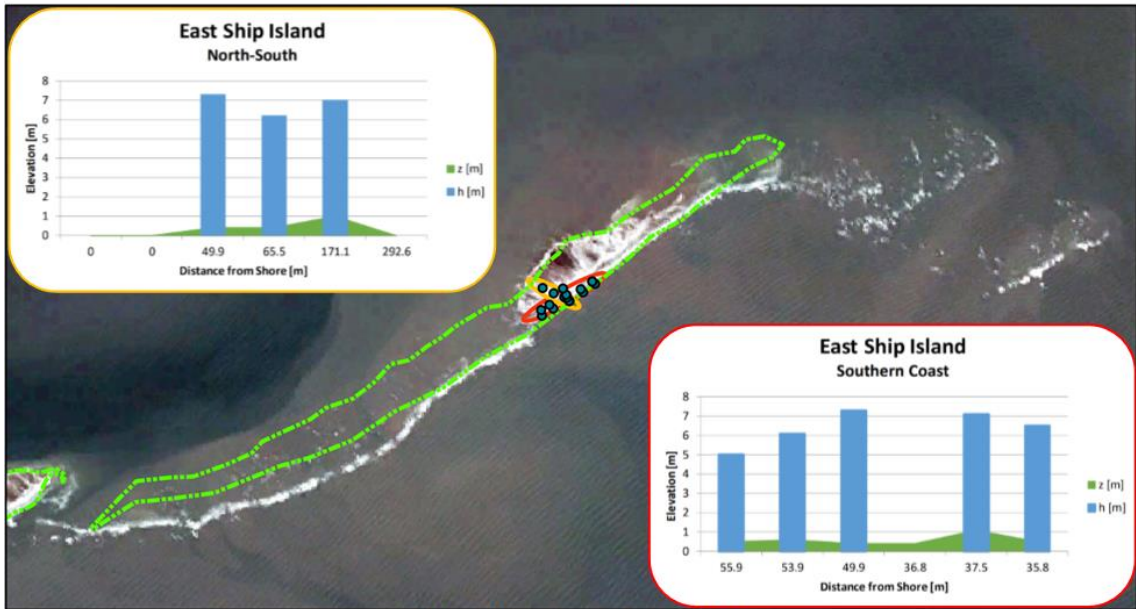


Figure 3.2 *Hurricane Nate*

Hurricane Nate's track showing landfall as a minor hurricane (minimum pressure was 981 mb) on the Mississippi coast the morning of October 8, 2017 (Beven & Berg, 2018).

After Hurricane Katrina, 2005



After Hurricane Nate, 2017



Figure 3.3 *East Ship Island after Hurricane Katrina and Hurricane Nate*

Terrain (z) and water (h) elevations measured on East Ship Island after Hurricane Katrina (top panel). North to south transects outlined in yellow and east to west transect is outlined in red with green dots representing surveyed locations. Terrain (z) and water (h) elevations measured on East Ship Island after Hurricane Nate (bottom panel). North to South transect outlined in yellow with pink dots representing surveyed locations. Green outline represents East Ship Island's outline prior to each storm (figure courtesy of Hermann Fritz).

3.3 Hypotheses

(H1) Due to the orientation of the prevailing wave energy and the downstream position in the littoral transport regime, West Ship Island sediment mobilized by Hurricane Nate should be smaller in grain size than that mobilized on East Ship Island. I assessed this hypothesis by comparing volume percentages, D10, D50, and D90 of storm deposits from both islands.

(H2) Due to faster settling rates of coarser particles, a fining trend of storm deposits should have occurred landward. I assessed this hypothesis by comparing grain size statistics of basinward storm deposits to landward deposits.

(H3) Hurricane Nate, a minor hurricane, was constructive to Ship Island as storm layers were deposited subaerially as overwash fans, whereas Hurricane Katrina, a major hurricane, was erosional, removing washover sediment to the back-barrier that was lost from the barrier platform. The volume of subaerial sediment deposited by Hurricane Nate in overwash fans was less than the volume of subaerial sediment eroded by Hurricane Katrina; however, this volume was additive. I tested this hypothesis by comparing: 1) subaerial area differences between pre-storm and post-storm imagery 2) erosion volume due to Hurricane Katrina from Eisemann et al. (2018) to an estimate of washover volume due to Hurricane Nate using post-storm imagery and trench deposition thicknesses, and 3) erosion volume due to Hurricane Katrina from Eisemann et al. (2018) to a flux estimate from a modified Meyer-Peter Müller equation.

3.4 Methods

To investigate Hurricane Nate storm effects on Ship Island, a survey was conducted on both islands one month after landfall and two trenches on each island were analyzed.

3.4.1 Survey

Both islands were extensively surveyed to examine Hurricane Nate effects. We searched for: high water marks, wrack lines, and inundation distances. High water marks were identified by lines of debris and abrasion on tree trunks (Figure 3.4). Wrack lines were identified by abrupt contiguous lines of debris with even elevation (Figure 3.4). Inundation distances were identified by toppled vegetation (Figure 3.4) and lines of debris on the ground. Leveling transects from the shoreline to high water marks and wrack lines on overwash fans were surveyed using a Trimble GPS rover with a Laser craft range finder to record elevations and distances from shore. Elevations were corrected to a concurrent base station previously set up in Biloxi and reduced to MSL using a tidal benchmark on West Ship Island (Station ID: 8744756) which was attached to a steel rod driven about 16 m to refusal. The station datum is 1.161288 m below MSL.

3.4.1.1 Trenches

Overwash sediments were surveyed using the procedures of Hong et al. (2018). Trench sites were selected to be representative of the overwash fans and were spaced in transects to examine lateral depositional trends. Four trenches ranging in depth from 30 cm to 55 cm were dug in storm deposits that overtopped preexisting vegetation. Two trenches were dug on West Ship Island (SI 1.1 and SI 1.2) and two trenches were dug on East Ship Island (ESI 1.1 and ESI 1.2) (Figure 3.5). Small nourishment projects on Ship

Island prior to Hurricane Nate were on the sound side to the northwest to protect Fort Massachusetts (Figure 3.5). Any sediment mobilized there would not have reached the trench sites. Trench site elevations and positions were surveyed, and elevations were reduced to MSL as positions were referenced to the nearest shoreline. The trenches on West Ship Island were 8.8 km apart from the trenches on East Ship Island. Lithology was noted for each trench and sediment samples were taken where there were facies changes down trench, resulting in seven samples from both trenches on West Ship Island and five samples from both trenches on East Ship Island. No grain size samples were taken in the organic-rich Hurricane Nate capping deposits. Descriptions of the trenches included lithological changes, color, structure, vegetation, and organics associated with deposits.

3.4.1.2 Grain Size

Grain size analysis was performed using a Malvern MASTERSIZER 3000 laser particle-size analyzer. Volume percentages and Folk and Ward graphical statistics were calculated for all samples using GRADISTAT (Folk & Ward, 1957; Blott & Pye, 2001). Volume percentages are the percent of sediment that is smaller than a given grain size by volume. The graphical statistics calculated were the mean grain size (average grain size), sorting (grain size variation), skewness (symmetry of grain size distribution), and kurtosis (the measure of the concentration of grain size distribution around its mean) (Folk & Ward, 1957; Hong et al., 2018). Also analyzed were D10, D50, and D90.

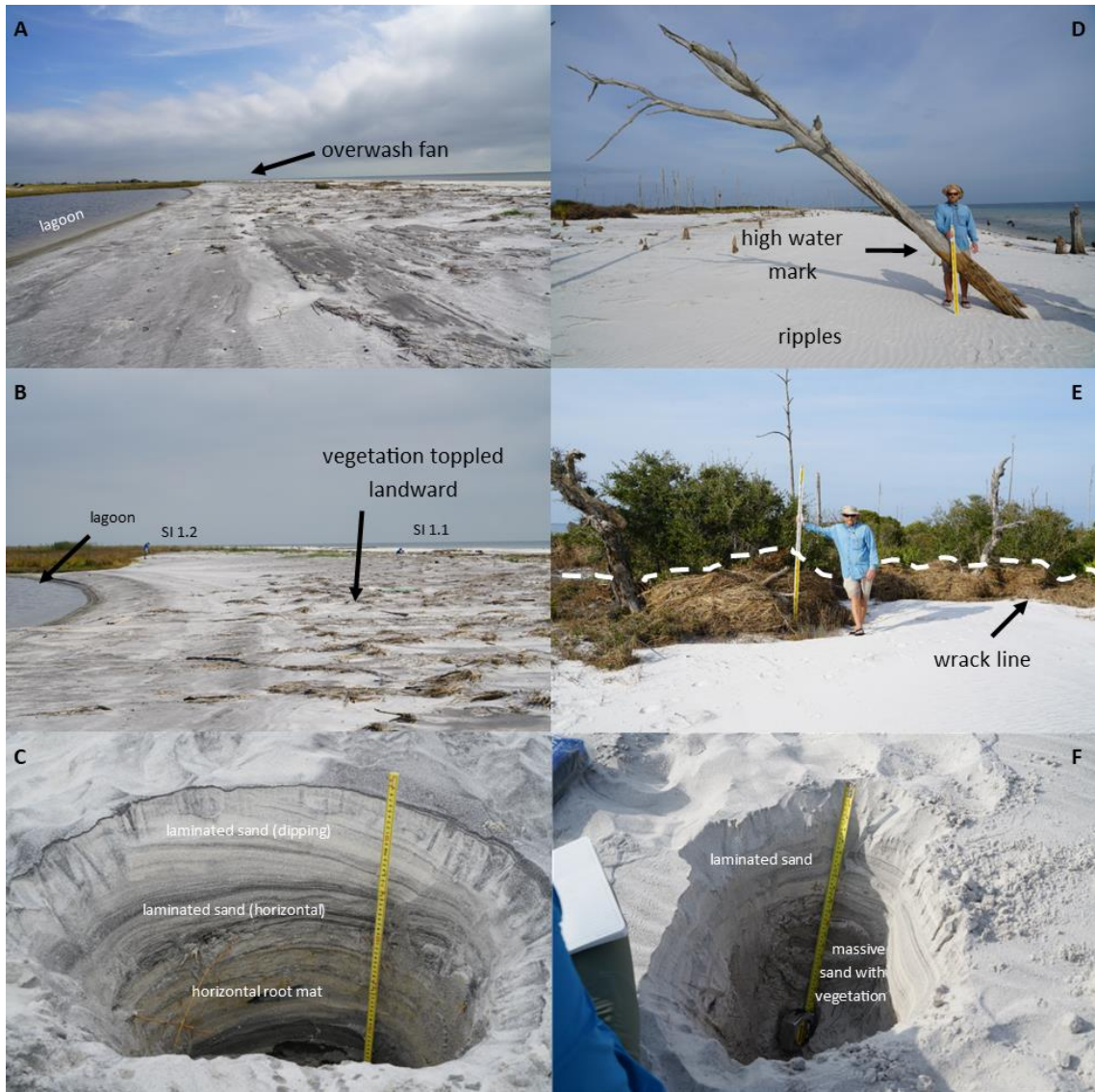


Figure 3.4 *Ship Island Survey*

Ship Island was surveyed on November 7, 2017, about a month after Hurricane Nate, resulting in four trenches sampled in overwash fans and elevations of water lines and wrack lines: A) easterly view of sampled overwash fan on West Ship Island B) trench locations SI 1.1 and SI 1.2 on overwash fan on West Ship Island C) Trench SI 1.1 D) high water mark on overwash fan on East Ship Island E) wrack line on overwash fan on East Ship Island F) trench ESI 1.1 (photos courtesy of Hermann Fritz).



Figure 3.5 *Trench Locations*

Trench locations on West Ship Island (SI 1.1 and SI 1.2) and East Ship Island (ESI 1.1 and ESI 1.2) located in overwash fans about 8.8 km apart, imagery taken post storm by National Geodetic Survey, 2022; Fort Massachusetts is located on the northwest area of West Ship Island.

3.4.2 Sediment Flux

Two modes of sediment transport occur during storm inundation: bed load and suspended load transport. As wave energy increases, a particle that is stationary on the seafloor during quiescence may roll or bounce along the seafloor (bedload) and/or become transported in the water column (suspended load). Sediment transport flux can be calculated using boundary shear stress, grain diameter, and density (Wiberg & Smith, 1989). When wave energy diminishes to the point where a particle comes out of suspension, due to a decrease in wave height and surge velocity, it will settle at velocity that can be calculated using kinematic viscosity, grain diameter, and density (Ferguson & Church, 2004).

To compare the sediment transport of Hurricane Katrina with Hurricane Nate, width-averaged sediment flux was calculated for each trench using a modified Meyer-Peter Müller equation:

Equation 1 modified Meyer-Peter Müller equation

$$q_s = \sqrt{\left(\left(\frac{\rho_s}{\rho_f} - 1\right) g D_{50}^3\right)} \times [1.6(\ln \tau + 9.8)] \times [\tau - \tau_{cr}]$$

where ρ_s and ρ_f are the densities of sediment, consisting of quartz, (2650 kg/m³) and seawater (1025 kg/m³), $\tau = u^2 / \left(\left(\frac{\rho_s}{\rho_f} - 1\right) g D_{50}\right)$, $u^2 = gHS$, $g = 9.81 \text{ m/s}^2$, $H = 2.7m - V$, S is slope, and V is vegetation layer elevation with respect to MHHW (Shaw et al., 2015). T_{cr} is the non-dimensional critical shear stress of 0.047 (Wiberg & Smith, 1989). As Equation 1 utilizes D_{50} , a complete sediment inventory is required i.e., a defined overwash fan where sediment did not washover into the lagoon. Flux was averaged across all four trenches, and this average was multiplied by the total island front

length, resulting in a volume of sediment moved per time landward along the entire island, not just into subaerial overwash fans. Subsequently, the total volume of erosion attributed to Hurricane Katrina, 5,300,000 m³ (Eisemann et al., 2018), was divided by the volume of sediment per time moved by Hurricane Nate to compare sediment transport of a major hurricane to that of a minor one.

3.4.3 Image Analysis

Ortho-rectified oblique imagery from April 2017 (NOAA, 2021) and emergency response imagery from October 10, 2017 (National Geodetic Survey, 2022) were analyzed utilizing GIS. The pre storm ortho-rectified oblique image had a horizontal accuracy in the 5–10 m range (~ 0.30 m per pixel) whereas the post storm emergency response imagery had a horizontal accuracy in the 3–5 m range (~ 0.15 m per pixel). “Measure Area” was used to obtain ellipsoidal areas of Ship Island before Hurricane Nate and overwash fans created by Hurricane Nate. The area of overwash was multiplied by the average overwash thickness found in this study to obtain the volume of overwash caused by Hurricane Nate. The lengths of the island fronts were also measured.

3.5 Results

3.5.1 Hurricane Nate Deposit Characteristics

All Nate sediment samples were well-sorted, skewness was symmetrical, and kurtosis was mesokurtic. From the trenches, the underlying sediment and the Hurricane Nate layer were of smaller grain size on West Ship Island than East Ship Island (Figure 3.6). The grain size found in all overwash fans ranged from 21.2 to 666 μm. In trench SI 1.1, the Nate layer was 26 cm thick, and was deposited at 0.23 m above MSL 57.2 m from the shoreline (Figure 3.7). It was demarcated from previous deposits by a horizontal

root mat underlying laminated sand capped by dipping laminations at the top of the trench. The D50 grain size of the bottom of the storm layer was 284 μm , coarsening to 290 μm towards the top of the deposit (Figure 3.6).

Trench SI 1.2 had a thinner storm layer of 18 cm (Figure 3.6 and Table 3.1) deposited at 0.72 m above MSL 81.5 m from the shoreline (Figure 3.7). The hurricane layer was found to have a D50 of 290 μm at the base of the deposit. There was finer deposition at 15 cm, with a D50 of 272 μm . The D50 was 305 μm in the upper most sample of trench SI 1.2. The top 10 cm of SI 1.2 consisted of a fine layer of organics.

In ESI 1.1, the Nate layer was 26 cm thick, and was deposited 101.3 m from the shoreline at 1.62 m above MSL (Figure 3.7). The storm deposit base was demarcated by massive sand with vegetation underlying laminated sand ranging in size from 21.2 to 666 μm . Above the root mat, hurricane deposits, having a D50 of 310 μm initially, fined slightly up trench with parallel laminations followed by an increase in D50 to 354 μm towards the top of the storm layer (Figure 3.6).

ESI 1.2 was 122.2 m from the shore and 1.62 m above MSL at the top (Figure 3.7). In ESI 1.2, the hurricane layer was found from 14.5 cm depth to the surface, and there was a slight coarsening from the base of the storm layer to the top, from a D50 of 305 μm to 310 μm (Figure 3.6). There was not a layer of pronounced fining in the storm layer of ESI 1.2 as found in SI 1.2.

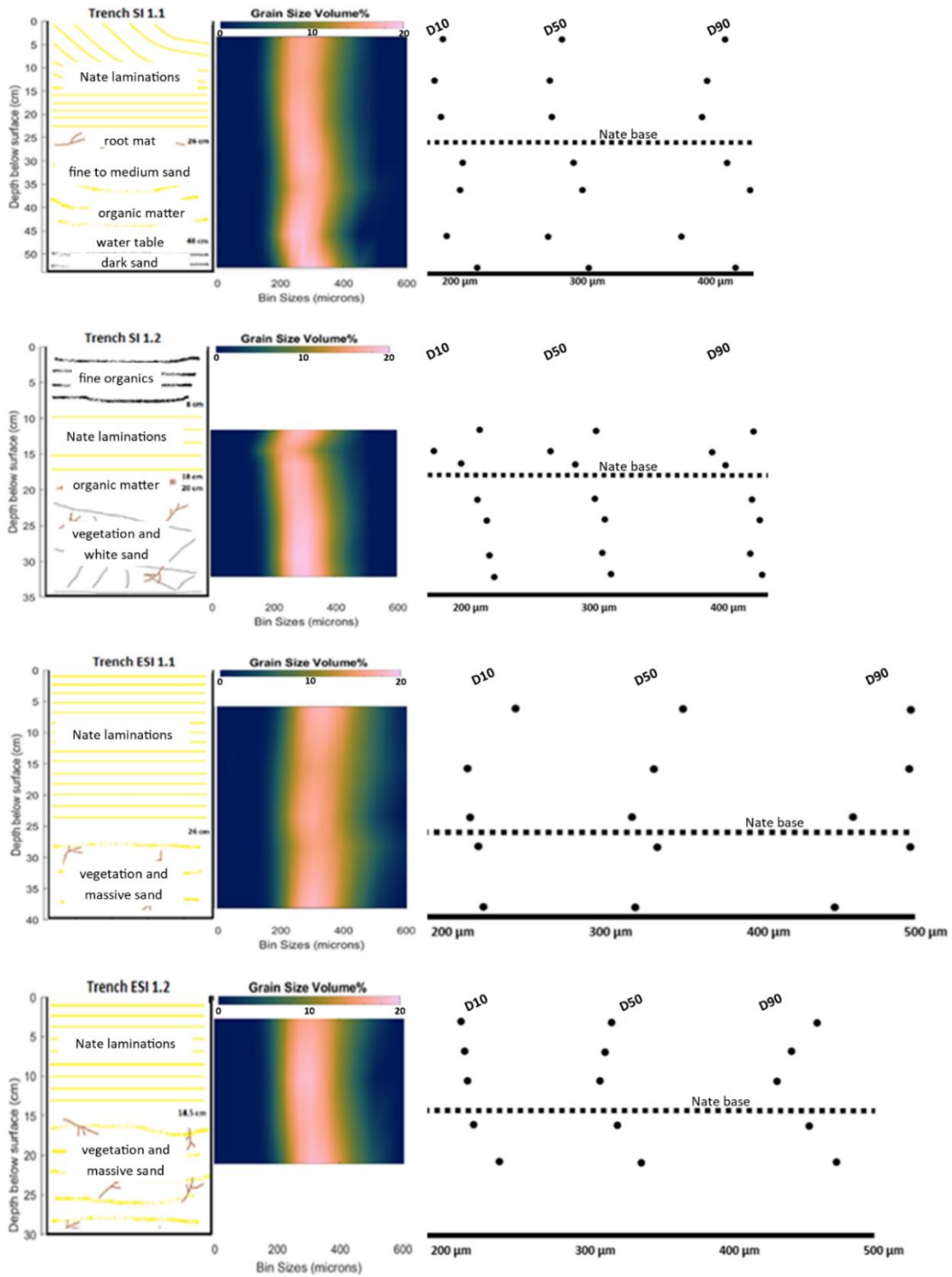


Figure 3.6 *Sedimentological Characteristics*

Volume percentages, lithology, and Folk and Ward statistics (samples above the Nate base were hurricane deposits) for all trenches.

Sediment was well-sorted, skewness was symmetrical, and kurtosis was mesokurtic in all samples; trench SI 1.2 was not sampled from 10 cm to the top due to a layer of fine organics.

Trench Distances from Shoreline and Hurricane Layer Elevations

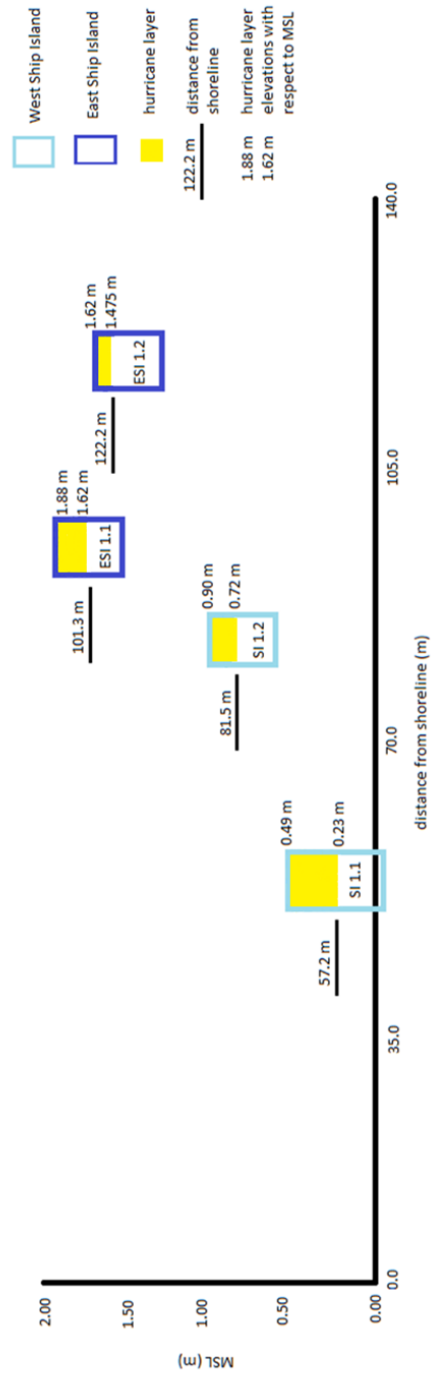


Figure 3.7 *Trench Distances from Shoreline and Elevations*

West Ship Island and East Ship Island trench distances from shoreline and hurricane layer elevations with respect to MSL. The Nate layer was 26 cm thick in both SI 1.1 and ESI 1.1, although ESI 1.1 was almost 1.8 x farther inland and 4 x as high.

Table 3.1

Hurricane Nate layer thicknesses and flux (from Equation 1)

Trench	Storm Layer Thickness (cm)	Distance from Shoreline (m)	Flux (m^2s^{-1})
SI 1.1	26.0	57.2	0.021
SI 1.2	18.0	81.5	0.023
ESI 1.1	26.0	101.3	0.025
ESI 1.2	14.5	122.2	0.019

3.5.2 Flux

Pre-Hurricane Nate, the areal extent of West Ship Island was 1.804 km^2 and East Ship Island was 0.934 km^2 , totaling 2.738 km^2 . Post Hurricane Nate, West Ship Island's area was 1.843 km^2 and the shoreline length was 5,307 m, and East Ship Island's area was 0.964 km^2 and shoreline length was 4,321 m. Therefore, the total area and shoreline length for Ship Island Post-Nate was 2.807 km^2 and 9,628 m, respectively. The total shoreline length, 9,628 m, multiplied by the average flux, $0.022 \text{ m}^2/\text{s}$ equals $212 \text{ m}^3/\text{s}$. This is equivalent to 5,665 s (1.57 h) of sediment transport by Hurricane Katrina on Ship Island ($\sim 5,300,000 \text{ m}^3$ [Eisemann et al., 2018] divided by $212 \text{ m}^3/\text{s}$).

3.5.3 Overwash Volume

The total overwash fan area was found to be $355,000 \text{ m}^2$ on West Ship Island (average thickness – 0.22 m) and $383,000 \text{ m}^2$ on East Ship Island (average thickness – 0.20 cm). Total overwash volume on Ship Island due to Hurricane Nate was $154,700 \text{ m}^3$.

3.6 Discussion

3.6.1 Storm Sediment Transport

Recently, an emphasis has been placed on reconstructing storm surge events on a geologic timescale by analyzing buried deposits (Williams, 2009; Hawkes & Horton,

2012; Xian et al., 2022). Scientists are attempting to quantify the frequency and intensity of washover events that occurred before the historical record by comparing historical sediment packages to modern analogues and differentiating them from tsunami deposits (Hong et al., 2018; Soria et al., 2017, 2018; Brill et al., 2016; Spiske et al., 2021). Over geologic timescales along the Mississippi coast, intense hurricanes frequently impacted the MS coast between 900 to 600 and 2200 to 1900 yr BP (Bregy et al., 2018).

A comparison of the stratigraphic and sedimentological features of these Hurricane Nate deposits to other storm deposits is given in Table 3.2 and Table 3.3. In all trenches, washover deposits were separated from underlying sediment by a vegetation layer with a sharp contact. All analyzed samples were well-sorted, symmetrical, and mesokurtic. The storm deposits were laminated horizontally except for the trenches on West Ship Island, where the top of the basinward trench, SI 1.1, had sub horizontal planar laminae and the top of the inland trench, SI 1.2, had a fine layer of organics. Sub horizontal planar laminae (dipping laminations) were found in washover terraces from deposits associated with Hurricane Rita (McGee et al., 2013), Typhoon Haiyan (Soria et al., 2017), and Hurricane Isabel (Morton et al., 2007) as shown in Table 3.2 and Table 3.3. This indicates these laminae are created when the surge reaches a landward increase in elevation, (i.e., the highest elevation of the runup, R_{HIGH} , is lower in elevation than the berm now being attacked [Sallenger, 2000]), creating a collision regime eroding the underlying soil that is deposited basinward in return flow. Horizontal laminations of organics associated with Tropical Cyclone Pam (Hong, et al., 2018) (Table 3.3) were attributed to backwash from a landward lake or from underlying soil. Similar organic

laminations were found on both West and East Ship Islands and are also likely associated with storm return flow.

3.6.2 Grain Size Comparison

3.6.2.1 West Ship Island and East Ship Island

Hurricane Nate deposits were well sorted on both islands like deposits of Hurricane Rita (McGee et al., 2013), Hurricane Carla (Morton et al., 2007), Typhoon Haiyan (Soria et al., 2017), and Hurricane Isabel (Morton et al., 2007) (Table 3.2 and Table 3.3). The grain size distribution for Hurricane Nate deposits on West Ship and East Ship differed slightly. For trench SI 1.1 the base of the deposit had a D50/D90 of 280/400 μm which coarsened slightly to 300/420 μm at the top (Figure 3.6). For trench SI 1.2 the base of the deposit had a D50/D90 of 290/405 μm which fined to 270/395 μm and then coarsened to 310/415 μm at the top (Figure 3.6). No other fining trend was observed in the Nate deposits, suggesting momentary landward decelerating flow velocities on West Ship, followed again by accelerating flow velocities. For trench ESI 1.1 the base of the deposit had a D50/D90 of 310/460 μm which coarsened to 350/500 μm at the top (Figure 3.6). For trench ESI 1.2 the base of the deposit had a D50/D90 of 305/440 μm which coarsened to 310/480 μm at the top (Figure 3.6). The significantly larger D90 values on East Ship compared with West Ship suggest more rapid, consistently accelerating flow velocities. This is also supported by coarser D90s values on East Ship Island trenches at higher elevation and inland distances compared to those of West Ship Island (Figure 3.8). Washover deposits on both islands coarsened upwards as observed with deposits from Hurricane Ike, Hurricane Rita, Typhoon Haiyan, and Tropical Cyclone Pam as shown in Table 3.2 and Table 3.3.

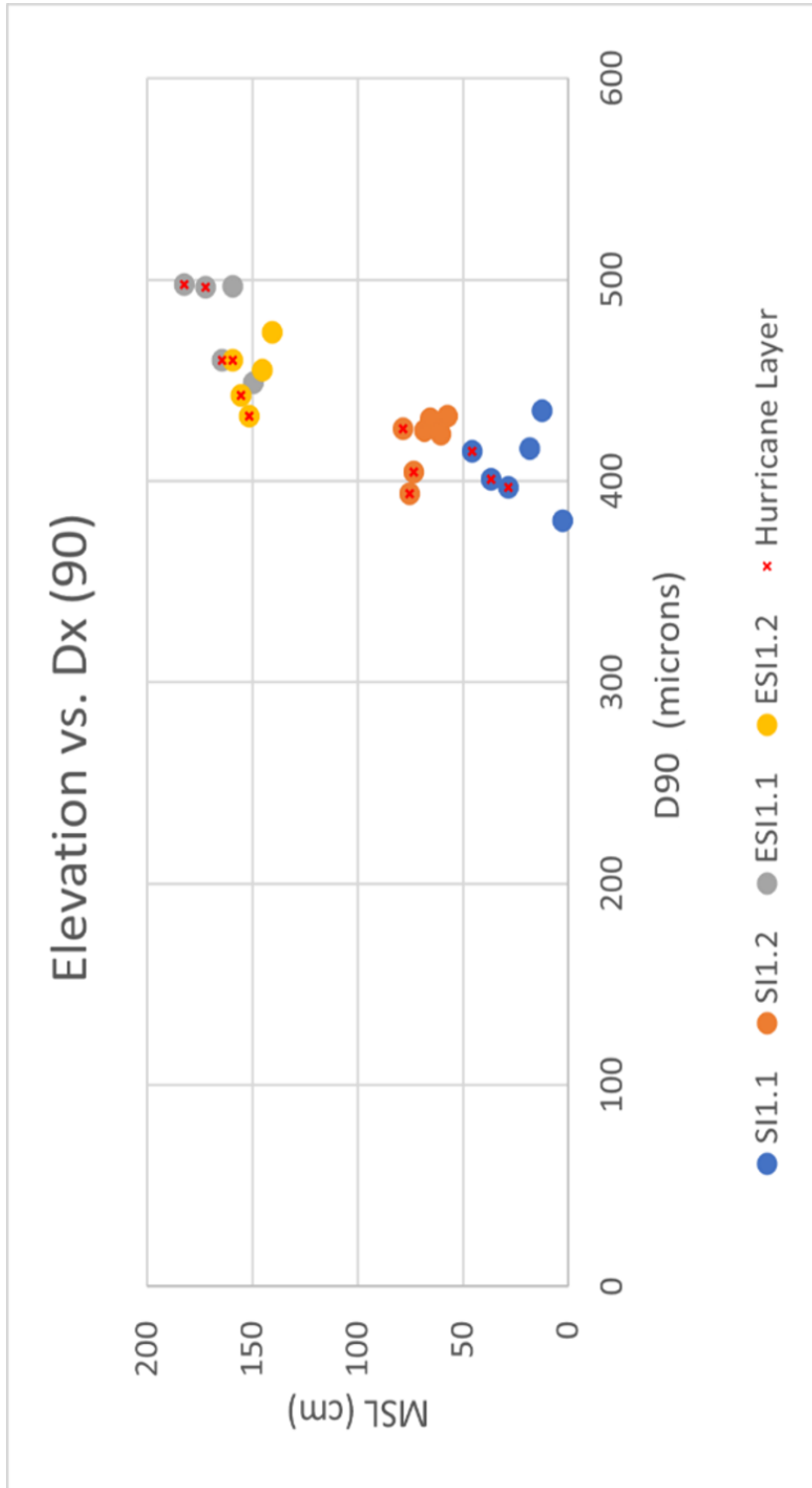


Figure 3.8 *Elevation Versus D90*

Elevation (MSL) versus D90 for all trenches showing Hurricane Nate samples with a red "x"; East Ship Island deposits were of larger grain size and at higher elevation than deposits of West Ship Island.

3.6.2.2 Landward Fining

There was evidence of landward fining on both islands, consistent with deposits associated with Hurricane Ike, Hurricane Rita, Typhoon Haiyan, Hurricane Carla, and Cyclone Yasi (Table 3.2 and Table 3.3). Landward fining is associated with both minor and major storms as wave energy abates landward and sediment sourced from the shoreface settles at a rate dependent on grain size (Ferguson & Church, 2004). At each trench, the initial Hurricane Nate deposits were finer yet better sorted than the underlying deposits indicating initial low energy deposition. This initial deposition was also finer than underlying sediments farther inland at both islands. As the storm intensity increased, the size of the deposited grains increased to that of the underlying sediment, indicating localized erosion and deposition into overwash fans, or a “steepening” of the island. Compared to basinward sedimentation, grain size increased farther inland on West Ship Island as the storm intensified, until organics were washed in; however, grain size fined farther inland on East Ship Island.

Table 3.2

Comparison of Stratigraphic and Sedimentological Features of Hurricane Nate Deposits to other NGOM Tropical Cyclone Deposits, with Local Setting, Meteorology, and Hydrodynamic Conditions (adapted from [Soria et al., 2017])

	Hurricane Nate (This study)	Hurricane Ike (Hawkes & Horton, 2012)	Hurricane Ike (Williams, 2010)	Hurricane Rita	Hurricane Katrina	Hurricane Carla
locality	Ship Island, Mississippi	Galveston and San Luis Islands, Texas	McFaddin National Wildlife Refuge, Texas	Constance Beach, Louisiana	Ocean Springs and St. Andrews, Mississippi	Matagorda Peninsula, Texas
date	October 2017	September 2008	September 2008	September 2005	August 2005	September 1961
storm deposit thickness (cm)	14.5-26	2-28	51-64 (within 200 m); 3-10 (> 200 m)	2-50	9-13	at least 25 to 30
vertical grading	coarsening upward	coarsening upward; alternate coarsening and fining upward	no analysis	Unit A (sand sheet): coarsening upward; Unit B (washover terrace): coarsening upward	massive	upward fining
sorting	well-sorted	not reported	not reported	well-sorted	not reported	poorly sorted (proximal) to well-sorted (distal)
sedimentary structures	horizontal laminae except at the top of SI 1.1 (sub horizontal planar laminae) and SI 1.2 (structureless)	not reported	ripple marks on the surface	Unit A: planar laminae; Unit B: foreset laminae	not indicated	Planar parallel laminae
basal contact	sharp, depositional	sharp, depositional with little or no erosion	sharp	sharp, erosional	sharp, erosional	sharp, erosional and depositional
cross-shore geometry	West Ship Island: berm crest with overwash fan thinning landward in front of line of lagoons; East Ship Island: berm crest in front of overwash fan thinning landward	landward thinning; thicker deposits on the swales	fining and thinning landward	landward thinning	no transect data	narrow thick terrace deposits, moderately thin broad fans, landward thinning
lateral grading	overall landward fining	not reported	thinning and fining landward	inland fining only on the distal deposit	no transect data	landward fining
inland extent (m)	101 to 122	110 to 320	2700	400 to 500	not reported	average at 193, up to 930

Table 3.2 (continued)

coastal geomorphology	barrier island (berm crest topography with landward lagoons on West Ship Island)	barrier islands (ridge and swale topography)	palustrine marshes and brackish lakes, sandy beach with low foredunes	beach ridges separated by low-lying, muddy marshes	salt marsh	barrier island
deposit elevation above sea level (m)	0.49 to 1.88	0.75 to 2.2	1 to 2	0.5 to 1 (ridges)	1.7 to 5	not reported
maximum storm intensity	minor hurricane (981 mb; 148 k/h)	Cat 4 (231 k/h)	Cat 4 (231 k/h)	Cat 5 (897 mb; 288 k/h)	Cat 5 (902 mb; 280 k/h)	Cat 5 (280 k/h)
landfall storm intensity	Cat 1 (117 k/h)	Cat 2 (175 k/h)	Cat 2 (175 k/h)	Cat 3 (190 k/h)	Cat 3 (920 mb; 288 k/h)	Cat 5 (280 k/h)
translation speed (km/h)	45	20	20	19	24	not reported
inundation (m)	< 3	3 to 4	> 3	4 to 5	~ 7	3 to 4
flow depth (m)	~ 1 to 2	1 to 4	not reported	at least 3	5 to 6	1 to 1.5
inundation duration (hrs.)	not analyzed	48 of flooding	48 of flooding	6	~ 24	24
inundation distance (m)	not analyzed	not reported	2500	not reported	725 to 780 (< 1 km)	1500 to 3000
distance from eye (km)	~ 0	25 to 50	~ 70	35	40 to 50	60
references	(Beven & Berg, 2018; Willingham, 2017)	(Doran et al., 2009; Morton & Barras, 2011; Hawkes & Horton, 2012)	(Doran et al., 2009; Morton & Barras, 2011; Williams, 2010)	(Williams, 2009; Morton & Barras, 2011; Williams, 2009; McGee et al., 2013)	(Morton & Barras, 2011; Fritz et al., 2007; Horton et al., 2009)	(Morton et al., 2007)

Table 3.3

*Comparison of Stratigraphic and Sedimentological Features of Tropical Cyclone**Deposits Outside of NGOM, with Local Setting, Meteorology, and Hydrodynamic**Conditions (adapted from [Soria et al., 2017])*

	Typhoon Haiyan (Soria et al., 2017)	Typhoon Haiyan (Soria et al., 2017)	Cyclone Yasi	Hurricane Isabel	Tropical Cyclone Pam
locality	Tanauan, Leyte	Basey, Samar	South of Cairns, northeast Queensland, Australia	Hatteras Is., North Carolina	Manuro: Efate Island; PRB: Port Resolution Bay, Tanna Island
date	November 2013	November 2013	February 2011	September 2003	March 2015
storm deposit thickness (cm)	2 (distal) 10-20 (proximal)	2-8	5 (87 m from shore); 20-50 (50 m from the shore)	40-97 (2 m thick overwash terrace)	Manuro: ≤ 10 (sand) and ≤ 18 (pumice); PRB: ≤ 44 (sand)
vertical grading	Unit 1 (sand sheet to mud): coarsening upward; Unit 2 (washover terrace): coupled fining and coarsening upward	no analysis	fining upward with fine-skewed trends	cycles of upward coarsening or upward fining	Manuro: coarsening upward; PRB: no vertical gradation except with finer grained laminae
sorting	moderate to well-sorted	poorly sorted	not reported	well-sorted	Manuro: moderately well-sorted; PRB: moderately to moderately well-sorted
sedimentary structures	Unit 1: massive to horizontal planar laminae; Unit 2: sub horizontal planar laminae	massive	horizontal planar laminae; basal coarse-grained sediment	sub horizontal planar stratification	Manuro: massive; PRB: horizontal planar laminae
basal contact	sharp, depositional	sharp, depositional	sharp; erosional	sharp	Manuro: sharp; PRB: gradational seaward and sharp landward
cross-shore geometry	washover terrace (proximal); sand sheet to mud (distal) with varying thickness landwards but generally thick in depressions	overall but not systematic landward thinning	highly variable thickness	narrow thick terrace deposits terminating in avalanche faces	Manuro: thickening sand landward with abrupt transition to pumice; PRB: variable thickness transitioning to pumice landward
lateral grading	overall landward fining	overall landward fining	landward fining in one site, no systematic trend in another site	not reported	Manuro: not analyzed; PRB: no systematic trend of sand deposits
inland extent (m)	1600	350	up to 87	up to 250	Manuro: 130 (sand); PRB: 100 (sand)
coastal geomorphology	sandy beach, coastal plain	sandy beach	sandy beach ridge plains	barrier island with dunes	Manuro: low-lying embayment; PRB: beach with berm crest topography and landward lake

Table 3.3 (continued)

surface elevation above sea level (m)	1.5 to 2	2 to 3	ridge crests at higher than 4 to 5	dunes at 3 to 4	Manuro: ~ 3.5 (sand); PRB: ~ 1.5 (sand)
maximum storm intensity	Cat 5 (895 mb; ~ 314 kph)	Cat 5 (895 mb; ~ 314 kph)	Cat 5 (929 mb ~ 205 kph)	Cat 4 (> 270 kph)	Cat 5 (> 270 kph)
landfall storm intensity	Cat 5 (~296 kph)	Cat 5 (~296 kph)	Cat 5	Cat 2	Cat 5
translation speed (km/h)	41	41	not reported	not reported	not reported
inundation (m)	5 to 6	5 to 6	3 to 6	2.7 (open coast; > 3 to 4)	Manuro: 1.95 to 5.29; PRB: 2.01 to 3.30
flow depth (m)	3 to 4	3 to 4	not reported	1.26 (landward limit overwash deposition)	Manuro: ~ 2; PRB: 1.51 over berm crest
inundation duration (hrs.)	~ 1	~ 1	12 (peak inundation lasting for 2)	9 (with peak inundation lasting for 5)	not reported
inundation distance (m)	2000	800	500	1500 to 3000	Manuro: ≥ 400; PRB: 320 m
distance from eye (km)	15	30	20 to 40	55	Manuro: 0; PRB: 15
references	(Takagi et al., 2015; Soria et al., 2016; Soria et al., 2017)	(Takagi et al., 2015; Soria et al., 2016; Soria et al., 2017)	(Boughton et al., 2011; Nott et al., 2013)	(Morton et al., 2007)	(Hong et al., 2018)

3.6.3 Flux Comparison: Major Hurricane and Hurricane Nate

In terms of the Sallenger (2000) storm impact scale, Hurricane Katrina caused an inundation regime whereas Hurricane Nate caused an overwash regime. The inundation regime occurs when the elevation of the base of the swash zone, the Sallenger (2000) R_{LOW} , exceeds the elevation of the first line of defense, a berm crest on Ship Island, hence the entire beach is inundated. This regime is associated with massive landward migration of sand bodies (Sallenger, 2000), sediment lost permanently to the barrier platform. The overwash regime occurs when the highest runup exceeds the berm crest elevation but R_{LOW} does not (Sallenger, 2000). Sand is transported and deposited landward resulting in net erosion of the foreshore but net accretion landward of the berm crest, contributing to landward migration (Sallenger, 2000). Ship Island lost 1,100,000 m² of subaerial area during Hurricane Katrina (Eisemann et al., 2018), whereas the island

gained 69,000 m² of subaerial area during Hurricane Nate due to overwash fans extending past the pre storm shoreline in the backbarrier. Hurricane Nate created 154,700 m³ of subaerial overwash, whereas 5,300,000 m³ of sediment was lost between from 2004-2007 due to Hurricane Katrina (Eisemann et al., 2018). Based on the calculation using average sediment flux caused by Hurricane Nate (0.022 m²/s) and island front length (9,628 m), a major storm such as Hurricane Katrina will move as much sediment in about an hour and a half as Hurricane Nate (212 m³/s) in its duration. Sediment moved by major storms is eroded from the barrier platform, whereas the sediment moved from Hurricane Nate was redeposited subaerially. Therefore, major storms are more responsible for Mississippi-Alabama barrier chain land loss than minor storms. A rollover scenario into Mississippi Sound would decrease the lagoon width and volume as infilling from inlets and washover from barriers occurs, whereas overstep could increase the size of the lagoon as the islands are suddenly drowned and appear shoreward while the lagoon transgresses shoreward (Rampino & Sanders, 1982).

The understanding of storm induced sediment processes on Ship Island may be applicable to other barriers in the region. Minor storms can be constructive as they deposit marine sediment onto land (Martin & Muller, 2021), and they provide more energy to transport shoreface sediment than that of fair-weather waves. For example, a Nor'easter type storm quickly provided energy to renourish the coast of Anegada of the British Virgin Islands with sediment eroded by a major hurricane about a half a year prior (Spiske et al., 2021).

3.7 Conclusions

Coastal environments are particularly vulnerable to storm surge as they are low lying and are affected by sinking land and oceanographic effects inducing higher rates of sea-level rise (Carter et al., 2018). The generally low elevation Gulf of Mexico barriers evolve based on the volume of sediment available for resupply, causing differential coastal change rates (Twichell et al., 2013) dominated by tropical cyclone effects (Byrnes et al., 2013; Eisemann et al., 2018) which have been modelled to increase in intensity (Carter et al., 2018). Surge enables storm waves to attack the supratidal region and to move sediment basinward to landward, resulting in dynamic coastal geomorphologic change. As most research has focused on major hurricane impacts, the effects of minor hurricanes on barrier islands have been less clear.

This study performed an analysis of a minor storm impact on a vulnerable barrier island of NGOM. The sedimentary characteristics can augment datasets providing analogues for studies of paleo storm deposits. The Hurricane Nate deposit was well sorted, symmetrically skewed, and mesokurtic containing either horizontally or sub planar laminae. Nate deposits on West Ship Island were finer than deposits on East Ship Island. More landward Nate deposits on West Ship Island slightly coarsened upwards, while basinward deposits on West Ship initially fined and then coarsened upwards. No other fining trend was observed in the Nate deposits, suggesting momentary landward decelerating flow velocities on West Ship, followed again by accelerating flow velocities. The landward and basinward Nate deposits on East Ship Island coarsened upwards more abruptly than those of West Ship Island. In general, Nate deposits on both islands fined landward. Based on a sediment flux calculation, the entire duration of Hurricane Nate

moved as much sediment in about an hour and a half of Hurricane Katrina on Ship Island. Furthermore, Hurricane Nate was a constructive event for Ship Island, based on areal and volumetric increases, in contrast to Hurricane Katrina which was a destructive event based on aerial and volumetric decreases. This highlights the important role that minor storms play in barrier island geomorphology.

3.8 References

- Anderson, J. B. et al., 2014. Variable response of the coastal environments of the northwestern Gulf of Mexico to sea level rise and climate change: Implications for future change. *Marine Geology*, Volume 352, pp. 348-366.
- Beven, J. L. & Berg, R., 2018. Hurricane Nate (AL 162017), Miami: National Hurricane Center.
- Blake, E. S. & Gibney, E. J., 2011. The Deadliest, Costliest, and Most Intense United States Tropical Cyclones from 1851 to 2010 (and Other Frequently Requested Hurricane Facts), Miami: National Weather Service.
- Blott, S. J. & Pye, K., 2001. GRADISTAT: a grain size distribution and statistics package for the analysis of unconsolidated sediments. *Earth Surface Processes and Landforms*, Volume 26, pp. 1237-1248.
- Boughton, G. N. et al., 2011. Tropical Cyclone Yasi: Structural Damage to Buildings.
- Bregy, J. C., Wallace, D. J., Minzoni, R. T. & Cruz, V. J., 2018. 2500-year Paleotempestological Record of Intense Storms for the Northern Gulf of Mexico, United States. *Marine Geology*, Volume 396, pp. 26-42.
- Brill, D. et al., 2016. Typhoon Haiyan's sedimentary record in coastal environments of the Phillipines and its palaeotempestological implications. *Natural Hazards and Earth System Sciences*, 16(12), pp. 27922-2822.
- Byrnes, M. R., Rosati, J. D., Griffee, S. F. & Berlinghoff, J. L., 2013. Historical Sediment Transport Pathways and Quantities for Determining an Operational Sediment Budget: Mississippi Sound Barrier Islands. *Journal of Coastal Research*, Volume 63, pp. 166-183.

- Cangialosi & Avila, 2017. Hurricane NATE. [Online]
Available at:
<https://www.nhc.noaa.gov/archive/2017/all16/all162017.update.10080530.shtml?>
[Accessed 25 March 2022].
- Carter, G. A. et al., 2018. Catastrophic storm impact and gradual recovery on the Mississippi-Alabama barrier islands, 2005-2010: Changes in vegetated and total land area, and relationships of post storm ecological communities with surface elevation. *Geomorphology*, Volume 321, pp. 72-86.
- Davis, R. E. & Dolan, R., 1993. Nor'easters. *American Scientist*, Volume 81, pp. 428-439.
- Dean, C., 2008. After Hurricane Ike, Finding the Coastline Rearranged, Again. [Online]
Available at:
https://www.nytimes.com/2008/09/23/science/23islands.html?no_interstitial
[Accessed 25 March 2022].
- Doran, K. S. et al., 2009. Hurricane Ike: Observations of Coastal Change: U.S. Geological Survey Open-File Report.
- Dupre, W. R., 1985. Geologic Effects of Hurricane Alicia on Upper Texas Coast: ABSTRACT. *AAPG Bulletin*, 69(9), pp. 1419-1419.
- Eisemann, E. R., Wallace, D. J., Buijsman, M. C. & Pierce, T., 2018. Response of a Vulnerable Barrier Island to Multi-Year Storm Impacts: LiDAR-Data-Inferred Morphodynamic Changes on Ship Island, Mississippi, USA. *Geomorphology*, Volume 313, pp. 58-71.

- Emanuel, K. A., 2013. Downscaling CMIP5 climate models shows increased tropical cyclone activity over the 21st century. *PNAS*, 110(30), pp. 12219-12224.
- Erdman, J., 2020. This Is Actually the Biggest Killer During Hurricanes and Tropical Storms. [Online]
Available at: <https://weather.com/safety/hurricane/news/us-deaths-hurricanes-tropical-storms-nhc-study>
[Accessed 25 March 2022].
- Ferguson, R. I. & Church, M., 2004. A Simple Universal Equation for Grain Size Settling Velocity. *Journal of Sedimentary Research*, Volume 27, pp. 3-26.
- Fleming, E. et al., 2018. Coastal Effects. In: D. R. Reidmiller, et al. eds. Impacts, Risks, and Adaptation in the United States: Fourth National Climate Assessment. Washington, DC: U.S. Global Change Research Program, pp. 322-352.
- Folk, R. L. & Ward, W. C., 1957. Brazos River bar [Texas]; a study in the significance of grain size parameters. *Journal of Sedimentary Research*, Volume 27, pp. 3-26.
- Fritz, H. M. et al., 2007. Hurricane Katrina Storm Surge Distribution and Field Observations on the Mississippi Barrier Islands. *Estuarine, Coastal and Shelf Science*, 74(1-2), pp. 12-20.
- Gremillion, S. L., Wallace, D. J., Wright, S. L. & Buijsman, M. C., 2020. Response and Recovery of Horn and Petit Bois Islands, Mississippi, USA to Tropical Cyclone Impacts: 2004 - 2016. *Geomorphology*, Volume 360.
- Hawkes, A. D. & Horton, B. P., 2012. Sedimentary records of storm deposits from Hurricane Ike, Galveston and San Luis Islands, Texas. *Geomorphology*, Volume 171-172, pp. 180-189.

- Hong, I. et al., 2018. Sedimentological characteristics of the 2015 Tropical Cyclone Pam overwash sediments from Vanuatu, South Pacific. *Marine Geology*, Volume 396, pp. 205-214.
- Horton, B. P., Rossi, V. & Hawkes, A. D., 2009. The Sedimentary Record of the 2005 Hurricane Season from the Mississippi and Alabama Coastlines. *Quaternary International*, 195(1-2), pp. 15-30.
- Hrvacevic, Z., 2020. MsCIP completes the restoration of Ship Island. [Online]
Available at: <https://www.dredgingtoday.com/2020/12/21/mscip-completes-the-restoration-of-ship-island/>
- Martin, T. & Muller, J., 2021. The geologic record of Hurricane Irma in a Southwest Florida back-barrier lagoon. *Marine Geology*, Volume 441, pp. 1-13.
- McGee, B. D. et al., 2013. Hurricane Rita Surge Data, Southwestern Louisiana and Southeastern Texas, September to November 2005.
- Mellet, C. L. & Plater, A. J., 2018. Drowned Barriers as Archives of Coastal Response to Sea-Level Rise. In: Moore, L., Murray, A. (eds) *Barrier Dynamics and Response to Changing Climate*. Springer, Cham, pp. 57-89.
- Meyer-Arendt, K. J., 1995. Historical Human Modification of Mississippi's Mainland Shoreline. Jackson: Mississippi Office of Geology.
- Morton, R. A., 2007. Historical Changes in the Mississippi-Alabama Barrier Islands and the Roles of Extreme Storms, Sea Level, and Human Activities, St. Petersburg: U.S. Geological Survey.

- Morton, R. A., 2008. Historical Changes in the Mississippi-Alabama Barrier-Island Chain and the Roles of Extreme Storms, Sea Level, and Human Activities. *Journal of Coastal Research*, 24(6), pp. 1587-1600.
- Morton, R. A., 2010. First-Order Controls of Extreme-Storm Impacts on the Mississippi-Alabama Barrier-Island Chain. *Journal of Coastal Research*, 26(4), pp. 635-648.
- Morton, R. A. & Barras, J. A., 2011. Hurricane Impacts on Coastal Wetlands: A Half-Century Record of Storm-Generated Features from Southern Louisiana. *Journal of Coastal Research*, 27(6A), pp. 27-43.
- Morton, R. A., Gelfenbaum, G. & Jaffe, B. E., 2007. Physical criteria for distinguishing sandy tsunami and storm deposits using modern examples. *Sedimentary Geology*, 200(3-4), pp. 184-207.
- Morton, R. A., Miller, T. & Moore, L., 2005. Historical Shoreline Changes Along the US Gulf of Mexico: A Summary of Recent Shoreline Comparisons and Analyses. *Journal of Coastal Research*, pp. 704-709.
- Morton, R. A. & Sallenger, A. H., 2003. Morphological impacts of extreme storms on sandy beaches and barriers. *Journal of Coastal Research*, pp. 560-573.
- National Geodetic Survey, 2022. 2017 NOAA NGS Emergency Response Imagery: Hurricane Nate from 2010-10-10. NOAA National Centers for Environmental Information.
- NOAA, 2021. National Oceanic and Atmospheric Administration (NOAA) Digital Coast Data Access Viewer. Charlestown(South Carolina): NOAA Office for Coastal Management.

- Nott, J., 2006. Tropical cyclones and the evolution of the sedimentary coast of northern Australia. *Journal of Coastal Research*, 221(221), pp. 49-62.
- Nott, J. et al., 2013. Anatomy of Sand Beach Ridges: Evidence from Severe Tropical Cyclone Yasi and its Predecessors, Northeast Queensland, Australia. *Journal of Geophysical Research: Earth Surface*, 118(3), pp. 1710-1719.
- Odezulu, C. I., Lorenzo-Trueba, J., Wallace, D. J. & Anderson, J. B., 2018. *Follets Island: A Case of Unprecedented Change and Transition from Rollover to Subaqueous Shoals*. In: L. J. Moore & A. B. Murray, eds. *Barrier Dynamics and Response to Changing Climate*. Springer, Cham, pp. 147-174.
- Oivanki, S. M., Meyer-Arendt, K. J. & Yassin, B., 1995. Analysis of Land Use and Land Cover Changes on the Mississippi Coast: 1950s-1992. [Online] Available at: <http://archives.datapages.com/data/gcags/data/045/045001/0467.htm>[Accessed 29 3 2022].
- Oppenheimer, M. et al., 2019. *Sea Level Rise and Implications for Low-Lying Islands, Coasts, and Communities*. Cambridge and New York(NY): Cambridge University Press.
- Otvos, E. G., 1970. Development and Migration of Barrier Islands, Northern Gulf of Mexico: Reply. *GSA Bulletin*, 81(12), pp. 3783-3788.
- Otvos, E. G. & Carter, G. A., 2008. Hurricane Degradation - Barrier Development Cycles, Northeastern Gulf of Mexico: Landform Evolution and Island Chain History. *Journal of Coastal Research*, 24(2), pp. 463-478.

- Otvos, E. G. & Carter, G. A., 2013. Regressive and transgressive barrier islands on the North-Central Gulf Coast - Contrasts in evolution, sediment delivery, and island vulnerability. *Geomorphology*, Volume 198, pp. 1-19.
- Penland, S., Boyd, R. & Suter, J. R., 1988. Transgressive depositional systems of the Mississippi Delta plain; a model for barrier shoreline and shelf sand development. *Journal of Sedimentary Research*, 58(6), pp. 932-949.
- Perez, M., 2019. Camille Cut is no more. A look at new changes to the barrier islands of the Mississippi Coast. Biloxi Sun Herald, 18 February.
- Pielke, R. A., Simonpietri, C. & Oxelson, J., 1999. Thirty years after Hurricane Camille: Lessons learned, lessons lost. National Center for Atmospheric Research.
- Rampino, M. R. & Sanders, J. E., 1982. Holocene Transgression in South-central Long Island, New York-Reply. *Journal of Sedimentary Petrology*, pp. 1020-1026.
- Romano, L. M., 2010. Hurricane Camille (August 1969). [Online] Available at: <https://encyclopediavirginia.org/entries/hurricane-camille-august-1969/>
- Rosati, J. D., Byrnes, M. R., Gravens, M. B. & Griffee, S. F., 2007. Mississippi Coastal Improvement Project Study, Regional Sediment Budget for the Mississippi Mainland and Barrier Island Coasts. U.S. Army Corps of Engineers.
- Rucker, J. B. & Snowden, J. O., 1990. Barrier Island Evolution and Reworking by Inlet Migration along the Mississippi-Alabama Gulf Coast. *Gulf Coast Association of Geological Societies Transactions*, Volume 40, pp. 745-753.
- Sallenger, A. H., 2000. Storm Impacts for Barrier Islands. *Journal of Coastal Research*, 16(3), pp. 890-895.

- Schwab, W. C., 2017. Change in morphology and modern sediment thickness on the inner continental shelf offshore of Fire Island, New York between 2011 and 2014: Analysis of hurricane impact. *Marine Geology*, Volume 391, pp. 48-64.
- Shaw, J., You, Y., Mohrig, D. & Kocurek, G., 2015. Tracking hurricane generated storm surge with washover fan stratigraphy. *Geology*, pp. 127-130.
- Soria, J. L. A. et al., 2017. Typhoon Haiyan overwash sediments from Leyte Gulf coastlines show local spatial variations with hybrid storm and tsunami signatures. *Sedimentary Geology*, Volume 358, pp. 121-138.
- Soria, J. L. A. et al., 2018. Surf beat-induced overwash during Typhoon Haiyan deposited two distinct sediment assemblages on the carbonate coast of Hernani, Samar, central Phillipines. *Marine Geology*, Volume 396, pp. 215-230.
- Soria, J. L. A. et al., 2016. Repeat Storm Surge Disasters of Typhoon Haiyan and its 1897 Predecessor in the Phillipines. *Bulletin of the American Meteorological Society*, Volume 97, pp. 31-48.
- Spiske, M. et al., 2021. Coastal erosion and sediment reworking caused by hurricane Irma - implications for storm impact on low-lying tropical islands. *Earth Surface Processes and Landforms*. Volume 47, pp. 891-907.
- Stewart, S. R., 2004. Tropical Cyclone Report Hurricane Ivan 2-24 September 2004, Miami: National Hurricane Center.
- Swift, D. J. & Moslow, T. F., 1982. Holocene Transgression in South-central Long Island, New York - Discussion. *Journal of Sedimentary Research*, pp. 1014-1019.

- Takagi, H. et al., 2015. Track Analysis, Simulation, and Field Survey of the 2013 Typhoon Haiyan Storm Surge. *Journal of Flood Risk Management*, Volume 10, pp. 42-52.
- Twichell, D. C., Flocks, J. G., Pendleton, E. A. & Baldwin, W. E., 2013. Geologic Controls on Regional and Local Erosion Rates of Three Northern Gulf of Mexico Barrier-Island Systems. Coconut Creek(Florida): US Army Corps of Engineers, 2020. USACE. [Online] Available at:
<https://www.sam.usace.army.mil/Media/News-Stories/Article/2451959/mobile-district-completes-ship-island-restoration/>
- Wiberg, P. L. & Smith, J. D., 1989. Model for Calculating Bed Load Transport of Sediment. *Journal of Hydraulic Engineering*, pp. 101-123.
- Williams, H. F., 2009. Stratigraphy, Sedimentology, and Microfossil Content of Hurricane Rita Storm Surge Deposits in Southwest Louisiana. *Journal of Coastal Research*, pp. 1041-1051.
- Williams, H. F. L., 2010. Storm Surge Deposition by Hurricane Ike on the McFaddin National Wildlife Refuge, Texas: Implications for Paleotempestology Studies. *Journal of Foraminiferal Research*, 40(3), pp. 210-219.
- Willingham, A., 2017. A look at four storms from one brutal hurricane season. [Online] Available at: <http://www.cnn.com/2017/10/10/weather/hurricane-nate-maria-irma-harvey-impact-look-back-trnd/index.html>[Accessed 27 5 2022].
- Xian, H. et al., 2022. High-resolution reconstruction of typhoon events since ~1850 CE based on multi-proxy sediment records in a coastal lagoon, South China. *Science of the Total Environment*, Volume 803.

APPENDIX A – Mississippi Offshore Sediment Resources Inventory

Sand resources off the coast of Mississippi and Alabama as well as on the Outer Continental Shelf have important implications for coastal resiliency. For example, the Army Corps of Engineers recently spent \$400 million on a sand nourishment project on Ship Island, having dredged and transported the resource from 32 to 56 km away from the project site (US Army Corps of Engineers, 2020). New sources of sand can be found through the study of core and geophysical data, some of which has already been collected by various agencies. These collected data, or legacy data, has not been compiled into one database, therefore, a cooperative agreement between the University of Southern Mississippi (USM) and the Bureau of Ocean Energy Management (BOEM) was created for this purpose: “Mississippi Offshore Sediment Resources Inventory: Late Quaternary Stratigraphic Evolution of the Inner Shelf.” A compilation of legacy geological data consisting of cores and geophysics from the NGOM, found in Table A.1, was compiled in a database. Taking into consideration salaries, ship time (with fuel), and equipment rentals, recollection of these data would cost over \$2,000,000 to recollect. The goal of this database is to holistically bring together numerous data sources into one ArcGIS framework and make them accessible for future assessment of sediment resource. The compiled core data were added to this ArcGIS framework (Figure A.1). Digitized geophysical data sets are displayed in the ArcGIS project for the inner shelf and outer shelf (Figure A.2). BOEM and USGS reports were also obtained identifying existing potential sand borrow sites as well as infrastructure in these areas. Collecting new core data offshore is one of the ongoing activities of this project. The ArcGIS framework will

be published through the BOEM Marine Minerals Information Systems database at the end of the project in September 2022.

This compilation focused on three areas: #1 near Petit Bois and Dauphin Islands (Lead by former USM student Robert Hollis), #2 near Horn Island (Lead by former USM student Nina Gal), and #3 western Mississippi Sound and the Outer Continental Shelf. I assisted the creation and organization of all three but for #3 I lead the effort. My contributions for #1 and #2, lead to coauthorship on the following publications:

- 1) Hollis, R.J., Wallace, D.J., Miner, M.D., Gal, N.S., **Dike, C.**, and Flocks, J.G., 2019, Late Quaternary Evolution and Stratigraphic Framework Influence on Coastal Systems along the North-Central Gulf of Mexico, USA: Quaternary Science Reviews, v. 223, 105910. First published online September 30, 2019, <https://doi.org/10.1016/j.quascirev.2019.105910>
- 2) Gal, N.S., Wallace, D.J., Miner, M.D., Hollis, R.J., **Dike, C.**, Flocks, J.G., 2021, Influence of antecedent geology on the Holocene formation and evolution of Horn Island, Mississippi, USA: Marine Geology, v. 431, 106375. First published online October 29, 2020, <https://doi.org/10.1016/j.margeo.2020.106375>.

Literature focused on the lowstand, transgression, and highstand fluvial deltaic system evolution for the NGOM that aids in outer shelf sand source identification and evolution was compiled in a Google Drive archive (Literature - Google Drive). Nearly 150 publications are contained herein, many of which provided new insight using data listed in Table A.1.

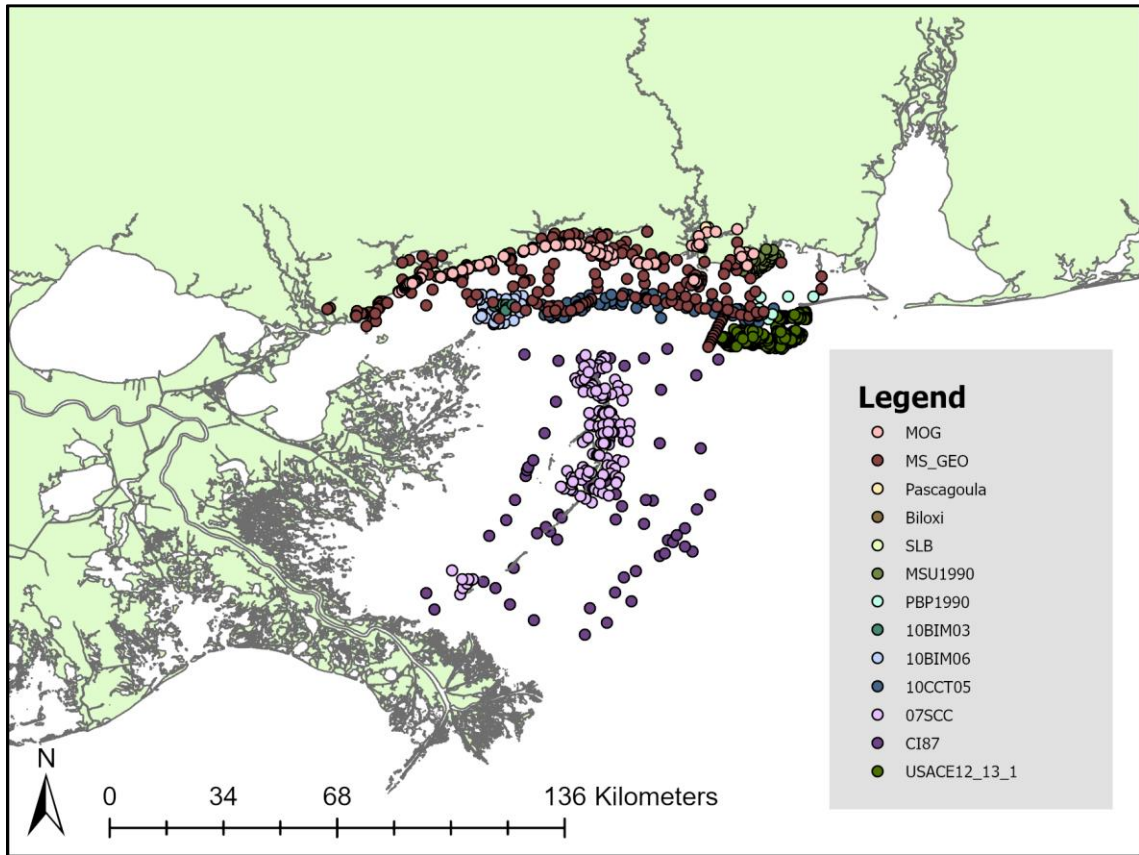


Figure A.1 *NGOM Legacy Core Data Compiled in the USM Database.*

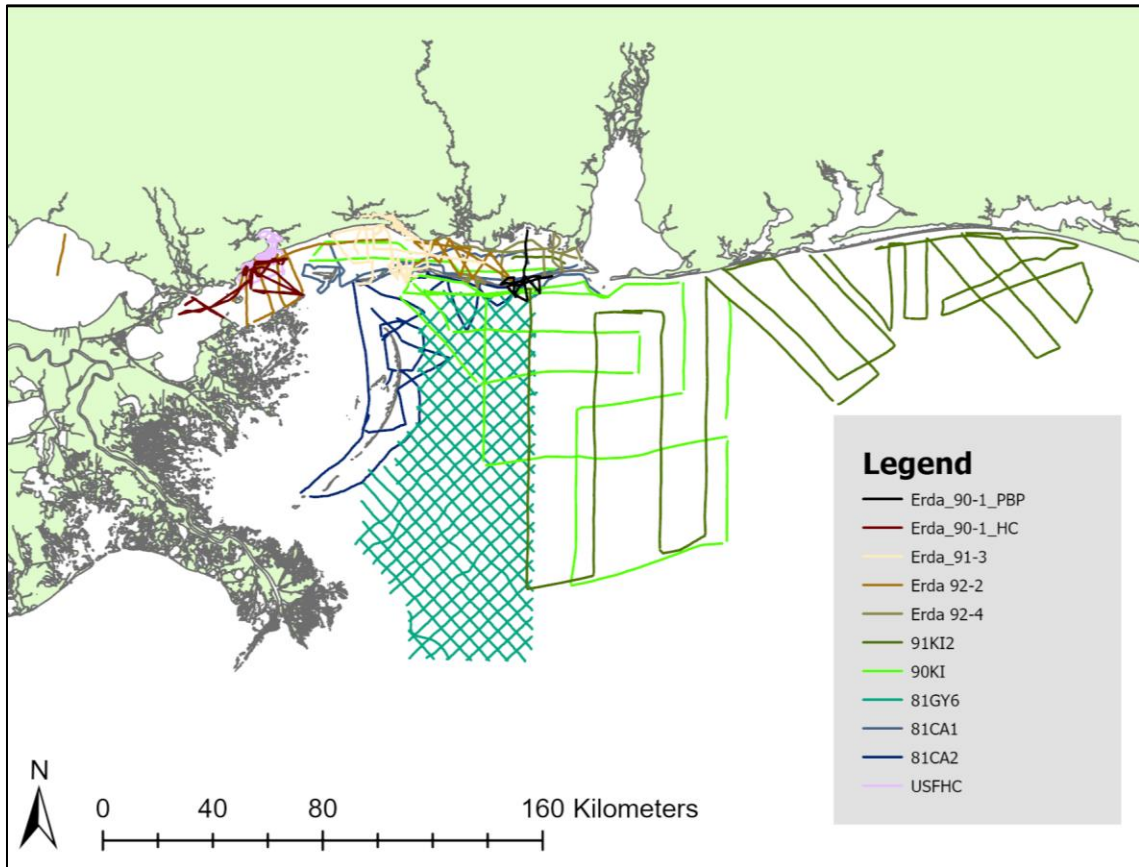


Figure A.2 *NGOM Legacy Seismic Data Compiled in the USM Database.*

Table A.1 *Legacy Core and Geophysical Data Collected in the USM Database*

Data Name	Location	Type	Dates	Associated Publications	Citation
MOG	Hancock County, Deer Island, Harrison County, Belle Fontaine and Round Island, Grand Bay NERR	vibracores, auger-cores, and hand-cores	1999-2003		(Gulf Coast Research Lab, 2004)
MS_GEO	Barrier islands, Gulf inner shelf, Hancock County, Harrison County, Jackson County, major bays (Bay St. Louis, Biloxi Back Bay), Mississippi Sound	vibracores and rotary cores	1980-2003	(Otvos & Giardino, 2004; Otvos, 2001)	(Gulf Coast Research Lab, 2021)
Pascagoula	Pascagoula River	rotary wash	2016		(Burns, Cooley, Dennis, Inc., 2009)
Biloxi	Biloxi River	rotary wash	2005-2006		(Burns, Cooley, Dennis, Inc., 2009)
SLB	Bay St. Louis		2005-2006		(HNTB Corporation, 2006)
MSU1990	Grand Bay National Estuary Research Reserve	vibracores	1990		(Kramer, 1990)
PBP1990	Petit Bois Island	vibracores	1990	(McBride et al., 1991)	(McBride et al., 1991)
10BIM03	Cat Island	vibracores	2010	(Kindinger et al., 2014; Miselis et al., 2014)	(Buster et al., 2014)
10BIM06	Cat Island	vibracores	2010	(Kindinger et al., 2014; Miselis et al., 2014)	(Buster et al., 2014)
10CCT05	Ship, Horn, and Petit Bois Islands	vibracores	2010		(Kelso & Flocks, 2015)
07SCC	Chandeleur and Breton Islands	vibracores	2007		(Dreher et al., 2010)
CI87	Chandeleur Islands	vibracores	1987	(Brooks et al., 1995; Kindinger et al., 1989)	(Dreher et al., 2010)
USACE12_13	Mississippi Sound and Mississippi-Alabama Barrier Islands	vibracores	2010-2013	(Flocks et al., 2015; Flocks et al., 2014)	
Erda_90-1_PBP	Petit Bois Pass	boomer	1990	(McBride et al., 1991)	(Bosse et al., 2017)

Table A.1 (continued)

Erda_90-1_HC	Lake Borgne and Mississippi Sound	boomer	1990		(Bosse et al., 2017)
Erda_91-3	Mississippi Sound	boomer	1991		(Bosse et al., 2017)
Erda_92-2	Grand, Cat, and Horn Islands	boomer	1992	(Hollis et al., 2019)	(Bosse et al., 2018a)
Erda_92-4	Horn and Petit Bois Islands	boomer	1992	(Hollis et al., 2019)	(Bosse et al., 2018a)
91KI2	Mississippi-Alabama-Florida Shelf	boomer	1991	(Kindinger et al., 1994)	(Bosse et al., 2018b)
90KI	Mississippi-Alabama Shelf	boomer	1990	(Kindinger et al., 1994)	(Bosse et al., 2018b)
81GY6	Mississippi-Alabama-Louisiana Shelf	minisparker	1981	(Greene et al., 2007; Kindinger, 1988; Kindinger et al., 1994; Roberts et al., 2004)	(Bosse et al., 2018b)
81CA1	Mississippi-Alabama-Louisiana Shelf	boomer	1981	(Penland et al., 1985)	(Bosse et al., 2018b)
81CA2	Mississippi-Alabama-Louisiana Shelf	boomer	1981	(Penland et al., 1985)	(Bosse et al., 2018b)
USFHC	Bay St. Louis and Mississippi Sound	boomer	1989		(Bosse et al., 2018c)

A.1 References

- Bosse, S. T., Flocks, J. G. & Forde, A. S., 2017. Digitized analog boomer seismic-reflection data collected during U.S. Geological Survey cruises Erda 90-1_HC, Erda 90-1_PBP, and Erda 91-3 in Mississippi Sound, June 1990 and September 1991. U.S. Geological Survey.
- Bosse, S. T., Flocks, J. G. & Forde, A. S., 2018a. Archive of digitized analog boomer seismic-reflection data collected during U.S. Geological Survey cruises Erda 92-2 and Erda 92-4 in Mississippi Sound, June and August 1992: U.S. Geological Survey data release, <https://doi.org/10.5066/F7RV0N0X>.
- Bosse, S. T., Flocks, J. G. & Forde, A. S., 2018b. Archive of digitized analog boomer minisparker seismic reflection data collected from the Northern Gulf of Mexico: 1981, 1990, and 1991: U.S. Geological Survey data release, <https://doi.org/10.5066/F7CN730G>.
- Bosse, S. T., Flocks, J. G. & Forde, A. S., 2018c. Archive of digitized analog boomer seismic reflection data collected during USGS cruise USFHC in Mississippi Sound and Bay St. Louis, September 1989. St. Petersburg(Florida): USGS.
- Brooks, G. R. et al., 1995. East Louisiana Continental Shelf Sediments: A Product of Delta Reworking. *Journal of Coastal Research*, 11(4), pp. 1026-1036.
- Burns, Cooley, Dennis, Inc., 2009. *Engineering Boring Reports*.
- Buster, N. A., Kelso, K. W., Miselis, J. L. & Kindinger, J. G., 2014. Sediment data collected in 2010 from Cat Island, Mississippi: U.S. Geological Survey, Reston: U.S. Geological Survey.

- Cipriani, L. E. & Stone, G. W., 2001. Net Longshore Sediment Transport and Textural Changes in Beach Sediments along the Southwest Alabama and Mississippi Barrier Islands, U.S.A., *Journal of Coastal Research*, 17(2), pp. 443-458.
- Dreher, C. A., Flocks, J. G., Kulp, M. A. & Ferina, N. F., 2010. Archive of Sediment Data Collected around the Chandeleur Islands and Breton Island in 2007 and 1987 (Vibracore Surveys: 07SSC04, 07SCC05, and 87039). St. Petersburg(Florida).
- Flocks, J. G., Kindinger, J. L. & Kelso, K. W., 2015. Geologic control on the evolution of the inner shelf morphology offshore of the Mississippi barrier islands, northern Gulf of Mexico, USA. *Continental Shelf Research*, Volume 101, pp. 59-70.
- Flocks, J. et al., 2014. Near-surface stratigraphy and morphology, Mississippi inner shelf, northern Gulf of Mexico, Reston: U.S. Geological Survey.
- Gal, N. S. et al., 2021. Influence of Antecedent Geology on the Holocene Formation and Evolution of Horn Island, Mississippi, USA. *Marine Geology*, Volume 431.
- Greene, D. L., Rodriguez, A. B. & Anderson, J. B., 2007. Seaward-Branching Coastal-Plain and Piedmont Incised-Valley Systems Through Multiple Sea-Level Cycles: Late Quaternary Examples from Mobile Bay and Mississippi Sound, U.S.A. *Journal of Sedimentary Research*, Volume 77, pp. 139-158.
- Gulf Coast Research Lab, 2004. Mississippi Office of Geology Vibracore Corelogs.
- Gulf Coast Research Lab, 2021. Historical Mississippi Corelogs. Mississippi Department of Environmental Quality, Mississippi Office of Geology, Coastal and Energy Division.

- HNTB Corporation, 2006. *Bridge Replacement on US 90 across St. Louis Bay Hancock and Harrison Counties, Mississippi*.
- Hollis, R. J. et al., 2019. Late Quaternary Evolution and Stratigraphic Framework Influence on Coastal Systems along the North-Central Gulf of Mexico, USA. *Quaternary Science Reviews*, Volume 223.
- Kelso, K. W. & Flocks, J. G., 2015. Archive of sediment data from vibracores collected in 2010 offshore of the Mississippi barrier islands, Reston: U.S. Geological Survey.
- Kindinger, J. L., 1988. Seismic stratigraphy of the Mississippi-Alabama shelf and upper continental slope. *Marine Geology*, Volume 83, pp. 79-94.
- Kindinger, J. L., Balson, P. S. & Flocks, J. G., 1994. Stratigraphy of the Mississippi-Alabama Shelf and the Mobile River Incised-Valley System. In: *Incised-valley Systems: Origin and Sedimentary Sequences*. Society for Sedimentary Geology.
- Kindinger, J. L., Miller, R. J., Stelting, C. E. & Bouma, A. H., 1982. Depositional history of Louisiana-Mississippi outer continental shelf, United States Department of the Interior Geological Survey.
- Kindinger, J. L., Miselis, J. L. & Buster, N. A., 2014. The Shallow Stratigraphy and Sand Resources Offshore from Cat Island, Mississippi, Reston: U.S. Geological Survey.
- Kindinger, J. L., Penland, S., Williams, S. J. & Suter, J. R., 1989. Inner Shelf Deposits of the Louisiana-Mississippi-Alabama Region, Gulf of Mexico. *Transactions-Gulf Coast Association of Geological Societies*, Volume XXXIX, pp. 413-420.

- Kramer, K. A., 1990. Late Pleistocene to Holocene Geologic Evolution of the Grande Batture Headland Area, Jackson County, Mississippi.
- McBride, R. A. et al., 1991. Geomorphic History, Geologic Framework, and Hard Mineral Resources of the Petit Bois Pass Area, Mississippi-Alabama. In: *Coastal Depositional Systems in the Gulf of Mexico: Quaternary Framework and Environmental Issues*.
- Miselis, J. L., Buster, N. A. & Kindinger, J. L., 2014. Refining the link between the Holocene development of the Mississippi River Delta and the geologic evolution of Cat Island, MS: implications for delta-associated barrier islands. *Marine Geology*, Volume 355, pp. 274-290.
- Otvos, E. G., 2001. H. Mississippi Coast: Stratigraphy and Quaternary Evolution in the Northern Gulf Coastal Plain Framework, USGS.
- Otvos, E. G. & Giardino, M. J., 2004. Interlinked barrier chain and delta lobe development, northern Gulf of Mexico. *Sedimentary Geology*, Volume 169, pp. 47-73.
- Penland, S., Suter, J. R. & Boyd, R., 1985. Barrier island arcs along abandoned Mississippi River deltas. *Marine Geology*, Volume 63, pp. 197-233.
- Roberts, H. H. et al., 2004. Depositional architecture of the Lagniappe Delta: Sediment characteristics, timing of depositional events, and temporal relationship with adjacent shelf-edge deltas. In: J. B. Anderson & R. H. Fillon, eds. *Late Quaternary Stratigraphic Evolution of the Northern Gulf of Mexico Margin*. Tulsa(Oklahoma): SEPM (Society for Sedimentary Geology), pp. 143-188.

US Army Corps of Engineers, 2020. *USACE*. [Online]

Available at: <https://www.sam.usace.army.mil/Media/News->

[Stories/Article/2451959/mobile-district-completes-ship-island-restoration/](https://www.sam.usace.army.mil/Media/News-Stories/Article/2451959/mobile-district-completes-ship-island-restoration/)